ROMA TRE
UNIVERSITÀ DEGLI STUDI

DOTTORATO DI RICERCA IN INGEGNERIA CIVILE

XXX CICLO

A MODIFIED JOINTED ROCK MODEL FOR MASONRY IN SOIL-STRUCTURE INTERACTION PROBLEMS

Wanda Guglielmina Lasciarrea

Nome e Cognome del dottorando — firma

Prof. Gianmarco de Felice

Prof. Angelo Amorosi

Ing. Marialaura Malena

Docente Guida/Tutor: Prof. — firma

Prof. Gianmarco de Felice

Coordinatore: Prof. — firma

Collana delle tesi di Dottorato di Ricerca
In Ingegneria Civile
Università degli Studi Roma Tre
Tesi n° 70

To my lovely friends and
my wonderful family.

Acknowledgements

First of all, I want to thank my Ph.D. thesis committee and especially Prof. Pere Roca Fabregat and Prof. Bahman Ghiassi for being such good reviewers. All the comments and questions I received allowed me to improve the scientific content of this Thesis.
I would like to particularly thank Professor Pere Roca Fabregat, of the Universitat Politecnica de Catalunya, because he gave me the opportunity to work with him in Barcelona closely investigating the structural behavior of the Church of Santa Maria del Mar. He gave me the opportunity of applying the notions acquired during my Ph.D. by allowing me to analyze the Church in its interaction with the soil for the first time ever. I want to thank him also for his time, constant availability, diligence, accounts of observations and for the invaluable data and information he provided with his contagious enthusiasm towards the conservation of historic buildings.
I would like to express my most sincere appreciation for all the people that helped me and encouraged me during my Ph.D., especially Professor Gianmarco de Felice, who gave me the opportunity to do a great variety of experiences during these three years and for everything I have learned thank to his careful and precious supervising. I am very grateful to my co-advisors, Professor Angelo Amorosi and Ing. Marialaura Malena for all the suggestions, the kind supervision and encouragements they have always given to me. I appreciate their time and patience to share their knowledge and their passion for this work. Special thanks also to Prof. Daniela Boldini for all the indications she gave me during this three years.
Thanks, too, to the students I had the occasion to interact with because their doubts have been for me a chance of growth.
Moreover, I would like to thank all my colleagues, in particular, the beautiful people I met in Barcelona, for their particular friendship that made the visiting period one of the most rewarding experiences ever.
I want to also thank Blerta, Tiziano, Riccardo and all the wonderful friends of Portanevia Residence for all the beautiful moments we spent together, for the suggestions and their constant presence, also from far. They have been my second family and I will bring them in my heart forever.

Special thanks to Covino's family for making me felt as a daughter. I will always remember all the attentions, encouragements and teachings I received from them and I learned by their example.
I would like to express my gratitude to all my friends of Bari, met at High School, University, San Marco's Church and Puntasveva Residence who have given me the energy to go on with this experience never giving up and believing in me.
Moreover, I want to thank all my grandparents, especially the ones who have passed away. Not being able to be there with them while they were going through their illnesses was by far one of the hardest challenges I had to deal with. "Pain is a lesson I learned with the love" as a song states, and it has definitely turned out to be true. I would like to show them I learned their lessons of love through all their teachings, examples and advice. I will keep it in my mind as precious treasures.
Thanks, too, to all my lovely uncles and cousins for their constant presence and all the beautiful moments spent together. In particular, I would thank Marco for his continuous availability, help and all the experiences shared despite the distance. His enthusiasm made this experience more fun and carefree.
Finally and most importantly a special and unique thanks to my family, my mum Enza, my dad Riccardo and my brothers and sister Maurilia, with her husband Antonio and their lovely Giorgio, Silvio with his wife Valentina, Ugo with Valeria, and Karol with Annarita: without them and their unwavering support this work would not have been possible at all. I want to thank them for allowing me to follow my dreams and especially because, thanks to their constant support, affection, and all their sacrifices I never felt lonely during all these years spent away from home.
Thank you all, your love is my secret to go on.

Sommario

La salvaguardia dei fabbricati esistenti rispetto ad interventi che possano insidiarne la stabilità e la funzionalità strutturale, per cause naturali o antropiche, è un problema di scottante attualità. Ciò è particolarmente vero nel caso di strutture storiche e monumentali, caratterizzate da una delicata ed estesa nel tempo interazione con l'area nella quale sono insediate. In questo contesto assume crescente rilievo la complessa problematica dell'interazione tra strutture storiche e scavi in ambiente urbano, questi ultimi finalizzati alla realizzazione di opere in sotterraneo quali parcheggi o linee metropolitane. Tale contesto è caratterizzato da numerosi e complessi problemi, la cui soluzione appare necessaria ai fini della realizzazione dell'opera nel massimo rispetto della salvaguardia del costruito interagente con essa.
Il presente contributo mira ad individuare un approccio di analisi che integri gli aspetti strutturali e quelli geotecnici allo scopo di prevedere in maniera più realistica il danno indotto in strutture storiche durante la realizzazione di opere geotecniche. A tal fine è stato utilizzato il codice di calcolo geotecnico agli Elementi Finiti tridimensionale Plaxis 3D, in cui la modellazione della struttura è stata affidata alla versione modificata del modello Jointed Rock, già implementato nel codice. Tale modello, nato originariamente per descrivere il comportamento di ammassi rocciosi fratturati, è stato modificato nel presente lavoro al fine di descrivere il comportamento meccanico delle strutture murarie caratterizzate da forte grado di anisotropia. Il confronto effettuato con modelli costitutivi avanzati per le murature e con tests sperimentali, ha dimostrato l'attendibilità del nuovo *Jointed Masonry Model* nel rappresentare il comportamento della muratura e nel cogliere gli aspetti salienti delle strutture murarie. La possibilità di poter descrivere questa classe di opere all'interno di un codice di calcolo geotecnico ha consentito che due importanti strutture in muratura come il Ninfeo di Genazzano, attribuito a Bramante, e la Chiesa gotica di Santa Maria del Mar a Barcellona, fossero analizzate per la prima volta nell'ambito di una modellazione tridimensionale che tenesse conto della loro interazione con il terreno, descrivendo quest'ultimo con modelli costitutivi avanzati. Per entrambe le opere, l'utilizzo di un approccio

integrato, geotecnico e strutturale, che prendesse in considerazione l'evoluzione delle condizioni che hanno caratterizzato la storia dei singoli monumenti durante la loro costruzione e nel corso della loro vita, ha consentito di comprendere e riprodurre con sufficiente grado di accuratezza quanto occorso ai monumenti nel tempo.

L'ulteriore aspetto investigato con Jointed Masonry Model si sostanzia, infine, dello svolgimento di analisi parametriche al fine di valutare il danno prodotto su strutture in muratura a causa della realizzazione dello scavo di una galleria. L'aver potuto tenere conto della tridimensionalità del problema ha consentito di comprendere la modalità con cui i meccanismi alla base del comportamento di strutture storiche siano influenzati dal campo di spostamenti indotto dalla realizzazione di questo tipo di opere.

Abstract

The preservation of existing buildings regard to interventions that can undermine its stability and structural functionality, for natural or human-made reasons, is a burning topic of concern. This is particularly true in the case of historical and masonry buildings, characterized by a long and delicate interaction with the area in which they are located. In this context, the complex problem of the interaction between historical structures and excavations in the urban environment is increasingly emphasised, the latter being aimed at the construction of underground works such as car parks or metropolitan lines. This context is characterized by numerous and complex problems, the solution of which is necessary for the realization of the work in the strictest respect of the preservation of the constructions interacting with it. With approximate methods, today it is possible to combine more sophisticated methods, based on non-linear Finite Elements numerical analyses performed with specific codes developed in the academic field. The present contribution aims to identify an analysis approach that integrates both structural and geotechnical aspects to predict in a more realistic way the damage induced in historical structures as a consequence of geotechnical works. For this purpose, the Geotechnical Finite Element Code Plaxis 3D was used, in which the masonry behavior was modelled through the modified version of the Jointed Rock Model, already implemented in the code in its original version. This model, initially developed to describe fractured rock mass behavior, was modified in this work to describe the mechanical behavior of masonry structures characterised by a high degree of anisotropy. The comparison with advanced masonry models and experimental tests has demonstrated the reliability of the new developed *Jointed Masonry Model* to describe masonry response and to grasp the salient aspects of masonry. The opportunity to describe this class of works within a geotechnical code thus allowed two significant masonry structures such as the Nymphaeum of Genazzano, attributed to Bramante, and the Gothic Church of Santa Maria del Mar in Barcelona, were analyzed for the first time in a three-dimensional modelling that took into account their interaction with the ground, describing the latter with advanced constitutive models. For both

works, the use of an integrated approach, geotechnical and structural, that takes into account the conditions evolution characterising the individual monument's history during their construction and their lifetime, allowed to understand and reproduce with sufficient degree of accuracy what happened to structures over time. The further aspect investigated with Jointed Masonry Model is, ultimately, the study of parametric analyses carried out to predict the effects induced in masonry structures as a result of a tunnel excavation. Having been able to take into account the three-dimensionality of the problem has enabled to grasp how the mechanisms underlying the historic structure's behaviour are influenced by the displacement field induced by this kind of works.

CONTENTS

LIST OF FIGURE

INDEX OF TABLE

1. INTRODUCTION

Preserving our monuments is a matter of vital importance as each one of them is the historical and artistic witness of the evolution of mankind, society and territory. This value is undoubtedly connected with the life of the monument itself. Particularly nowadays, this matter has to be highlighted and discussed because of the numerous natural and anthropological interventions that can affect our historic buildings, characterized by a strong interaction with the area where they are located. Due to their indisputable importance, this kind of structures has to be preserved: the valuation of their state with regards to any interventions that can undermine their functionality is needed and fundamental. For this reason, it is crucial to produce a specific kind of analysis that integrates structural and geotechnical aspects in order to predict the damage induced in historical structures as a result of human intervention and natural phenomena.

Despite the great relevance of relevant studies conducted in the past, such as those devoted to the Leaning Tower of Pisa (Burland and Viggiani, 1994), the Ghirlandina Tower in Modena (Lancellotta, 2013) and the Pienza Cathedral (Calabresi G., 2013), a unified approach for the integrated analysis of structure and foundation soils is rare.

Traditionally, the prediction of effects on existing structures has been carried out with empirical methods that completely neglect the phenomenon of soil-structure interaction (Mair et al., 1993; Moh et al., 1996; O'Reilly & New, 1982), resulting very conservative with respect to damage assessment. Furthermore, these methods are based on significant simplifications that produce an effects prediction not sufficiently representative of the real case. It is recent the possibility to adopt new methods able to take into account the interaction with pre-existing structure, although in a simplified manner (Burland J.B., Wroth C.P., 1974; Potts D.M., Addenbrooke T.I., 1997; Boscardin M.D., Cording E.J., 1989; Burland J.B., 1995; Franzius, J.N., 2004). In fact, it consists in using a relatively simple analytical approach to describe the building considering it as an elastic beam that deforms according to the greenfield tunnel-induced ground movements that are estimated to occur at foundation level. Furthermore, the simplifications made with respect to particular geometric configurations of the problem, the sensitivity of the building and the complexity of the structure are still significant.

As opposed to approximate methods, it is possible today to combine more sophisticated methods based on non-linear Finite Elements numerical analysis, thanks to specific calculation programs developed in the academic field. The use of advances methods is, in fact, indispensable during the design process of works characterised by a particular complexity and in all that cases where the use of the Elastic Beam Assessment method is inconclusive (Potts & Addenbrooke, 1997). Besides, numerical modelling allows to take into account also the three-dimensionality of the problem that is an essential aspect to understand the mechanisms on which the behaviour of buildings subjected to the field of displacement induced by geotechnical works is based on. This is especially true in the case of galleries excavation, where the three-dimensionality condition strongly influences the numerical prediction, even with regard to the simulation of free field conditions. In fact, as highlighted by Burland & Wroth, 1974, Boscardin & Cording, 1989, and Burland, 1995, the advancement of the excavation front causes the propagation of the subsidence span generated by the excavation itself in the longitudinal direction, affecting at different moments, several parts of the structure. It follows that, at different times each part of the building is affected by a different settlements distribution, up to the full passage of the excavation front. This is the reason why the traditional methods for estimating masonry buildings at risk of tunnel-induced settlement damage are based on a phased sequence of calculations of rising sophistication (e.g. Mair et al., 1996; Harris & Franzius, 2005; Burland et al., 2012).

Actually, in the literature the examples comparing finite element modelling results with field data for buildings that have been affected by tunneling, are provided by Amorosi et al., 2012 - 2014, Sebastianelli et al., 2012, Fargnoli et al., 2015, Bilotta et al., 2017 and Yiu et al., 2017.

However, in civil engineering practice for project-based assessment purposes, there are no clear examples of application of this type of approach. This could be due to the relatively complex soil-structure interaction modelling, the difficulties in calibration procedure for masonry models, or the high computational cost sometimes required by the analyses.

The aim of this work is to reproduce a specific kind of analysis that integrates both structural and geotechnical aspects to reproduce the masonry behaviour and all the several failure mechanisms that concern it, especially in soil structure interaction problems. The emphasis is on the development of a Jointed Masonry Model to describe masonry structure mechanical response starting from an already existing Jointed Rock Model.

The Jointed Rock model, originally developed to describe rock mass behaviour and implemented in a Geotechnical Code called Plaxis 3D, has been adapted to the description of a masonry building. This strategy has allowed to take into account the real soil structure interaction since in this way it is possible to describe with advanced constitutive model both structure and soil in a unique program. To validate the Jointed Masonry Model in describing masonry behaviour, different kinds of analyses were carried out. These were then compared with both experimental and numerical tests performed with advanced constitutive models developed for masonry.

2. CONSTITUTIVE MODEL FORMULATION

Studies geared to the conservation of historical structures recourse to structural analysis to better understand the main mechanical features of masonry buildings, to characterise the current condition and try to quantitatively justify the actual damage state. The comprehension of masonry behaviour cannot disregard from the knowledge of its constitutive materials and its constructive typology.
In this chapter, the constitutive elements and their influence on masonry mechanical response are presented in more detail. Then, an overview of different modelling technique is presented before the Jointed Masonry Model description, adopted in this work to simulate the masonry structural behaviour, is illustrated.

2.1. Masonry properties and Micro-Macro modelling

Historic buildings, consisted of brick or stone masonry assembled together with mortar joints, are characterised by a complex mechanical behaviour due to its components. The main features of this kind of structure can be summarised in its composite character, in its brittle response in tension, a frictional response in shear and its anisotropy (P. Roca et al., 2009). The principal mechanical peculiarities of this kind of structures are the relatively large intrinsic stiffness and strength of the blocks as compared with those of the joints. Therefore, the behaviour of such assemblies is strongly influenced by the properties of the joints, the geometry of the units and their texture (de Felice et al., 2009).
In fact, the geometry and layout of joints play an essential role in the response of the wall and in the mechanism of failure (Fig.2.1).

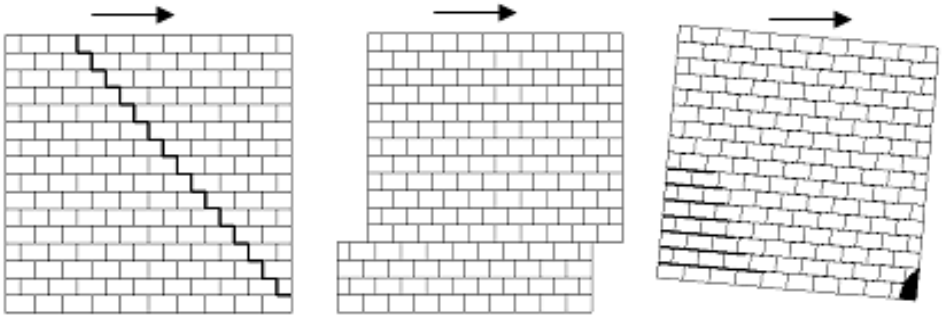

Figure 2.1 In-plane failure mechanisms of masonry walls.

It followed that, when dealing with these assemblies, a numerical approach should be able to describe the essential mechanical and strength feature of the real construction, taking into account its morphology. In particular, an accurate model should also allow to describe the structural damage including cracks and construction defects.
In particular kind of analysis, like the dynamic one, the numerical model capacity to describe some important aspects such as initial and historical soil settlements, architectural alterations and the historical construction stages should allow catching with a higher level of accuracy, the deformations occurred on the structure.
Depending on the level of accuracy and the simplicity desired, it is possible to use different modelling strategies.
Traditionally, the linear elastic analysis is performed, prior to the use of more advanced approach, to obtain a first estimation of the structural model capability regarding the mesh level accuracy and the values and load distribution. The reduced computer costs and the easy availability have encouraged its use as a supplemental tool aiding in the diagnosis of important masonry structures like San Marco in Venice (Mola and Vitaliani, 1995), the Tower of Pisa (Macchi et al., 1993) the Colosseum of Rome (Croci G., 1995), and the Church of the Guell Colony in Barcelona (Gonzales et al., 1993; Roca P., 1998).
Nevertheless, this model is inadequate for masonry structures since it is not able to model the non-tension response and the other essential features already described. In particular, this model cannot be used to estimate the ultimate response of masonry structures and hence to provide details about their structural safety.
One of the more direct approaches to the study of masonry buildings relies on the Finite Element Method. In detail, two main modelling strategies are

available namely the micro-modelling and the macro-modelling. One modelling strategy cannot be preferred over the other because different application fields exist for micro- and macro-models.

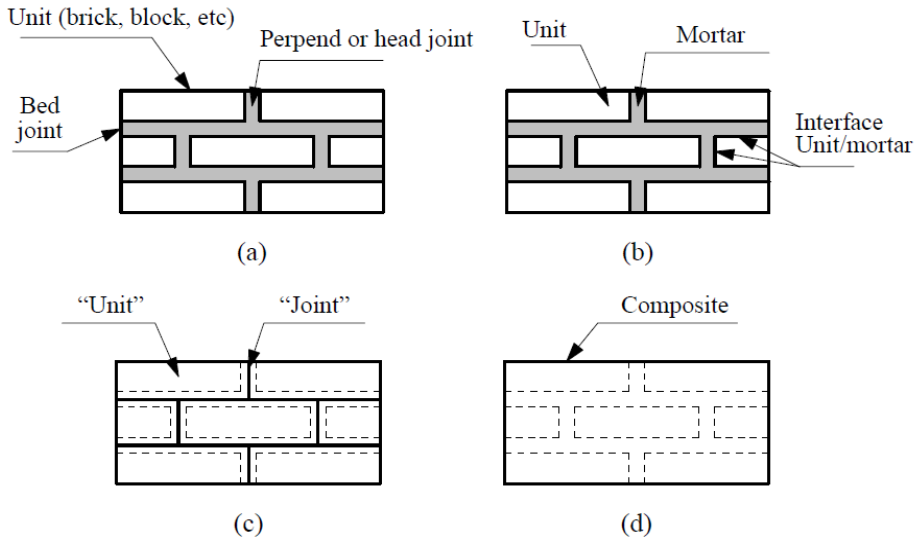

Figure 2.2 Modeling strategies for masonry structures: (a) masonry sample; (b) detailed micro-modeling; (c) simplified micro-modelling; (d) macro modelling.

In the micro-model, two different strategies are available depending on the way in which the masonry components are described.
The more accurate approach is the so-called detailed micro-model in which units and mortar joints are described through continuum finite element, whereas the unit-mortar interface is modelled by discontinuous elements able to take into account potential crack or slip planes (Fig. 2.2). In this approach, Young's modulus, Poisson's ratio and inelastic properties of both unit and mortar are taken into account. The interface represents a potential crack/slip plane with initial dummy stiffness to avoid interpenetration of the continuum.
The capability of this strategy in taking into account elastic and inelastic properties of both unit and mortar, it makes sure that this approach is particularly suitable for describing the local response of the material. Nevertheless, although the detailed micro model leads very realistic results, it requires a high computer effort. In order to overcome this problem, the simplified micro model is adopted in which continuum elements are used to model both units and mortar material, while the behaviour of the mortar

joints and unit mortar interfaces is described by discontinuous elements (Lofti and Shing, 1994; Tzamtzis A.D., 1994; Lourenco and Rots, 1997; Gambarotta and Lagomarsino, 1997; Sutcliffe et al., 2001).
In this way, it is possible to describe masonry as a set of elastic blocks bonded by potential fracture lines corresponding to the joints but, due to the fact that in this case the Poisson's effect of the mortar is not included, the accuracy is lost.
However, although micro modelling allows describing in a very accurate way the mechanical response of masonry structures and giving a better understanding about their local behaviour, some features of this approach make it suitable only for small individual members (Fig. 2.3), as structural details, with particular attention to strongly different states of stress and strain.

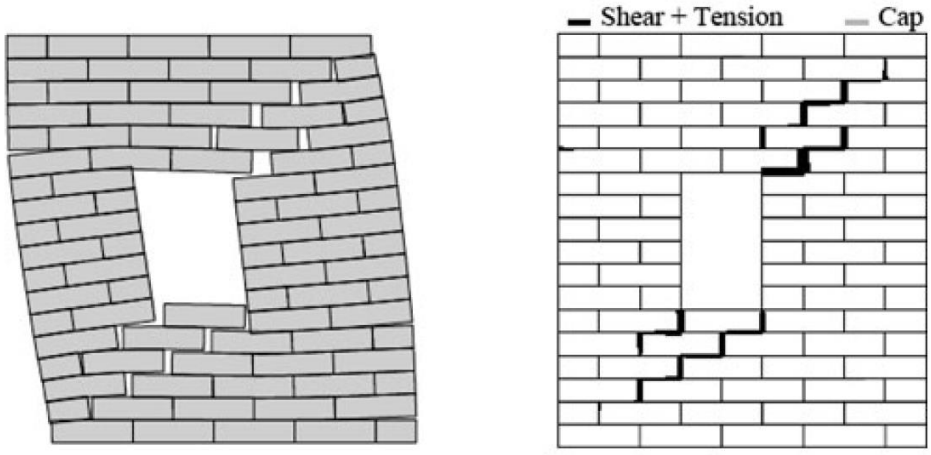

Figure 2.3 Micro-modelling of masonry shear walls: Deformed mesh (left) and damage (right) at a lateral displacement of 2.0 mm (Lourenco, 1996).

These aspects could be found in the high level of refinement required joined to the increase of the computational effort and to the request of complex material properties, which can only be obtained through costly and sophisticated laboratory tests.
This is the reason why, due to its lesser calculation costs, the macro-modelling is probably the most common approach used in this field.
This approach does not make any distinction between units and joints since its use is oriented to analyses on large structural portions or full buildings for which an accurate description of the interaction between units and mortar may not be necessary. For this reason, this kind of approach is

largely used to analyse also the seismic response of complex masonry structures and historical buildings (Pela et al., 2009; Mallardo et al, 2008; Roca et al., 2004; Murcia-Delso et al., 2009).
In the macro modelling, the masonry is modelled as a fictitious homogeneous orthotropic continuum for which a particular relation between average masonry strains and average masonry stresses is stabilized. In particular, this kind of approach should take into account different tensile and compressive strengths and different inelastic properties along the material axes.

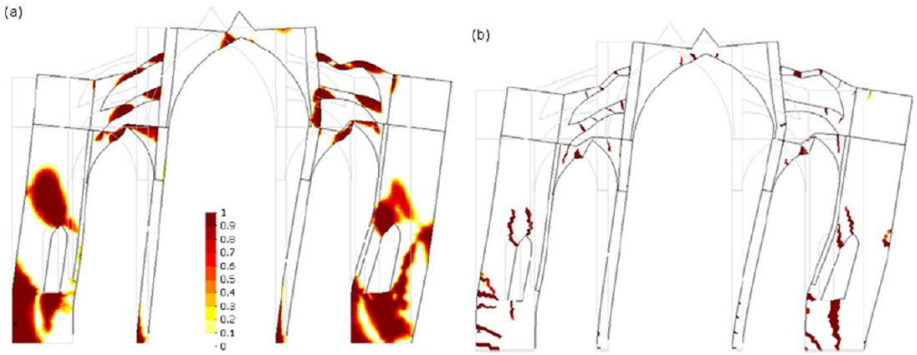

Figure 2.4 Tensile damage at the end of seismic analysis of Mallorca Cathedral: (a) smeared damage approach; (b) localized damage approach (Clemente et al., 2006).

Depending on the experimental tests available, the macro-modelling continuum parameters could derive from a numerical homogenization of the data obtained experimentally or, if it is possible, directly from tests on specimens of large size subjected to homogeneous states of stress.
The main advantage of the macro modelling technique lies in the simpler Finite Element mesh because it is not needed to make a detailed description of the internal masonry structure, and the finite elements can have dimensions bigger than the single brick units. This allows that the computational effort decreases with respect to the micro model case.
In the macro model, the isotropic criteria are usually used due to their mathematical simplicity and the low number of material parameters required, but also several orthotropic models (Papa E.A., 1996; Berto et al., 2002, Ghiassi et al., 2012) and a few anisotropic model (de Felice et al., 2009) have been proposed.
Nevertheless, the macro model strategy does not allow to describe masonry structure damage usually localized in isolate large cracks, since in the

macro approach the damage is smeared over a large volume of the structure (Fig. 2.4). Due to this, a spread modelling of damage could provide an unrealistic description of damage and may result in predictions either inexact or hard to associate to real measurements.
However, it is worth noting that in the case of the study of real buildings, for which all the material parameters required to obtain a more accurate masonry response are not normally available, the macro model approach is recommended. In particular, this kind of approach is applicable when the structure is composed of solid walls with sufficiently large dimensions so that the stresses across or along a macro-length will be essentially uniform. Furthermore, macro modelling is more practice oriented due to the reduced time and memory requirements as well as a user-friendly mesh generation. Therefore, this type of modelling is most valuable when a compromise between accuracy and efficiency is needed.

2.2. Jointed Masonry Model

The Jointed Masonry Model is an anisotropic elastic perfectly plastic constitutive model (Amorosi et al., In prep.). This model is a multilaminate model with isotropic elastic part. It is developed to describe the behaviour of masonry walls, as it allows to take into account the directional properties of the medium by the definition of the orientation of a maximum three different sliding planes.

2.2.1. Constitutive model formulation

The formulation of plasticity is similar on all the planes. On each of them a local Mohr-Coulomb yield condition applies to limit the shear stress |t|. Moreover, a tension cut-off criterion is adopted to limit the tensile stress on a plane. For the plane *i* the yield functions are defined as:

$$f_i^C = |\tau_{si}| + \sigma_{ni} \tan \varphi_i - c_i \qquad 2.1$$

$$f_i^t = \sigma_{ni} - \sigma_{t,i} \quad with \ \sigma_{t,i} \leq c_i \cot \varphi_i \qquad 2.2$$

where τ_s, σ_n are the local normal and shear stresses, while c_i, φ_i, $\sigma_{t,i}$ the cohesion, the friction angle and the tensile strength.
As such one of the key ingredients of the mechanical behaviour of masonry, i.e. its anisotropy at yielding, can be accounted for. As a matter of fact, the original Jointed Rock model already accounts for some features that characterise both jointed rocks and block structures, as discussed in Amorosi et al. (2015, 2016). Nonetheless, some specific and essential aspects of masonry behaviour were missing: this has triggered this research activity aimed at improve the original formulation adapting it to structural applications. More specifically, the original Jointed Rock model was modified to more realistically account for some specific features of the nonlinear mechanics of masonry stemming from the interlocking of the bricks. In fact, this latter feature can play a relevant role in the development of damage within a masonry structure, such as that occurring when vertical and shear cracks develop, leading to overturning and/or horizontal sliding of the system. This is because in the vertical direction of an ideal wall the bricks are arranged in a staggered way, resulting in an increased tensile and shear strength of the overall masonry along the corresponding head joint's direction.

The modifications introduced to the original Jointed Rock model can be easily discussed with reference to two families of joints reported in Fig.2.5: one related to the head joints and represented by the plane 1 and one related to the bed joints and represented by the plane 2.

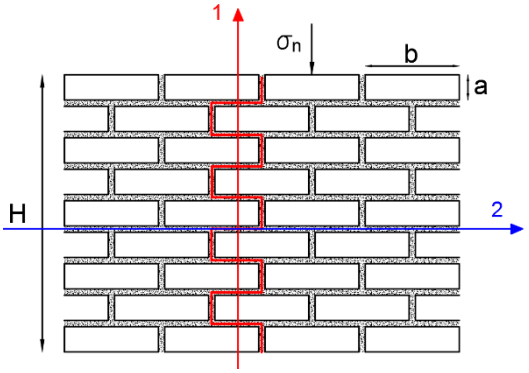

Figure 2.5 Definition of Plane 1 and plane 2 in the Jointed Masonry Model.

The modification consists in taking into account for Plane 1 the enhanced tensile strength available due to the contribution of the bed joints, which are subjected to a vertical stress state which increases with depth. This feature is responsible for the classical tendency, observed in many masonry structures, to exhibit tensile cracks that propagate downward from the top portion of the walls. This contribution depends on the dimensional ratio of the blocks that, in this new model, is accounted for through the parameter named *Strength Factor beta*. Related to the above enhanced tensile strength, a corresponding increment of the available shear strength is introduced in the model, such that the ratio between these two contributions keeps constant. In this way the overall strength along Plane 1 increases as a function of depth, both in terms of tensile and shear components.
Under plastic regime, the values of cohesion and tensile strength along Plane 1 are no longer constant, as they were in the original formulation, but end up depending on the stress according to:

$$c_1 = c_1 + SF_{beta} \cdot \sigma_{1,2} + c_2 \cdot \frac{SF_{beta}}{\tan \varphi_2} \qquad 2.3$$

$$\sigma_{t,1} = \sigma_{t,1} + SF_{beta} \cdot \sigma_{1,2} + c_2 \cdot \frac{SF_{beta}}{\tan \varphi_2} \qquad 2.4$$

where:

$$SF_{beta} = \tan \varphi_2 \cdot \frac{b}{2a} \qquad 2.5$$

In both expressions the first term represents the standard cohesive/tensile contribution along the head joints direction (Plane 1) while the second and third terms correspond to the frictional and cohesive contributions to the shear strength available along Plane 1 of the of the bed joints, respectively. In other terms, the second and third terms accounts for the interlocking effects.
It is worth noting that, although the model is formulated in a continuum context, the geometrical character of the single block composing the masonry is retained and entered via the SF_{beta} parameter. Furthermore, the failure mechanism can be continuously distributed through each element portion, along all the endless planes that are parallel to the one characterized by the orientation selected and not only along the contact plane between two blocks.
All the above holds along Plane 1 of Fig. 2.5, while no modification are introduced for the strength along Plane 2, as, for obvious geometrical reasons, not interested by the interlocking effects. Remarkably, this latter plane results as the weakest one, consistently with experimental observations.

2.2.2. Parameters of the Jointed Masonry Model

All the parameters of the Jointed Masonry Model coincide with those of the Original Jointed Rock Model, except for the new parameter SFbeta discussed above. The model parameters are the following:

Overall elastic isotropic parameters for the masonry:

G	: Shear modulus	[kN/m^2]
ν	: Poisson's ratio	[-]

Strength parameters of the Mohr-Coulomb model for the continuum (block's) part of the masonry:

c_{mc}	: Cohesion	[kN/m^2]
φ_{mc}	: Friction angle	[°]
ψ_{mc}	: Dilatancy angle	[°]
σ_{mc}	: Tensile strength	[kN/m^2]

Strength parameters for the joints/planes oriented along direction 1:

SF_{beta}	: Strength factor	[-]

c_1	: Cohesion	[kN/m^2]
φ_1	: Friction angle	[°]
ψ_1	: Dilatancy angle	[°]
σ_1	: Tensile strength	[kN/m^2]

Strength parameters for the joints/planes oriented along direction 2:

c_2	: Cohesion	[kN/m^2]
φ_2	: Friction angle	[°]
ψ_2	: Dilatancy angle	[°]
σ_2	: Tensile strength	[kN/m^2]

The orientation of the sliding planes in the proposed model is defined as in the original Jointed Rock model.

2.2.3. Calibration procedure

The isotropic elastic parameters used in the Jointed Masonry Model are referred to the overall masonry response. As a consequence, when the elastic properties of blocks (E_b, υ_b) and joints (E_m, υ_m) and the dimensions of the blocks (a, b) are provided, a homogenization procedure can be adopted to derive them (de Felice et al., 2009). In detail:

$$\frac{1}{G} = \frac{1}{a\,K_t} + \frac{4a}{b^2\,K_n + 4ab\,K_t} + \frac{1}{\mu_b} \qquad 2.6$$

$$\frac{\nu_{12}}{E_1} = \frac{\nu_{21}}{E_2} = \frac{\lambda_b}{2(3\mu_b\lambda_b + 2\mu_b^2)} \qquad 2.7$$

$$\frac{1}{E_1} = \frac{4a}{4ab\,K_n + b^2 K_t} + \frac{1}{4\,\mu_b} + \frac{\lambda_b + 2\mu_b}{4(3\mu_b\lambda_b + 2\mu_b^2)} \qquad 2.8$$

$$\frac{1}{E_2} = \frac{1}{a\,K_n} + \frac{1}{4\,\mu_b} + \frac{\lambda_b + 2\mu_b}{4(3\mu_b\lambda_b + 2\mu_b^2)} \qquad 2.9$$

where:

$$\mu_b = \frac{E_b}{2(1+\nu_b)}; \quad \lambda_b = \frac{\nu_b E_b}{(1-2\nu_b)(1+\nu_b)};$$

$$K_n = \frac{E_b E_m}{t_m(E_b - E_m)}; \quad K_t = \mu_b \cdot \mu_m \cdot \frac{1}{t_m} \cdot \frac{1}{\mu_b - \mu_m}$$

being t_m the mortar joints thickness. The parameters adopted for the analyses are the shear modulus G comes from eq. 2.6 and the Poisson's ratio n is the average value of those obtained by eq. 2.7.
It is worth noting that in the homogenization procedure the direction 1 corresponds to the horizontal bed joints and the direction 2 corresponds to the vertical head joints. Instead, in the Jointed Masonry Model the direction 1 is related to the vertical head joints, along which an enhanced tensile strength contribution is expected, and the direction 2 corresponds to the mortar bed joints.

3. STRUCTURAL MODEL VALIDATION

3.1. Traction test

The first comparison test consists in bringing up to failure a masonry panel subjected to self-weight, vertical pressure applied on top and a prescribed horizontal displacement imposed at the lateral sides. The panel has a dimension of 1.50 x 0.98m^2, and is constituted by 14 courses of bricks Boundary conditions are represented in Figure 3.1.

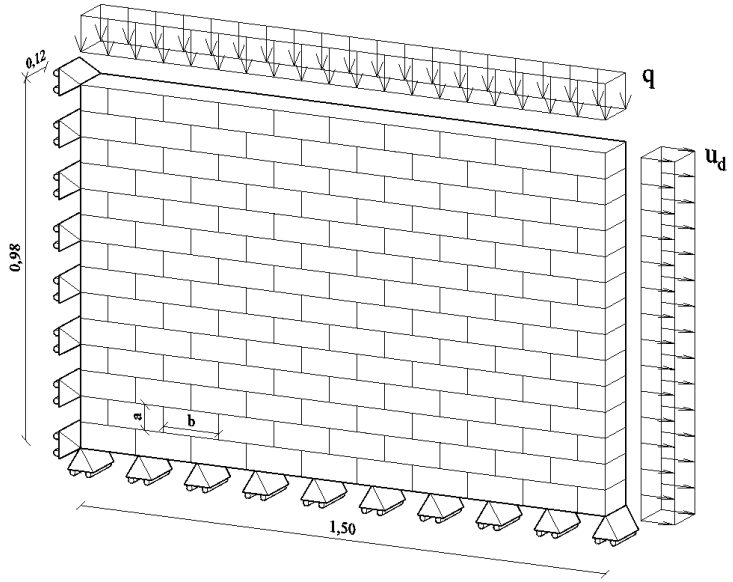

Figure 3.1Geometrical characteristics of the wall.

The analysis is carried out first applying the self-weight and the vertical pressure q = 10 kPa, followed by a stage characterised by a uniformly increasing horizontal component of the displacement u_d. The performance of the model is validated comparing its predictions to the results obtained by a corresponding numerical analysis carried out adopting a more advanced and well validated constitutive model, originally formulated by de Buhan and de Felice (1997) and then extended in de Felice et al. (2009), in which the masonry is represented as a continuous homogeneous anisotropic medium with an elastic-perfect plastic behaviour whose

constitutive relation depends on the mechanical and geometrical properties of block and joints.
The values of the mechanical parameters used in the numerical analysis are summarised in Table1. High values of cohesion and tensile strength are assigned to the blocks in order to induce the development of failure conditions along the sliding planes. These latter are characterised by the mechanical parameters provided in de Felice et al. (2009). The tensile strength on the sliding planes is assumed to be equal to its limit, in according to the tension cut off yield function.

Material properties	
γ (kN/m^3)	15
G (kPa)	477093
ν (-)	0.12
c_{mc} (kPa)	10E5
φ_{mc} (°)	31
ψ_{mc} (°)	31
σ_{mc} (kPa)	10E5
SF_beta (-)	0.687
$c_{planes\ 1\text{-}2}$ (kPa)	5
$\varphi_{planes\ 1\text{-}2}$ (°)	31
$\psi_{planes\ 1\text{-}2}$ (°)	31
$\sigma_{planes\ 1\text{-}2}$ (kPa)	8.32

Table 3.1 Parameters of the Jointed Masonry Model for traction tests

As reported in de Felice et al. (2009) the problem admits an analytical solution for the ultimate horizontal resultant tensile force T_{lim}.

$$T_{lim} = H\left[\frac{c}{\tan\varphi} + \frac{c}{\mu} + \frac{\gamma H}{2\mu}\tan\varphi + \frac{q}{\mu}\tan\varphi\right] \qquad 3.1$$

For the test values, a traction T_{lim}=25.42 kN/m is obtained. The value of the resulting traction obtained by the numerical analysis performed with the Jointed Masonry Model is equal to 25.3 kN/m; this is rather similar to that obtained by the more advanced constitutive model proposed by de Felice et al. (2009). Both solutions are thus consistent with the analytical one, as shown in Fig.3.2, where the results for the continuum models are represented in terms of the lateral traction versus edge horizontal displacement.

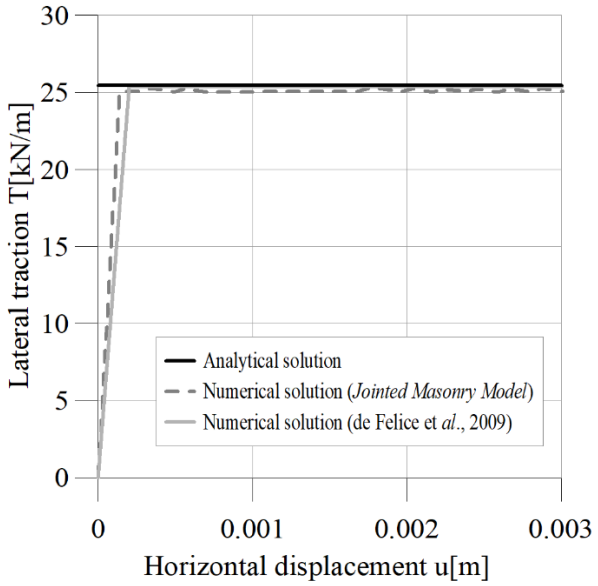

Figure 3.2 Lateral traction versus upper edge horizontal displacement.

3.2. Body force tests

A block masonry wall subjected to its weight and a horizontal force proportional to the weight, is here considered. The wall, constrained at its base, is analysed for six different values of the aspect ratio r, defined as H/L (Fig. 3.3). Two masonry textures A and B are considered, which correspond to SF_{beta} values respectively equal to 1.370 and 0.686. Even in this case, the results of the analyses are compared to those obtained by the advanced constitutive model de Felice et al. (2009).

The mechanical characteristics of the masonry are the same as those of the previous example, with the only exception of the cohesion, assumed null in this case. The two textures provide different values of G, n and SF_{beta}.

The results are shown with reference to the proportionality factor λ, defined as the ratio between the horizontal and the vertical components of the body forces. Figures 3.4 and 3.5 shows the comparison between the numerical analyses, performed with both the advanced constitutive model and the Jointed Masonry Model, and the analytical upper bound predictions of the λ value at failure for several aspect ratio and different texture.

ρ	0.5	1	1.5	2	2.5	3
$L \times H$	5.66×2.83	4×4	3.27×4.90	2.83×5.66	2.53×6.32	2.31×6.93

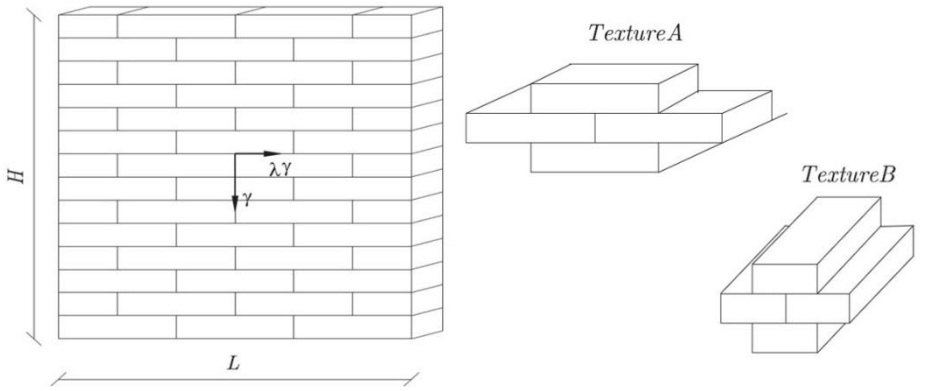

Figure 3.3 Geometric characteristics of blocks and masonry wall for tilting tests.

Material properties	Texture A	Texture B
γ (kN/m^3)	15	15
G (kPa)	511490	477093
ν (-)	0.14	0,12
c_{mc} (kPa)	10E5	10E5
φ_{mc} (°)	31	31
ψ_{mc} (°)	31	31
σ_{mc} (kPa)	10E5	10E5
SF_{beta} (-)	1.37	0,687
$c_{planes\ 1\text{-}2}$ (kPa)	0	0
$\varphi_{planes\ 1\text{-}2}$ (°)	31	31
$\psi_{planes\ 1\text{-}2}$ (°)	31	31
$\sigma_{planes\ 1\text{-}2}$ (kPa)	8.32	8.32

Table 3.2 Parameters of the Jointed Masonry Model for tilting tests.

The λ values, summarised in Table 3, indicate a maximum error lower than 3%. As shown in Fig.3.6, the Jointed Masonry Model correctly predicts also the plastic strain distribution as indirectly detected in both experimental tests (Fig. 3.6) and numerical analyses (Fig. 3.7-3.9) carried out for the same set of parameters (φ=31°, Texture B) and considering two different aspect ratios (ρ = 0.5, 1).

ρ		0.5	1	1.5	2	2.5	3
Texture A	Advanced model	0.477	0.461	0.422	0.367	0.312	0.270
	Modified JRM	0.485	0.470	0.420	0.359	0.310	0.266
	Deviation	-2%	-2%	0%	2%	1%	1%
Texture B	Advanced model	0.410	0.410	0.391	0.348	0.301	0.262
	Modified JRM	0.420	0.421	0.390	0.343	0.296	0.257
	Deviation	-2%	-3%	0%	1%	2%	2%

Table 3 λ values obtained by numerical analyses.

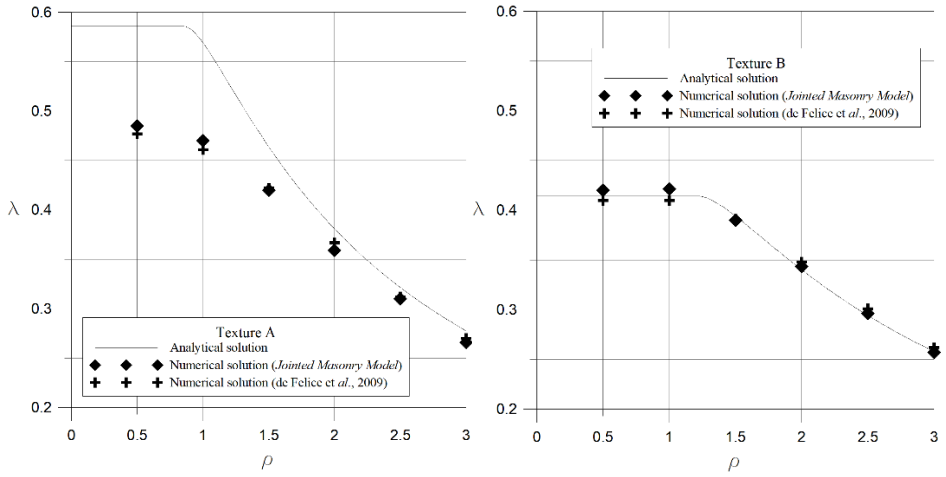

Figure 3.4 Texture A- B: λ values at failure for different aspect ratio.

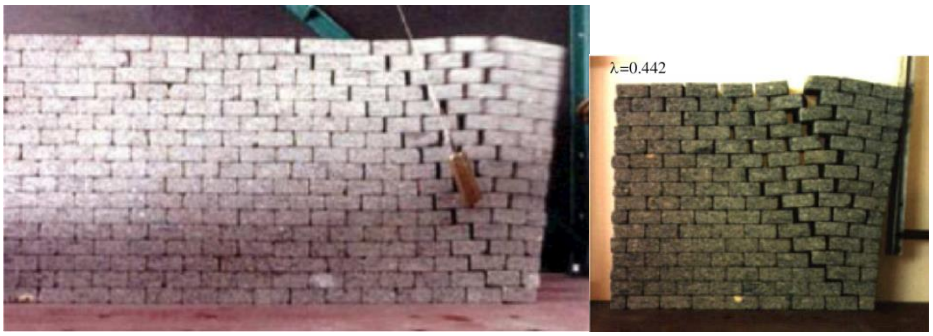

Figure 3.5 Experimental analysis for r=0.5 (left) and r=1 (right), texture B.

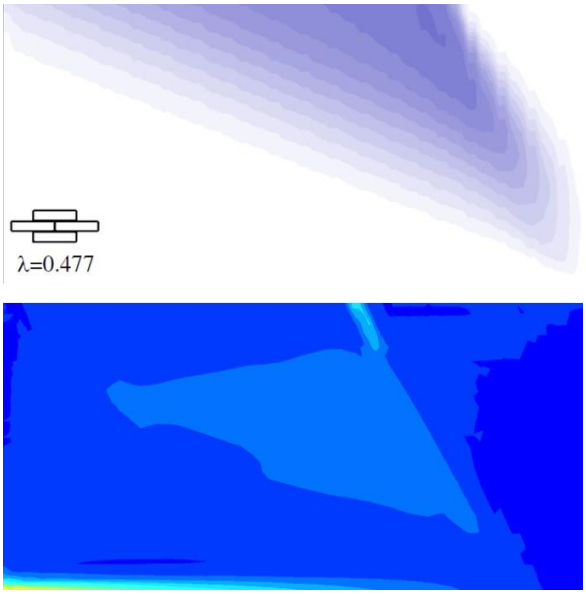

Figure 3.6 Plastic strain distribution of the simulation performed with an advanced constitutive model (de Felice et al., 2009) (up) and Jointed Masonry Model (down) for ρ=0.5 and texture A.

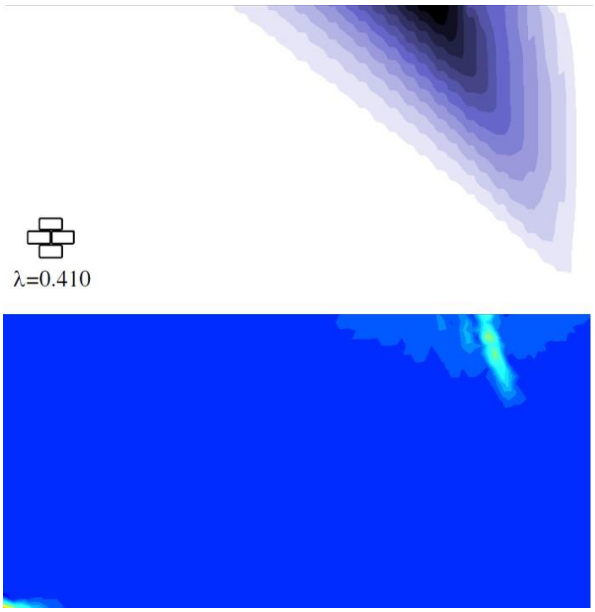

Figure 3.7 Plastic strain distribution of the simulation performed with an advanced constitutive model (de Felice et al., 2009) (up) and Jointed Masonry Model (down) for ρ=0.5 and texture B.

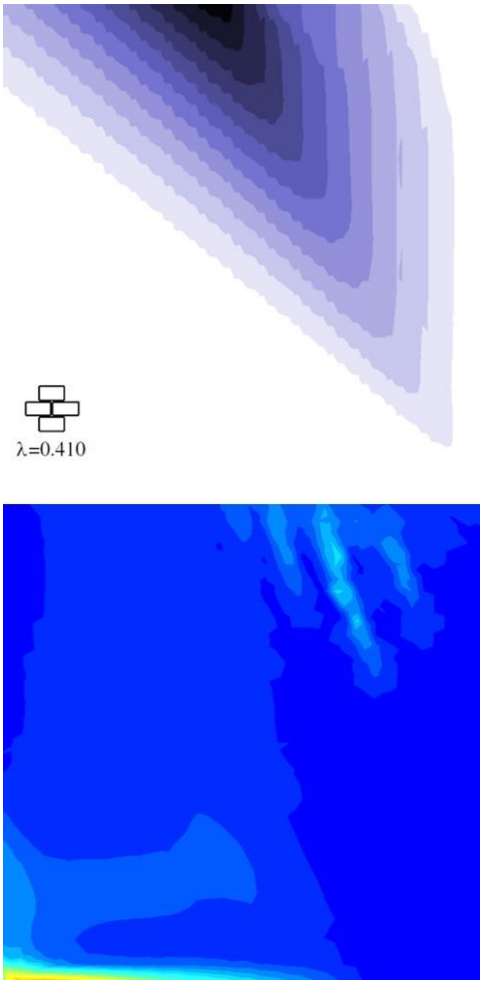

Figure 3.8 Plastic strain distribution of the simulation performed with an advanced constitutive model (de Felice et al., 2009) (up) and Jointed Masonry Model (down) for ρ=1and texture B.

As already discussed in de Felice et al. (2009), the λ value decreases with increasing values of r for both the textures (Fig. 3.4). For decreasing values of ρ the value of λ at failure tends toward a constant value: this can be related to the observed concentration of the plastic strain in a limited portion of the wall for decreasing values of the slenderness ρ (Fig. 3.9), such that the actual width of the wall does no longer influence the failure mechanism and the corresponding λ value. This latter feature does not hold for larger values of ρ, for which the entire width of the wall is involved in

the plastic strain localization mechanism as shown in Fig. 3.10. The role of the masonry texture parameter SF_{beta} can be assessed by comparing the plastic strain localization pattern shown in Figures 3.10: the larger the value of SF_{beta} (e.g. texture B as compared with Texture A of the same figure), the more enhanced the plastic strain localization, i.e. failure is concentrated in a narrower zone. The analytical and numerical solutions match satisfactorily in the case of texture parameter SF_{beta}=0.687, while tend to diverge for low values of r in SF_{beta}=1.370 case (Figure 3.4).

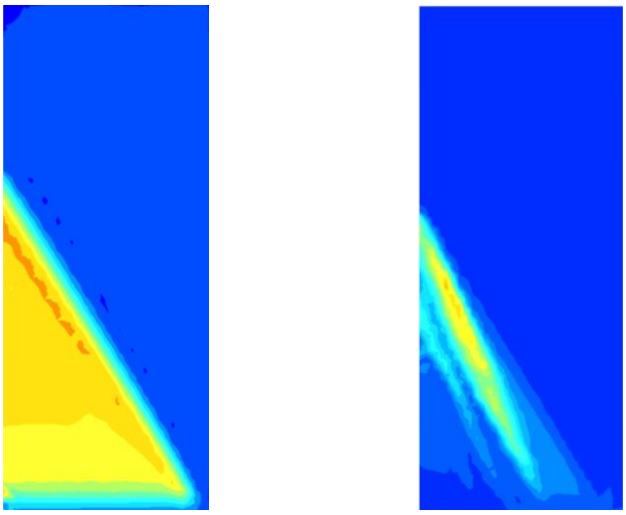

Figure 3.9 Plastic strain distribution of the simulations performed with Jointed Masonry Model for texture A (left) and texture B (right), ρ=2.5.

This should be related to the different assumptions on which the solutions relay: the analytical solution was obtained assuming a rigid block failure mechanism, characterized by a rotation around a point at the base of the wall and the related development of a discontinuity plane, while the FE solution is based on a continuum approach characterized by the development of either diffuse or more concentrated plastic strain localization zone. The more concentrated the localized zone, the closer the numerical solution is to the analytical one: this justifies the accordance of the results for relatively large values of r for both values of SF_{beta}, the better match observed for the SF_{beta}=0.687 case, characterized by a more concentrated localization pattern due to the texture characteristics.

3.3. Diagonal compression tests

The predictive capability of the proposed modified model was also investigated by a comparison with *in situ* diagonal compression tests conducted on a masonry wall of irregular blocks. Since the cohesion value was not provided for some tests, its value was determined through Calderini Lagomarsino model (2009). The tests results show that the obtained average cohesion value has to be further reduced to match the shear strength coming from the experimental test.

3.3.1. Panel PD13OR

The specimen tested has dimensions equal to 122x122x48 cm^3. The bricks size was obtained as an average dimension of blocks, such that the ratio height *b* versus base *a* of the blocks is equal to 3. During the numerical test, carried out under displacement control, the specimen was first subjected to its weight, and then a displacement orthogonal to the upper steel shoe and equal to 20.00mm was applied in ten steps. The diagonal load was transferred to the specimen through two steel elements placed on the two diagonally opposite corners of the panel and modelled here as made by an elastic material. In the experiments, the strain was calculated based on the measurements carried out with reference to four points placed along the two diagonals, whose coordinates are shown in Table 4. The numerical analyses are performed using 27364 tetrahedral 10-node elements, with an average size equal to 60mm, for a total number of nodes equal to 40333.

Point	Node	x (m)	z (m)
1	38075	0.22	0.24
2	2874	0.94	0.96
3	20336	0.94	0.26
4	25415	0.23	0.96

Table 3.4 Coordinates of the control points

The material properties used in the numerical analysis are shown in Tab.5. Except for the weight, obtained by the Tab. C8A.2.1 of the Italian code NTC as not available in the reference paper, all the other parameters are the same as those determined by the authors and used by them to carry out their

numerical analyses. The only discrepancy refers to the shear modulus G, which in the analyses was assumed as half of that declared by the Authors.

Material properties	
γ (kN/m^3)	19
G (kPa)	20000
ν (-)	0.25
c_{mc} (kPa)	10E6
φ_{mc} (°)	32
φ_{mc} (°)	32
σ_{mc} (kPa)	10E6
SF_beta (-)	0.94
$c_{planes\ 1\text{-}2}$ (kPa)	55
$\varphi_{planes\ 1\text{-}2}$ (°)	32
$\psi_{planes\ 1\text{-}2}$ (°)	32
$\sigma_{planes\ 1\text{-}2}$ (kPa)	60

Table 3.5 Parameters of the Jointed Masonry Model for diagonal compression test, Panel PD13OR.

The τ-γ curve illustrated in Fig. 3.11 indicates a satisfactory match of the experimental results obtained by our model. The maximum tangential strength attained in the experiments 0.059 MPa, was obtained by the numerical analysis with reference to the strain value equal to 5x10e+3. Both load and strain were calculated as the average value among four points located in the same position of those used to carry out the experimental results.

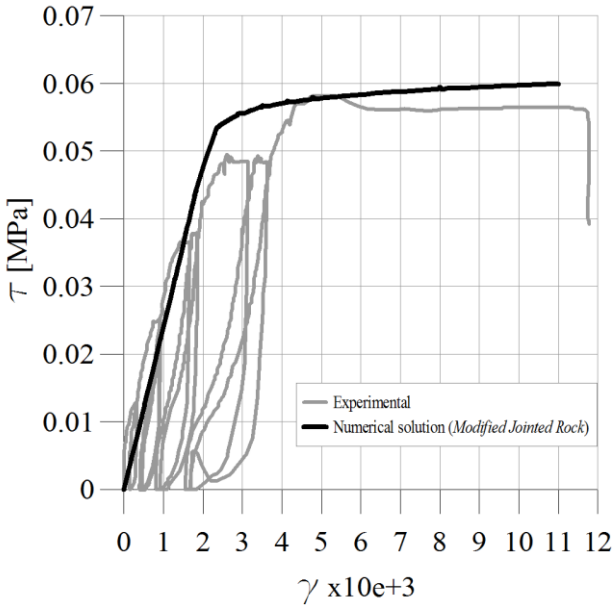

Figure 3.10 τ-γ curve.

Fig.3.12 shows how the total cartesian strains distribution, carried out with the Modified Model, is in good agreement with the damage obtained by Borri et al. (2004). The crack delivers in the direction of the supports until a full diagonal crack is obtained.

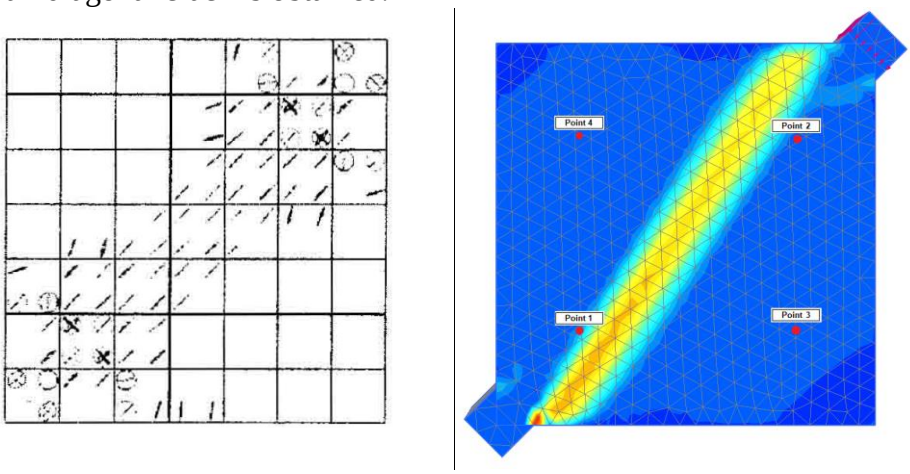

Figure 3.11 Crack pattern distribution obtained by Borri et al. (left) and total cartesian strain performed with Jointed Masonry Model (right).

3.3.2. Panel 7-P1

In this paragraph, a description of a tuff stone masonry panel tested during the experimental campaign in Tuscany Region (Italy), is presented. In particular, a ratio of mortar tensile strength to joint cohesion equal to 1 is assumed, since the vertical joints are very regular and made up with good mortar; for both panels the same material properties in compression and the same interlocking parameter are used, according with the masonry typology. The different behaviour of the two panels is related to a different quality of the mortar or to a different thickness of joints; these aspects influence the elastic and inelastic deformability, as well as the mortar joint strength. These features were surveyed qualitatively during the *in-situ* test.

Material properties	
γ (kN/m^3)	15
G (kPa)	470000
ν (-)	0.20
c_{mc} (kPa)	10E5
φ_{mc} (°)	21
ψ_{mc} (°)	21
σ_{mc} (kPa)	10E5
SF_beta (-)	2
$c_{planes\ 1\text{-}2}$ (kPa)	139
$\varphi_{planes\ 1\text{-}2}$ (°)	21
$\psi_{planes\ 1\text{-}2}$ (°)	21
$\sigma_{planes\ 1\text{-}2}$ (kPa)	60

Table 3.6 Parameters of the Jointed Masonry Model for diagonal compression test, Panel 7-P1.

The comparison between numerical and experimental results is made with the sxy-curve. In particular, two curves were extracted from each numerical analysis, evaluating the strain from the displacements of the panel corners or from internal points, located where the LVDT were fixed (the influence of the base of measure on the evaluation of the shear strain appears to be

negligible). For both panels, the numerical curves approximate very well the experimental results.

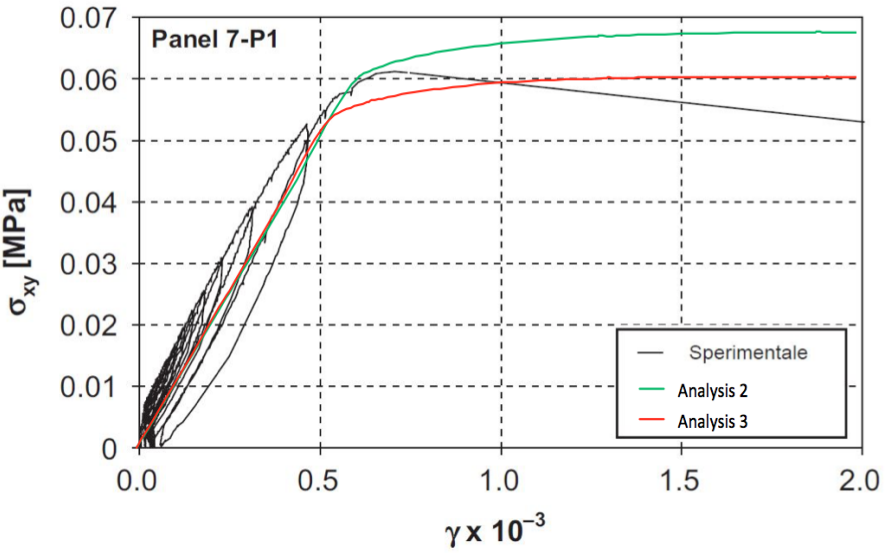

Figure 3.12 $\tau - \gamma$ Curve for Panel 7-P1

3.3.3. Panel 13-P1

The panel determined by the symbol 13 - P1 is also part of the campaign experimental conducted by Anna Brignola et al. in the Tuscany region. The masonry was tested in the municipality of Filattiera in the province of Massa-Carrara, and consists of blocks of irregularly double-faced stone, characterized by brick walls. The masonry thickness was 54 cm.
For the analysis, the parameters are determined using the model Calderini Lagomarsino (2009). The parameters are shown in the following table.

Material properties	
γ (kN/m^3)	15
G (kPa)	150000
ν (-)	0.20
c_{mc} (kPa)	10E5
φ_{mc} (°)	21.8
ψ_{mc} (°)	21.8
σ_{mc} (kPa)	10E5
SF_beta (-)	2
$c_{planes\ 1\text{-}2}$ (kPa)	120-93
$\varphi_{planes\ 1\text{-}2}$ (°)	21.8

$\psi_{planes\ 1\text{-}2}$ (°)	21.8
$\sigma_{planes\ 1\text{-}2}$ (kPa)	60

Table 3.7 Parameters of the Jointed Masonry Model for diagonal compression test, Panel 13-P1.

Two different analyses were made when the cohesion c varied. In the case of analysis 1, determined with a cohesion value equal to that determined by the Calderini Lagomarsino model, the shear strength is overestimated. To ensure a better estimate of the shear strength for the numerical model, cohesion has been reduced by 22.5%. A reduced stiffness of 50% is used to best estimates the linear trend of the experimental curve. The analyses and the parameters used are below:

1. Φ=21.8°; G=150 MPa; c=0.120 MPa
2. Φ=21.8°; G=150 MPa; c=0.093 MPa

Figure 3.15 shows the collapse configuration that is characterized by the creation of plastic points on the diagonal compression of the wall panel, where the shear strength of the material is exceeded. There are areas where a limited cracking is visible to overcome traction resistance.

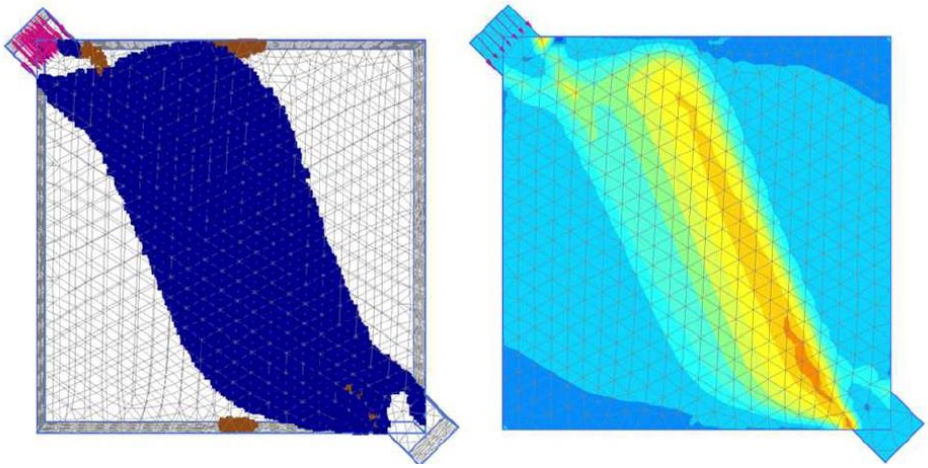

Figure 3.13 Plastic points (left) e Total strain distribution zx (right), analysis 1.

Figure 3.16 shows the τ curve obtained from the first analysis. Stiffness is reduced since experimentally during the first load steps the deformation of the masonry is very small and results in a very high initial stiffness.

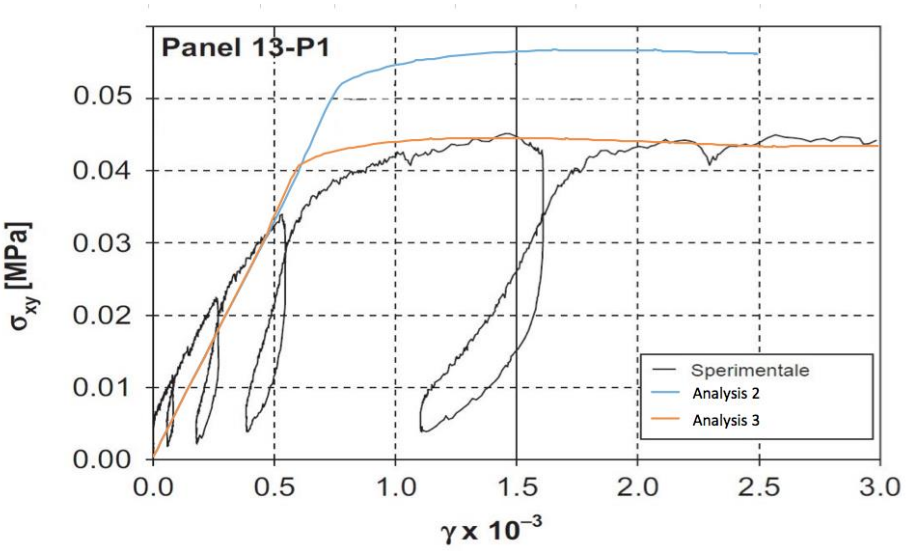

Figure 3.14 τ – γ Curve for Panel 13-P1

The estimate of the maximum tangential strength on the panel varies, depending on the interface cohesion. The variation of the tangential strength τmax takes very little values in the case of reduced cohesion (analysis 2), assuming a value of 31.83% if the analysis is carried out leaving unaltered the cohesion of the masonry interface.

3.3.4. Panel BD-02-OR

The BD 20 OR panel is a panel tested in a building built in the early 20th century to host the school in the locality of Belfiore, (Foligno) in province of Perugia. It was tested in the experimental campaign by Corradi et al. The masonry panel is made up of bricks, tied by a lime mortar. The size of the bricks is 30x15x6.5 cm, so the wall thickness is 30 cm. Two different analyses were made changing the cohesion value. The analyses and the parameters used are shown below:

1. Φ=31°; G=131 MPa; c=0.103 MPa
2. Φ=31°; G=131 MPa; c=0.069 MPa

The diagonal test was carried out on panels 120=120 cm2 with a maximum cross-section thickness of 30 cm. The panel remained anchored to the rest of masonry wall through a part of the 30 cm of the lower horizontal edge. The remaining three edges and a part of the fourth were cut and isolated from the rest of the masonry wall. The test is constituted of a set of metallic

elements fixed at the two corners of a panel's diagonal. A jack, placed at one corner, is interposed between two metallic elements which allow it, on the one hand, to act directly on a corner of the panel, while at the same time resulting in a rigid connection to an analogous metal element located at the opposite corner (Corradi et al., 2003).

Material properties	
γ (kN/m^3)	15
G (kPa)	131000
ν (-)	0.25
c_{mc} (kPa)	10E5
φ_{mc} (°)	31
ψ_{mc} (°)	31
σ_{mc} (kPa)	10E5
SF_beta (-)	0.65
$c_{planes\ 1\text{-}2}$ (kPa)	103-69
$\varphi_{planes\ 1\text{-}2}$ (°)	31
$\psi_{planes\ 1\text{-}2}$ (°)	31
$\sigma_{planes\ 1\text{-}2}$ (kPa)	103

Table 3.8 Parameters of the Jointed Masonry Model for diagonal compression test, Panel BD02OR.

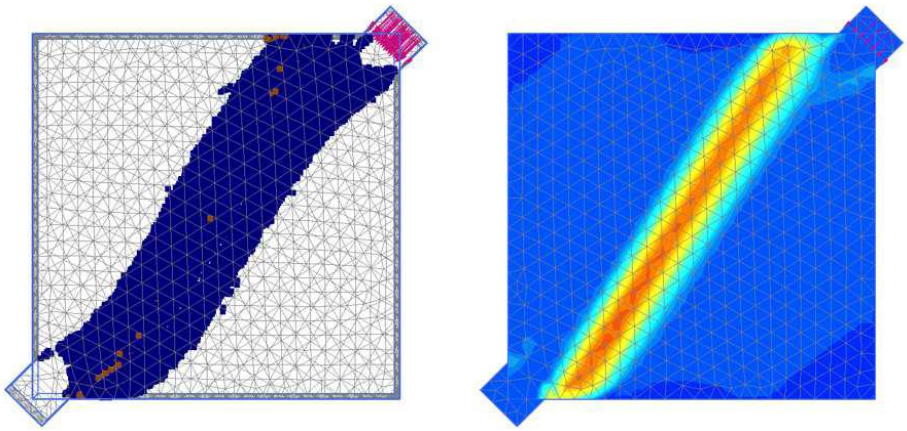

Figure 3.15 Plastic points e flat deformation zx

The figure 3.17 shows the collapse of the panel relative to the last load step of the analysis 2. It shows that the fracture occurs along the compressed diagonal, and is mostly characterized by a break to overcome the shear strength. From the plot of deformations on the surface zx of the panel it is clear how the displacements are in the diagonal area of the panel where negative traction deformations are concentrated.

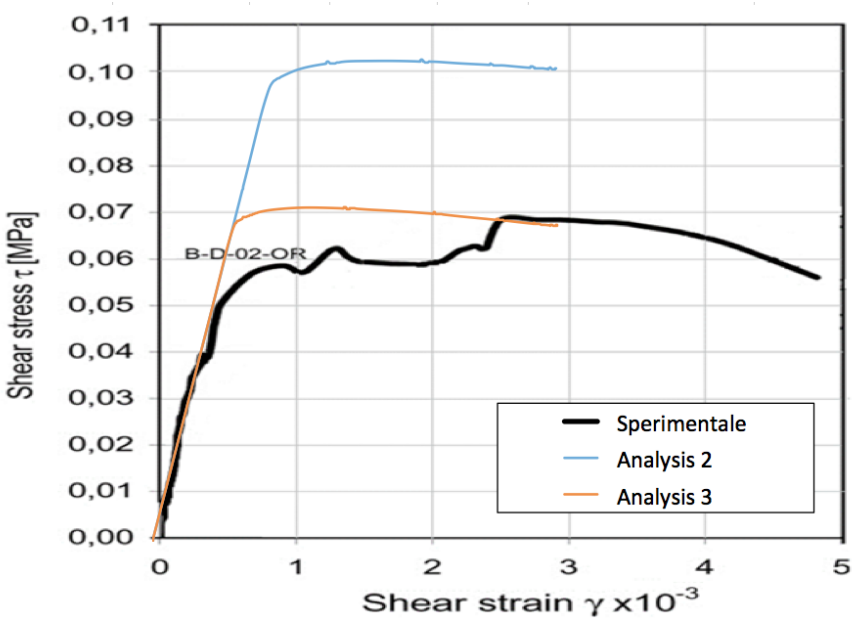

Figure 3.16 Curva T-g for Panel BD-02-OR

The graph τ in Figure 3.18 reports the results of both the analyses. Analysis 1, with the cohesion determined through the Calderini Lagomarsino model, proves to overestimate the tangential voltage τmax of a coefficient equal to 42%. Analysis 2 carried out with a 32.5% reduction in the value of cohesion proves to better approximate the tangential voltage τmax with a coefficient of variation of 1.5%.

3.4. TU Eindhoven shear walls

Two panels with and without opening tested at TU Eindhoven are here considered. The panels have dimensions of 0.99x1.00x0.10m^3, and are composed of wire-cut solid clay bricks with dimensions 210x52x100mm^3 (Raijmakers and Vermeltfoort, 1992). The tests were carried out by first applying the self-weight of the panels, followed by a vertical pressure equal to 300kPa, and then a uniform horizontal displacement distribution applied at the top of the wall (shear conditions), precluding any rotation of this upper surface. The numerical analyses are performed using 11375 tetrahedral 10-node elements, with an average size equal to 35mm, for a total number of nodes equal to 18927.
The material parameters adopted in the numerical analyses are provided in (Lourenco, 1996) and summarised in Tab. 9. Also in this case, the elastic parameter G stems from a homogenization procedure and its value is consistent with that used in Pelà et al. (2013).

Material properties	
γ (kN/m^3)	15
G (kPa)	1404494
ν (-)	0.06
c_{mc} (kPa)	10E5
φ_{mc} (°)	36.9
ψ_{mc} (°)	36.9
σ_{mc} (kPa)	10E5
SF_beta (-)	1.514
$c_{planes\ 1\text{-}2}$ (kPa)	350
$\varphi_{planes\ 1\text{-}2}$ (°)	36.9
$\psi_{planes\ 1\text{-}2}$ (°)	36.9
$\sigma_{planes\ 1\text{-}2}$ (kPa)	250

Table 3.9 Parameters of the Jointed Masonry Model for shear wall tests.

3.4.1. Shear walls without opening

A similar pattern of damage is obtained by our model as compared to the model advanced one by Lourenco, as illustrated in Fig. 3.17, which refer to a displacement of 2.00mm for the wall without opening. The experimental test is also well reproduced by the numerical analyses in terms of load-displacement curves (Fig. 3.18). The numerical results are compared with

those obtained numerically by a composite interface model for masonry formulated by Lourenco (1996). In his formulation, interface elements are used as potential crack, slip or crushing planes. The model includes a tension cut-off and a cap for compressive failure. All the inelastic phenomena occur at the interface elements, where the degradation of stiffness and strength is also accounted for by the Author. It is worth mentioning that the formulation of the Jointed Masonry Model proposed does not account for the decay of strength along the joints (as the plastic formulation does not include negative hardening or damage ingredients): as such, the model cannot reproduce the final decay of strength shown in the figure 3.18 by the experimental test. Nonetheless, the Jointed Masonry Model's formulation is capable of picking the maximum strength, which can be sufficient in many practical applications.

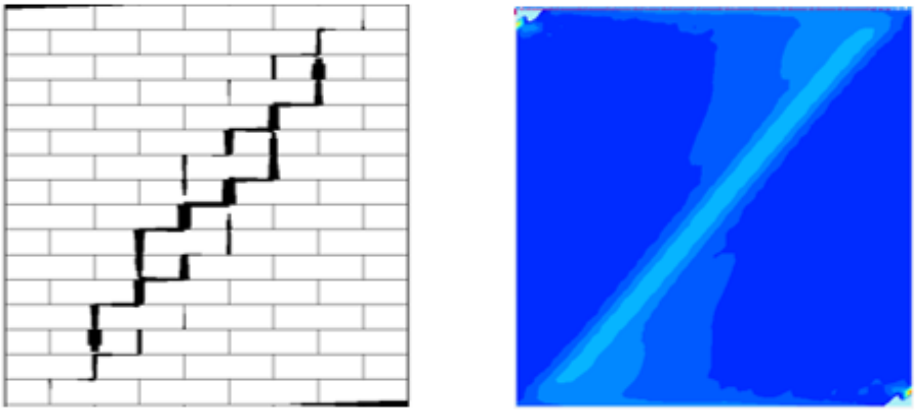

Figure 3.17 Damage at a displacement of 2.00mm: (left) composite interface model; (right) Total Cartesian Strain zx in the Jointed Masonry Model.

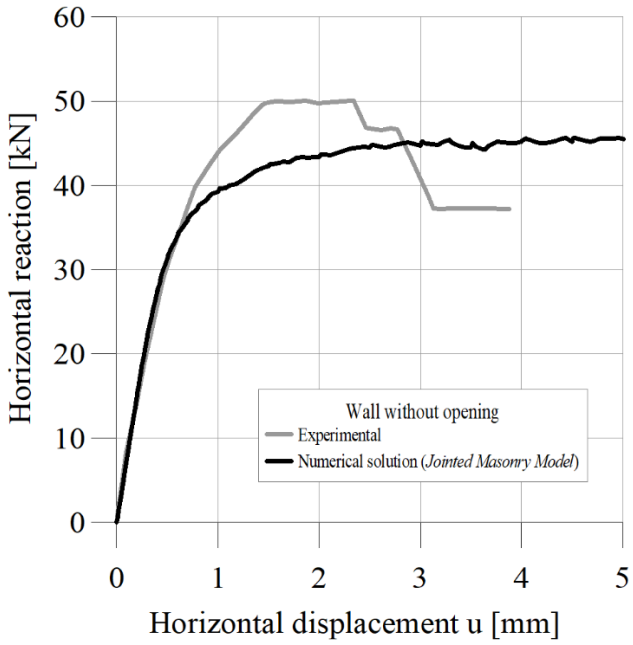

Figure 3.18 Comparison between experimental and numerical reaction vs. displacement diagram for the wall without opening.

3.4.2. Shear walls with opening

The analysis concerns the test carried out for a wall with a central opening subjected to the same initial vertical load of the previous case and to a horizontal displacement increased to 25.00mm. A similar pattern of damage is obtained also in this case by the Jointed Masonry Model as compared to the model advanced one by Lourenco, as illustrated in Fig. 3.19, which refer to a displacement of 25.00mm. The tensile damage stems from the two opposite corners of the opening and develops towards the top and the base of the wall. The model is also capable to predict the tensile damage arising from the vertical external sides of the wall, involving the top left pier next to the opening and the bottom right one, and it clearly

resembles what observed on both experimental test (Raijmakers and Vermeltfoort, 1992) and numerical analysis (Lourenco, 1996).
Furthermore, the model is formulated under 3D conditions, differently from all the others mentioned in this work and, as such, can be used to simulate rather more complex structures as compared to the others.

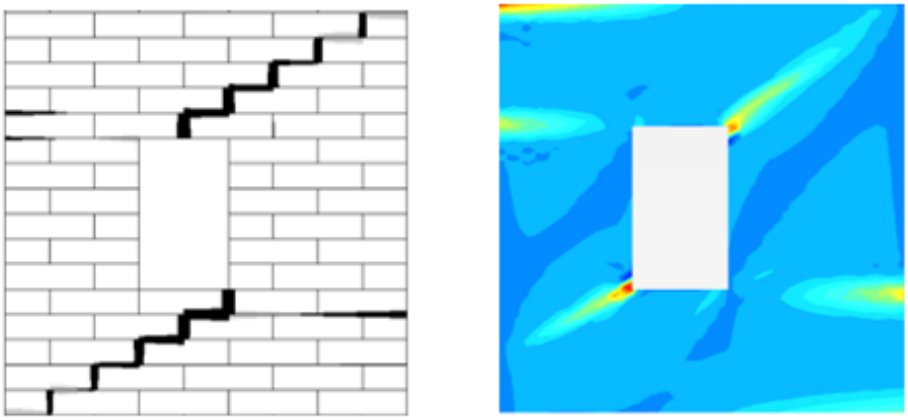

Figure 3.19 Damage at a displacement of 25.00mm: (left) composite interface model; (right) Total Cartesian Strain zz in the Jointed Masonry Model.

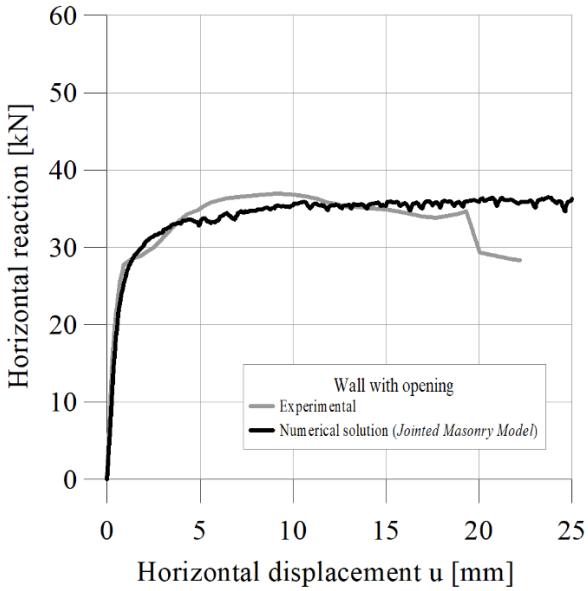

Figure 3.20 Comparison between experimental and numerical reaction vs. displacement diagram for the wall with opening.

4. APPLICATIONS

4.1. Nymphaeum of Genazzano

An advanced numerical approach for the analysis of the degradation processes that affected the Nymphaeum of Genazzano is here presented. It is a Renaissance structure attributed to Bramante and located in the southern portion of the Lazio region (Italy). The work aims to quantitatively assess whether the current state of the structure could be attributed to the erosion phenomena mentioned above through describing the structure with Jointed Masonry Model.

4.1.1. History

The Ninfeo of Genazzano is a structure dating back to the sixteenth century, attributed to the famous architect Bramante and located about 60 km South-East of Rome (Fig. 4.1). The structure is about 46 meters wide; its facade has a central loggia with three spans that finish, on the short sides, in two exedras adjacent to two square rooms (Fig. 4.2). These rooms are bordered to the west by two rectangular rooms. The three bays were originally covered, presumably, with vaulted ceilings.

Figure 4.1 The Nymphaeum of Genazzano.

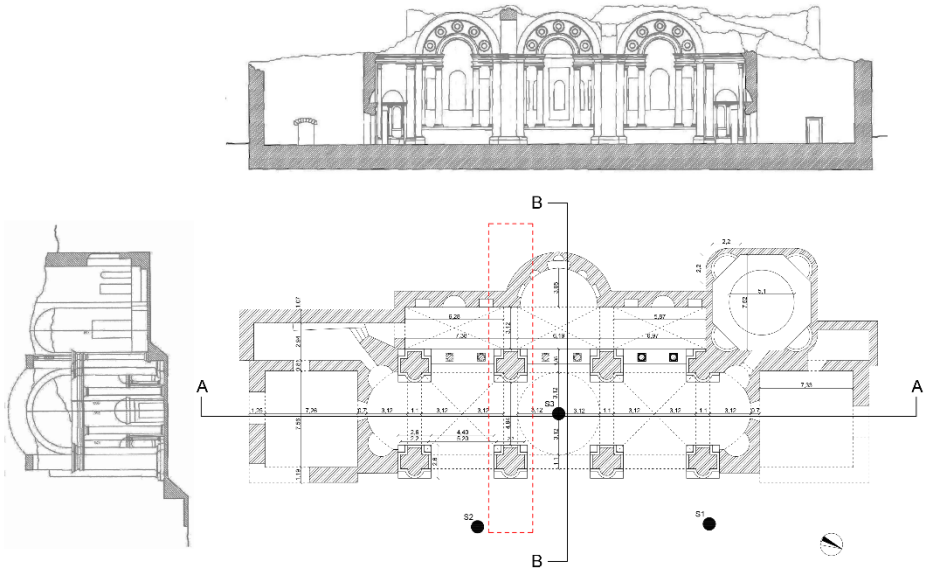

Figure 4.2 Plan, longitudinal A-A and transversal B-B sections.

The back of the structure receives the actions of the soil backfill, directly related to the sloping shape of the hill were it was build. Three serlianas (Fig. 4.3), framed by large pillars and central arches, separate the loggia from a space located westward at a higher elevation, which is the proper Ninfeo.

Figure 4.3 Detail of the serliana element.

This latter is close, to the North, to an octagonal room which contains inside a circular tank. The serlianas entablature is aligned with that of the adjacent interior pillars, although their architrave extends below that of the pillars. In this way the serlianas appear on a farthermost plan causing a perspective effect typical of Bramante's work (Frommel, 1969). Research on materials and construction methods have revealed asymmetries both in plan and elevation, as for example the different widths of the side spans of the loggia and the different depth of the niches opening in the wall located to the west. Several studies show that the older elements are present in the central part of the structure, i.e the lodge, with its two exedras, and the octagon. In fact, the small niches opening in the exedras corner, designed to accommodate the statues, are the basic units of the module that reproduces itself proportionally throughout the structure.

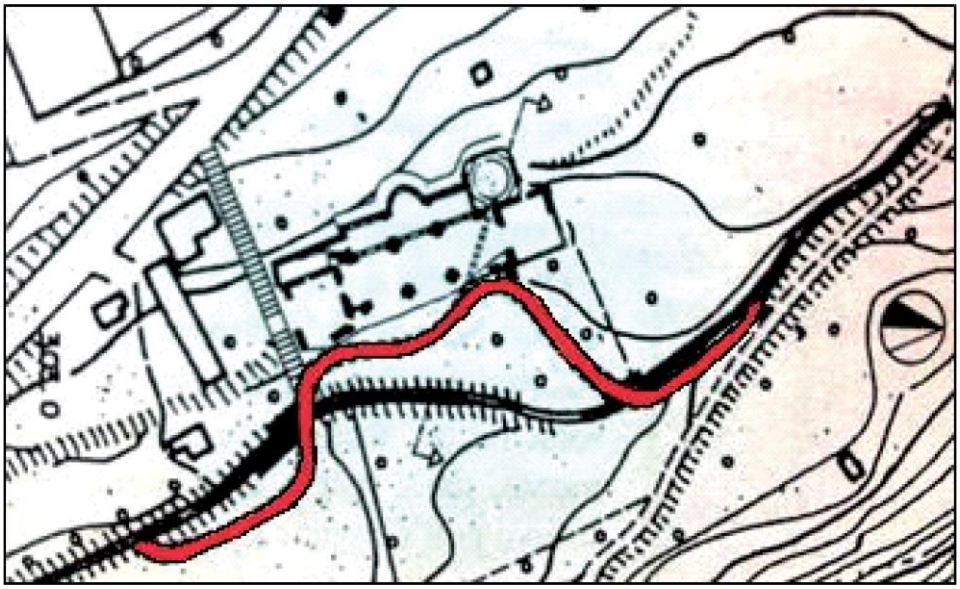

Figure 4.4 Planimetry and evolution in time of the river (modified from Barucco, 2001).

Since the early 19th century the Ninfeo appears in ruins. The structure was subjected to various restoration works in order to improve its precarious stability conditions, focusing mainly but not only on the entire East front, characterised by the most unstable conditions due to the erosion exerted by the stream flowing in front of it. In fact, the major instabilities suffered by the construction are concentrated near the original riverbed: one at the North semiesedra and another one on the South wall of the square room, where it was characterised by some curvatures. Such a mechanism might have caused the partial loss of stability of the vaults system and the consequent rotation of the columns. The monument stability was likely to be also influenced by the thrust exerted by the embankment at its back. During the first restoration work, the key intervention was concentrated on the small stream by changing its route and filling its former bed with made ground (Fig. 4.4). In addition, a buttress was realized to support the Northern semiesedra to prevent its collapse (Fig. 4.5). In the two following interventions arches and piers were also reinforced.

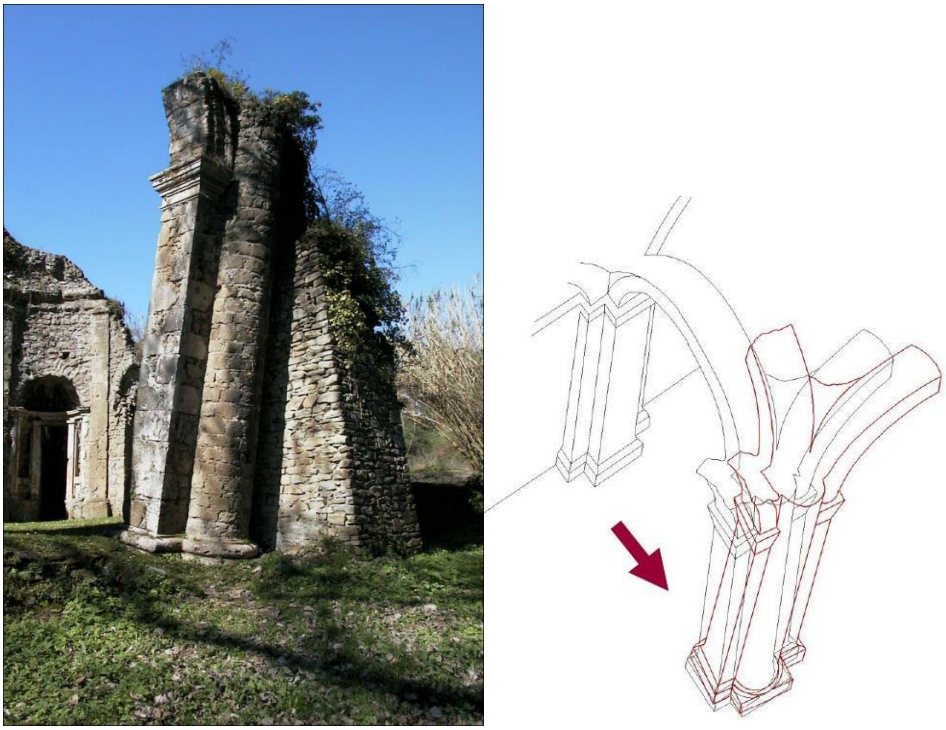

Figure 4.5 Buttress supporting the Northern semiesedra (left) and hypothesis of collapse mechanism (right) modified from Trovalusci, 2014.

4.1.2. Geotechnical characterization and soil model

During the last restoration of the Ninfeo of Genazzano, occurred in 2006, some site investigation and laboratory tests were carried out to characterize the foundation soils. Three boreholes with continuous core retrievalwere conducted to a depth of 15 meters below the ground level. Two of them, S1 and S2, were located outside the monumental area, while a third one, indicated as S3, was realized inside the Ninfeo (Fig. 4.2). From the analysis of the stratigraphic sequence it appears that the subsoil is constituted by a first layer of backfill of variable thickness, equal to about 0.5min the borehole S3 and to 4m in the borehole S1. In the latter case, the larger thickness of the backfill is probably due to the presence of the original river bed at this location. Under this stratum, a layer composed by sandy silt of high consistency and characterised by the presence of cracks was identified. From a depth of about 5– 6m below ground level a layer of silty

clay of high consistency, sometimes characterized by a rather stiff shale structure, was encountered. The hydraulic conditions were evaluated through two open standpipe piezometers installed within the boreholes S2 and S3, indicating a position of the water table 1m below ground level (approximately 300m above sea level). This elevation coincides with the water level in the tank situated in the octagonal room of the Ninfeo. SPT tests were performed in the backfill providing a value of the friction angle ϕ equal to 40◦ (Skempton, 1986). Laboratory tests were conducted on three undisturbed samples collected along the boreholes S1 and S2 between 8.0 and 12.7m below ground level. They are characterised by a fine matrix of about 89% (the silt fraction is predominant) and a plasticity index of *IP* =15%. The average values of the unit weight and water content are equal to γ =19.0 kN/m3 and $w0$ =22.5%, while the void ratio $e0$ is equal to 0.57. The consistency index *IC* is equal to 1, thus confirming the consistent state of the soil. The oedometric test performed during the campaign survey interested only the reloading-unloading braches, not having exceeding the preconsolidation pressure of the sample. The swelling index *CS* has a value equal to 0.03, while it is reasonable to assume for the material an overconsolidation ratio *OCR* larger than 8. The strength properties in terms of effective stresses were obtained by direct shear tests, indicating a cohesion c =76 kPa and a friction angle ϕ =23◦. The undrained strength *cu*, equal to 238 kPa, was determined by two undrained unconsolidated triaxial tests that were carried out on a sample taken between 12.4 and 12.7m below the ground level. The embankment, located at the back of the structure, was described by a linear elastic-perfectly plastic Mohr-Coulomb model, characterized by the following parameters: γ =19 kN/m3,E =30MPa, v =0.20, c =10 kPa, φ =30◦ and ψ =30◦. The backfill layer was neglected due to its modest thickness. The mechanical response of the foundation soils was described by the advanced constitutive *Hardening Soil model with small strain stiffness* (HSsmall, Benz, 2007), capable of taking into account important aspects of soil behavior, such as the high stiffness at very small strain levels, the reduction of stiffness with the increasing strain level and the developmentof plastic deformations from the earliest stages of loading. The soil reversible response is accounted for by a non-linear elastic isotropic model. The small strain shear modulus is a function of the stress state by the following expression:

$$G_0 = G_0^{ref} \left(\frac{c' \cdot \cos\phi' + \sigma'_3 \cdot \sin\phi'}{c' \cdot \cos\phi' + p^{ref} \cdot \sin\phi'} \right)^m \qquad 4.1$$

where *Gref*0 is the small strain shear modulus at the reference pressure *p ref* =100 kPa, σ_3 is the minimum principal effective stress and *m* is a constant. The shear modulus evolution with increasing shear strain is included in the formulation by the expression of the stiffness decay curve proposed by Hardin and Drnevich (1972) and modified by Santos and Correia (2001):

$$\frac{G_s}{G_0} = \frac{1}{1 + a\left|\frac{\gamma}{\gamma_{0.7}}\right|} \qquad 4.2$$

where *Gs* is the secant shear modulus, *a* is a constant equal to 0.385 and γ 0.7 is the shear deformation at which the shear modulus is reduced to about 70% of the initial value. The derivative of Eq. (2) with respect to the shear deformation provides the value of the tangent shear modulus, *Gt* , which has a lower limit corresponding to the shear module *Gur* :

$$G_t > G_{ur} = \frac{E_{ur}}{2(1+\nu_{ur})} \qquad 4.3$$

The shear modulus *Gur* is selected by the user with reference to an average shear deformation level, beyond which the reversible response is characterized by tangent shear modulus that is constant with the deformation. The corresponding Young's modulus is also dependent on the stress state by a function similar to (1):

$$E'_{ur} = E'^{ref}_{ur}\left(\frac{c'\cdot\cos\phi' + \sigma'_3\cdot\sin\varphi'}{c'\cdot\cos\varphi' + p^{ref}\cdot\sin\varphi'}\right)^m \qquad 4.4$$

Similar expressions are used in the model to define the secant stiffness at 50% of the ultimate load in drained triaxial tests, *E*_50, and the tangent stiffness of the first loading in oedometric tests, *E_oed*. The irreversible response of the *HSsmall* model is controlled by two yield surfaces that evolve by two isotropic hardening laws: the deviatoric yield surface *fs*, which changes its opening as a function of the deviatoric plastic strains, and the volumetric yield surface *fv*, introduced to limit the elastic domain with reference to compression stress paths and depending on the volumetric plastic strains. The elastic domain is also further reduced with reference to tensile stress states by a tensile cut-off surface. The flow rule of the yield surface *fv* is associated, while it is not associated for the deviatoric surface

fs. The physical and mechanical parameters of the sandy silt and clayey silt are summarized in Table 10.

Parameter	Sandy Silt	Clayey Silt
γ (kN/m^3)	19.0	19.9
c' (kPa)	10	76
φ' (°)	26	23
ψ (°)	0	0
m (-)	1	0
$E'_{50}{}^{ref}$ (kPa)	20800	40960
$E'_{oed}{}^{ref}$ (kPa)	20800	40960
$E'_{ur}{}^{ref}$ (kPa)	62400	122880
ν_{ur} (-)	0.20	0.20
G_0^{ref} (kPa)	130000	256000
$\gamma_{0.7}$ (-)	0.00025	0.00025
p^{ref} (kPa)	100	100
K_0^{nc} (-)	0.562	0.610
R_f (-)	0.9	0.9
$\sigma_{tension}$ (kPa)	0	0
$c_{increment}$ (kPa/m)	0	0

Table 4.10 Parameters of the HSs model for the soil strata for the Nymphaeum of Genazzano.

where the meaning of the symbols is explained below:

- $E'_{50}{}^{ref}$: secant stiffness in standard drained triaxial test;
- $E'_{oed}{}^{ref}$: tangent stiffness for primary oedometer loading;
- $E'_{ur}{}^{ref}$: unloading/reloading stiffness at engineering strains;
- ν_{ur}: Poisson's ratio for unloading-reloading;
- K_0^{nc}: K_0-value for normal consolidation;
- R_f: failure ratio;
- $\sigma_{tension}$: tensile strength;
- $c_{increment}$: increase of cohesion per unit of depth.

The unit weight (γ) and the strength parameters (c and ϕ) of the clayey silt were derived from the geotechnical characterisation. In the absence of direct measurements, the same value of the unit weight was assumed for the sandy silt layer, while the cohesion was reduced to c= 10 kPa due to the less cohesive nature of the material and to take into account the swelling phenomena whichare likely to have affected this superficial layer. The friction angle was set equal to ϕ =26◦. For both soil layers a zero dilatancy was assumed. The profile of the small strain shear modulus $G0$ was

estimated from the SPT tests results, adopting the following expression by Otha and Gotho (1978) for the shear wave velocity:

$$V_S = C\left(N_{SPT}\right)^{0.171} z^{0.199} f_A f_B \left(m/s\right) \qquad 4.5$$

where C is a constant equal to 68.8, z is the depth below ground level, fA is a constant dependent on soil type (here assumed to be 1.15 for the backfill and 1 for the silty soil) and fB is a constant depending on the geological period of deposition (here assumed to be 1 for the backfill and 1.3 for the silty soil). In order to have a continuous profile for $G0$, these values were interpolated by the expression proposed by Viggiani and Atkinson (1995) with the following parameters: A=3500, n=0.7 and m=0.21. This allowed to calibrate the parameters of the constitutive model, $Gref$ 0 and m, with reference to the sandy silt and clayey silt layers (Fig. 3). In particular, for the clayey silt, a constant value of $G0$ with depth (m=0) was assumed. The parameter γ 0.7 was selected with reference to the decay curves of $G/G0 - z$ proposed by Vucetic and Dobry (1991) for soils of low plasticity (plasticity index IP =15%).

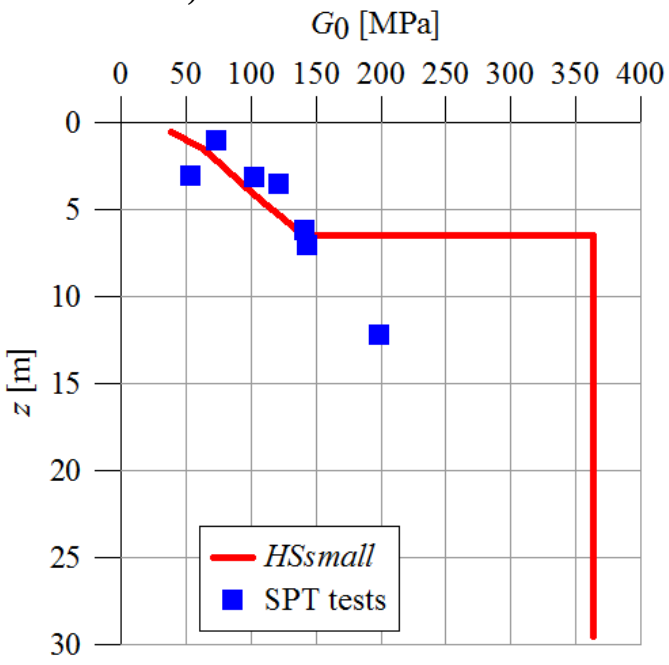

Figure 4.6 Profile of the small strain shear modulus G0 with depth.

The reference value of the small strain Young's modulus, E_ref_0 ,was related to $Gref_0$ by the Poisson's ratio for unloading/reloading, v_{ur}, assumed

to be equal to 0.2. The reference value of the unloading/reloading Young's modulus, E_ref_{ur}, assumed to be 0.2 E_ref_0, was calculated with reference to the stiffness decay curves. The parameters E_ref_0 and E_refo_{ed} were set equal to 0.33 E_ref_{ur}, as proposed in the literature (Schanz, 1998).

4.1.3. Structural model

The masonry structure of the Ninfeo is made up of several blocks of tuff, lime mortar and pozzolan, with horizontal joints not perfectly regular, inner core of rubble and corner bricks of travertine. Architectural elements such as columns, pilasters and capitals are also made up of blocks of travertine. The arches are made of tuff at full depth. The vaults, collapsed today, were in concretion, made up of irregular stones of tuff and mortar.
The arches are made of tuff at full depth. The vaults, collapsed today, were in concretion, made up of irregular stones of tuff and mortar. The portion of the Ninfeo analysed in this study is located along a cross-section (Fig. 4.2) that includes the soil, the embankment, part of the West wall of the monument, two arches and two columns that delimit, northwards, the center span of the loggia. The section thickness is equal to 4.95 m, which corresponds to the distance between the columns of the loggia. The soil extends for 30 m below ground level and, to the West, reaches an elevation of 49.86 m. In this way it was possible to represent the natural inclination of the slope, already characterising the site during the construction of the Ninfeo. The columns, 9.43 m high, have a square base of side 2.8m and height of 1.2 m, and start at −0.35m from ground level.

Parameter	Arches	Walls and columns
γ (kN/m^3)	16.0	16.9
G (kPa)	723378	1040590
ν (-)	0.16	0.20
C_{mc} (kPa)	10000	10000
φ_{mc} (°)	31	31
ψ_{mc} (°)	31	31
σ_{mc} (kPa)	10000	10000
SFβ (-)	0.70	0.375
$C_{planes1\text{-}2}$ (kPa)	2	1
$\varphi_{planes1\text{-}2}$ (°)	31	31
$\psi_{planes1\text{-}2}$ (°)	31	31
$\sigma_{planes1\text{-}2}$ (kPa)	3.33	1.66

Table 4.11 Parameters of the Jointed Masonry Model for the Nymphaeum of Genazzano.

The arch supported by the two columns, having a span equal to 5.34 m, is a pointed one and is made by blocks having a height of 0.55m and a thickness of 1.1 m. The arch between the central column and the back wall has a span of 3.49m and a height equal to 1.62 m; it is composed by blocks of the same size of the other arches. The spring of this arch coincides with the upper surface of the wall. This latter, 1.25m wide and 8.97m high, has the same thickness of the section and it is positioned to −0.35m from ground level. The behavior of masonry structures was described by the Jointed Masonry Model. The physical and mechanical parameters are summarized in Table 11.

4.1.4. Structural model validation

Some preliminary numerical analyses were also carried out by the Finite Element code Abaqus in order to validate the Plaxis model: a homogenisation-based advanced model for masonry (de Felice et al., 2009) was adopted as reference. In this formulation, the masonry is represented as a continuous homogeneous anisotropic medium with an elastic-perfect plastic behavior, whose constitutive relation depends on the mechanical and geometrical properties of blocks and joints.

The simplified geometry adopted in such preliminary 2D calculations is shown in Figure 5. It is a two-arch structural model, laying on a rigid soil and subjected to a distributed vertical load *q* acting on top of the two arches, and increased up to collapse. The Plaxis analysis predicted a collapse pressure of 125 kPa, while the reference Abaqus analysis lead to a value of 127 kPa (Fig. 4.9). The very good agreement between the two results, as well as the almost coincident deformative mesh and strain patterns shown in Figures 4.7-4.8, prove the reliability of the Jointed Masonry Model in describing the mechanical behavior of the investigated masonry structures.

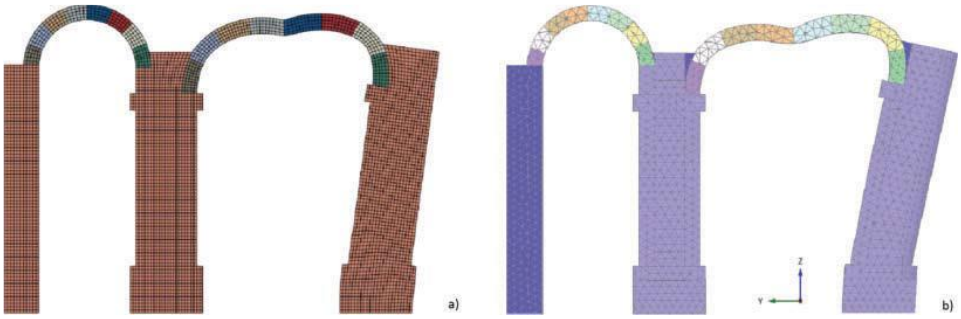

Figure 4.7 Deformed configuration in Abaqus a) and Plaxis 3D b).

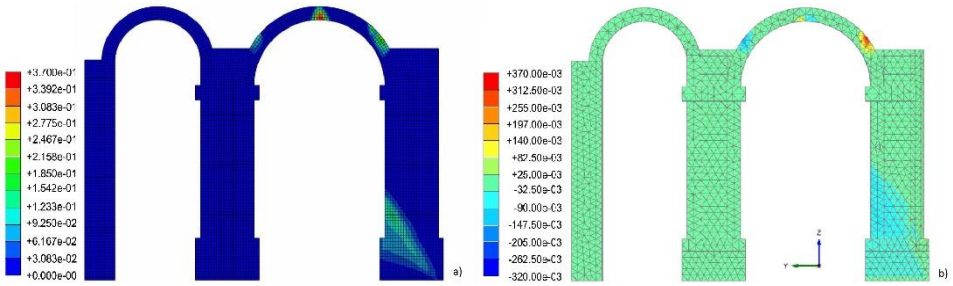

Figure 4.8 Distribution of the maximum principal total strains in Abaqus (left) and of the total strain in Plaxis 3D (right); (Continuum Mechanics sign convention).

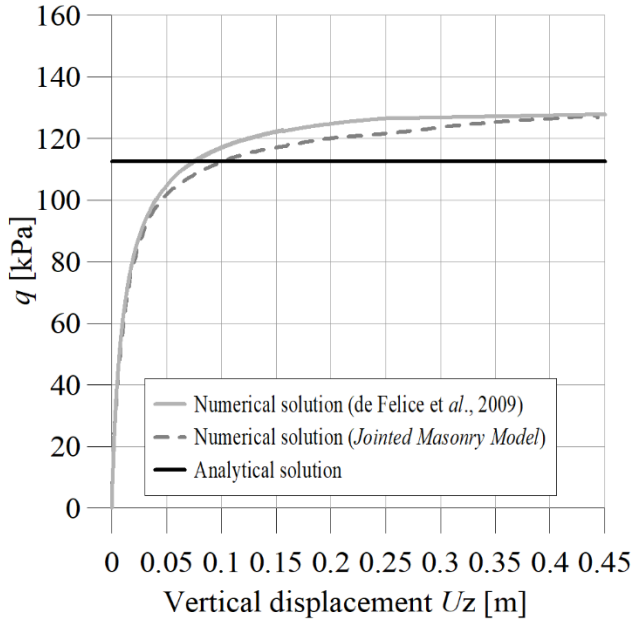

Figure 4.9 Load-displacement curve of the key point of the right end side arch.

4.1.5. Soil structure interaction analysis

The full interaction analysis was then performed by the code Plaxis 3D. The 3D FE model, corresponding to the selected portion of the structure (Fig. 4.2), was obtained using 10-node tetrahedral elements without any interface between the soil and the structure. The boundary conditions

adopted in the analysis were as follows: the bottom nodes were constrained with respect to all directions whereas those on the vertical sides were fixed along the horizontal direction. The subsoil and embankment's behaviour were modelled by the constitutive assumptions and related parameters illustrated in 4.1.2.

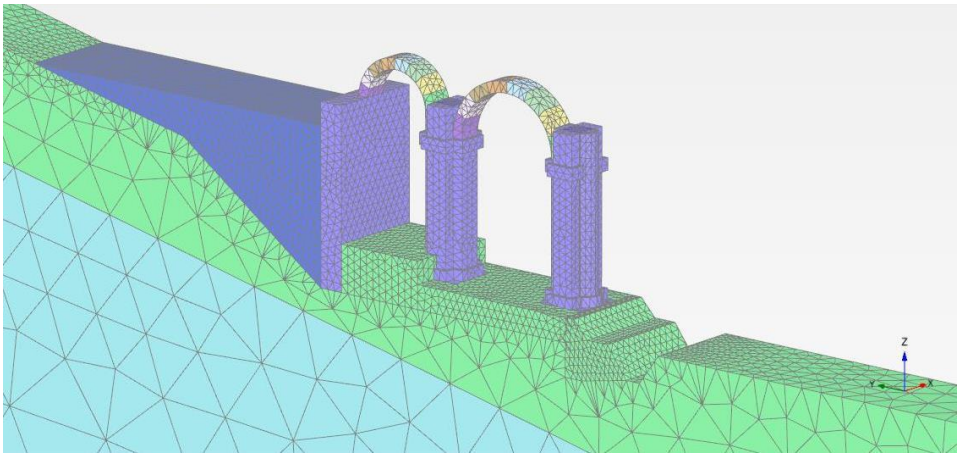

Figure 4.10 Mesh of the modelled portion of the Nymphaeum of Genazzano.

Drained conditions were assumed for the soil through all the stages of analyses, given the relatively slow processes under study. Given the strong non-linearity of the soil and structural behaviour, all the relevant construction stages of the Ninfeo were simulated step-by-step: the initialization of the state of stress according to the initial ground profile, including the slope behind the future structure; excavation of the bed river that flowed by the Ninfeo at the time of its construction; excavation for construction of the Ninfeo, with subsequent activation of the foundation elements, columns and arches; activation of the embankment on the left side (Fig. 4.11)

These stages were followed by the modelling of the erosive action of the river, simulated by a deepening and enlargement of the rived bed at the toe of the external column.

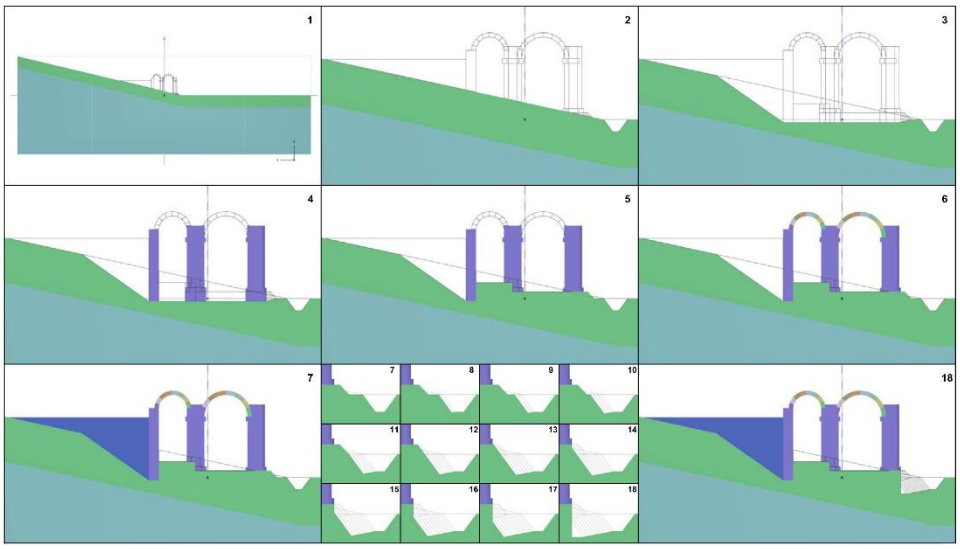

Figure 4.11 Construction phases sequence during the numerical analysis.

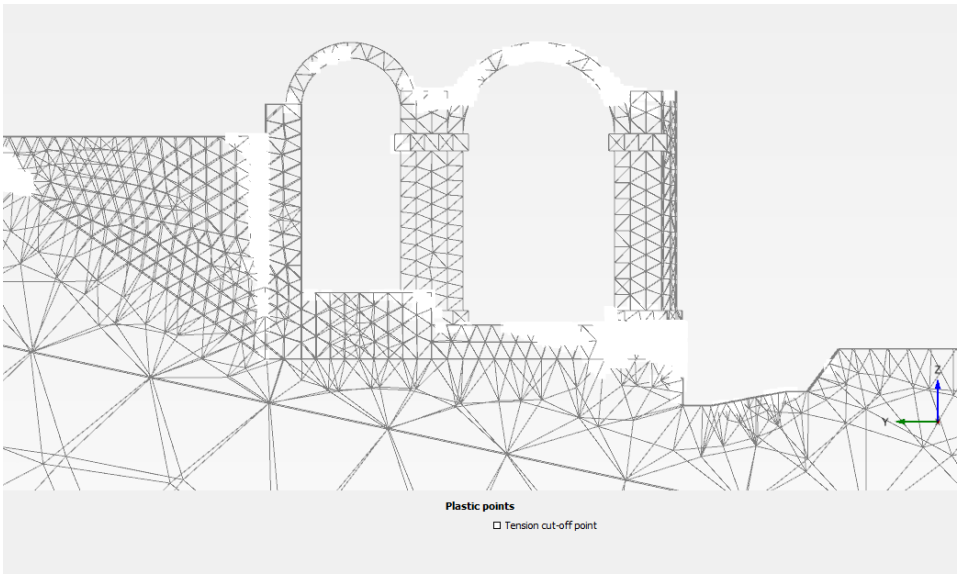

Figure 4.12 Distribution of tension cut-off points at the end of the numerical simulation.

At the end of the excavation stage some portions of the arches and the columns were characterised by shear and tensile failure. The corresponding plastic point's distribution is illustrated in Figure 4.12, which clearly resembles what observed on the validation model illustrated in the previous

paragraph under similar conditions. In this final configuration, the external column suffers a considerable rotation.

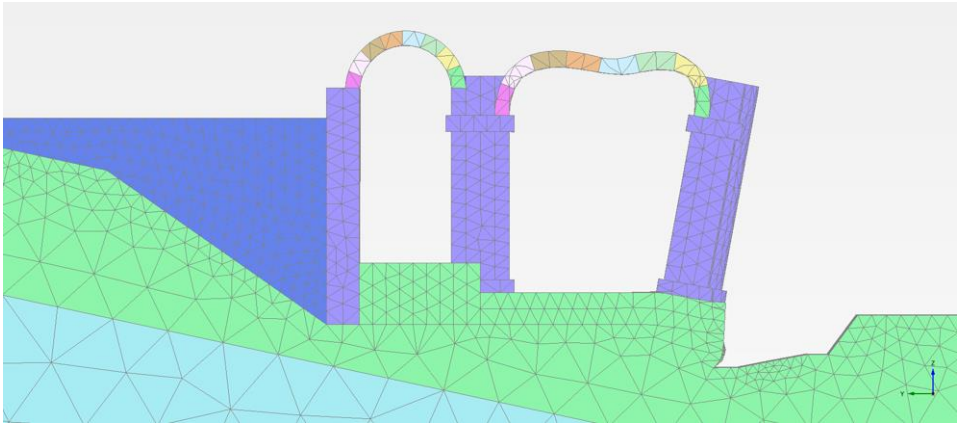

Figure 4.13 Deformed configuration at the end of the interaction analysis of the Nymphaeum of Genazzano.

The corresponding horizontal displacement of a point located at the top of it is equal to 7.40 cm. An in situ survey of the structure indicated a horizontal displacement of the top of this column being approximately equal to 8 cm, a very similar figure to that reproduced numerically (Figs 7a, b).

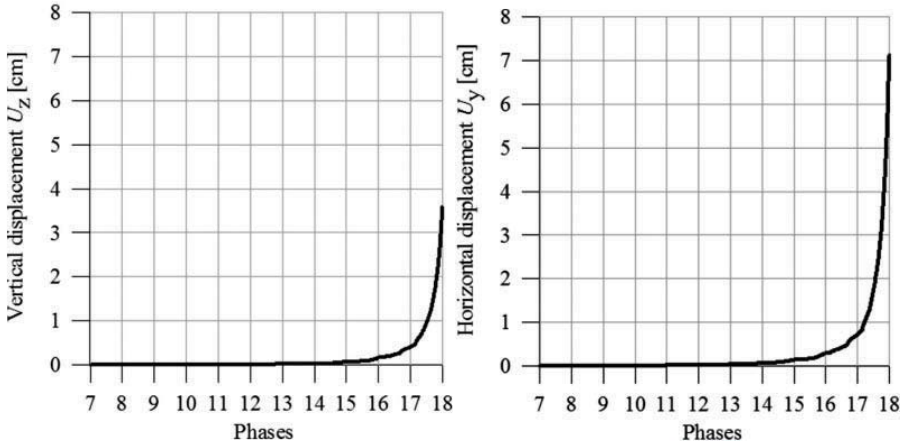

Figure 4.14 Vertical (left) and Horizontal (right) displacement evolution of the key point of the right end side column during different calculation phases.

4.1.6. Conclusion

Any modification of the state of the soil interacting with a surface structure can be fatal for the equilibrium or the structural functionality. This is particularly true for historic buildings, characterized by a long and delicate interaction with the site where they were built. Accordingly, an integrated approach to the analysis of this class of problems should simultaneously take into account the mechanical behaviour of soil, the hydraulic conditions of the site, the structural characteristics of the historic buildings and the sequence of the construction and post-construction phases, given the strongly non-linear behaviour of the materials involved. This paper illustrates this approach as based on a 3D finite element modelling, carried out adopting advanced constitutive hypotheses for both the structure and the soil. The key factors affecting the overall response of such a system were accounted for, including the construction sequence and interaction with the surrounding environment. The numerical results allowed to quantitatively justify the current damaged state of the Ninfeo of Genazzano as a consequence of its interaction with an existing river that has continuously exerted an erosion action at the base of the external columns.

4.2. Church of Santa Maria del Mar

In this chapter, the state of the art in the study of the structural performance of Santa Maria del Mar Church is presented. After a general description of the church, the history of the building and its past seismic performance are reviewed. Then, the morphology of the structure and the current damage patterns are described. The results of the gravity load analysis conducted on a rigid base are presented together with the study of the seismic performance of the structure. Finally, interaction analyses of the church in its interaction with the soil are described after that the geotechnical characterization is shown.

4.2.1. General description of the building

The building is composed of three naves, formed by four sections and an altar that consists of a polygon of seven sides, all covered by cross-vaults. The octagonal pillars are 26 m high and are separated by 13 meters from each other, forming four central parts of 13 by 13 meters. The Catalan gothic style uses buttresses instead of flying arches, and the spaces between the end of the lateral naves and the end of the buttresses are incorporated in the structure, using them to locate little chapels. A top view and an internal view of the building are shown in figures 4.16 and 4.17.

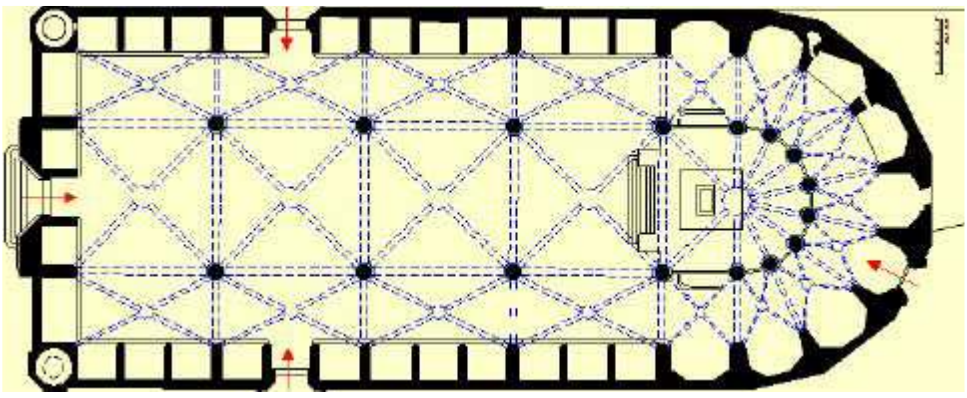

Figure 4.15 Plan view of the Santa Maria del Mar.

Figure 4.16 Internal view of Santa Maria del Mar.

The building is almost 85 meters long, 35.30 meters wide and has a maximum height of 34 meters from the ground to the roof. The plan view of the church is known as basilica plan, as no transept crosses the three naves. In the Northern part of the building there is a semi-circular apse and in the Southern façade one tower at each side (47m high the Western one and 46m high the Eastern one). The towers are integrated into the lower part of the perimeter of the façades. There are four entrances: one at each visible face of the building, two to the lateral naves at the lateral façades, one to the central nave at the main façade and one at the head. All the faces of the building have similar features, with the first level of walls around 16m high, defining the height of the lateral chapels (figure 4.18).

Figure 4.17 External view of Santa Maria del Mar.

In fact, the lower part of the buttresses is embedded in this wall, connecting them to make them work together. This wall has two levels: the first one is 6-7m high and the second 10m with windows at each lateral chapel of about 8x2m. In the main façade there is the main entrance to the Church with a big portal 12 high (figure 4.19).

Figure 4.18 Main portal of Santa Maria del Mar.

The other entries are similar but smaller and simpler. The upper part of the main façade is a vertical plan interrupted by two longitudinal buttresses (carrying the longitudinal thrust of the vaults) and the towers at the sides. A 9m diameter rose window in the centre of the wall is the most characteristic element of the façade. The rest of the perimeter is composed by the walls, the lateral chapels and the transversal buttresses. There are four buttresses at each side, two in the main façade and six at the head. They are all 14m high (from the chapel cover level to the top), with an average wide of 1.45 m. Next level is the lateral nave cover. The roof is composed of tiles and has a shape that enables water drainage. The roof is only interrupted by triangular walls aligned with the diaphragmatic arches that can have both structural and drainage functions. At the last level, the

cover of the central nave is done with a tiled surface with different slopes adapted to the vault shape and enabling drainage (Figure 4.20).

Figure 4.19 View of the roof of the central nave of Santa Maria del Mar.

The interior of the church shows the characteristics of the Southern Gothic: a very clear volume creating almost a single space, with a preference for the longitudinal orientation (no transept), as shown in figure 4.20. The church is composed by three naves with 13x13m square sections in the central nave and rectangular sections in the lateral naves (figures 4.21).

Figure 4.20 Square and rectangular cross vaults of the central (left) and lateral (right) nave of Santa Maria del Mar.

The altar consists of a polygon of seven parts. The piers have an octagonal shape and are 26m high and are 1.56m wide. The squared sections are covered by cross vaults surrounded by diaphragmatic arches at a height of 32m. The lateral vaults have a significant height compared to the central one (26m) and are also covered by rectangular cross vaults (figure 4.21). The altar of the church is covered with a vault with palm shape and has a big circular keystone in the centre, as shown in figure 2.15.

4.2.2. History and past seismic performance

Santa Maria del Mar Church started to be built in 1329, and the works finished in 1383 when the last section was covered. However, there are pieces of evidence that in the 1340s the new Gothic church was already accessible to the cult. Between 1339 and 1352, the majority of the lateral chapels were already made. The head chapels were erected afterwards, between 1360 and 1370. There is evidence of two events causing damage to the structure during construction. In 1373 an earthquake caused the partial collapse of the Eastern tower. In 1378 there was an important fire that caused significant damages to the interior of the church. No more information is available about the construction process, except that the last vault was closed in 1383. The existing towers were finished a long time afterwards (1496 and 1902). In Fig. 4.22, Vendrell et al. (2007) draw the construction phases of the building.

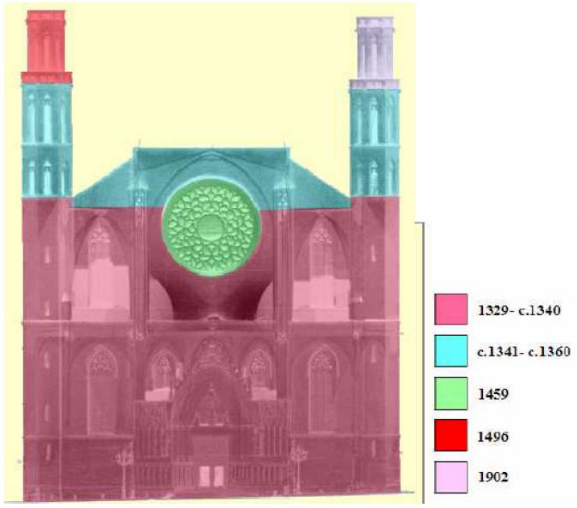

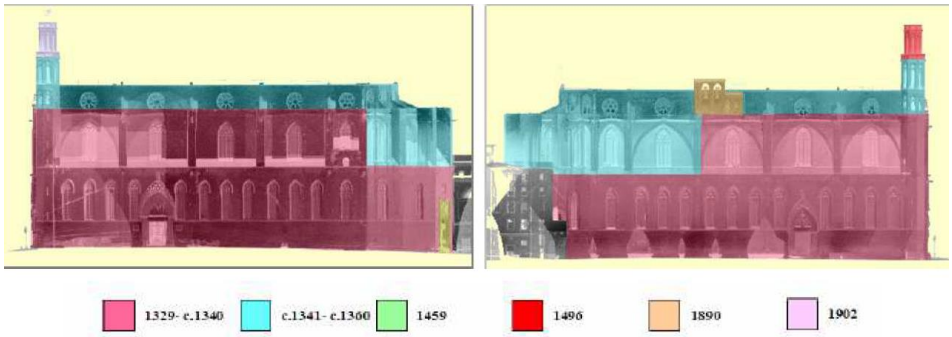

Figure 4.21 Façade and lateral view of construction phases, according to Vendrell et al. (2007).

There is also the indication of a relevant earthquake in 1428 that caused the partial collapse of the rose window of the façade, killing 25 people. This piece was restored in 1459. Several interventions have been carried out later: little architectural changes for functional reasons, repair interventions due to bombing 17th, 18th and 19th Centuries, restorations. In the 20th Century, there was an important intervention after a big fire in 1936. The three main important events causing damage were:

- Fire in 1378, concerning almost all the church. Some of the pathologies usually associated to 1936 fire could correspond in fact to this one. Essentially, this fire could have affected the vault of the second section, which was being built at this moment. In 1379 there were important works to repair the damages caused.
- The earthquake of 1428: it was an important earthquake causing damage to the façade and fall of the rose window. The damage was however caused probably by a series of events and not a single one, as between 1427 and 1428 the seismic activity in Barcelona was important. The existing cracks in the façade can be a consequence of these earthquakes (at the beginning of the 20th Century these cracks were described as stable).
- Fire in 1936: the most affected areas were the old presbyterium, the head of the church and the old organ. Nowadays the damage is still visible in some of the piers (figure 4.23). The most important earthquakes that the building has experienced were in the 14th and 15th Century.

1. 1373 Earthquake with Epicentre in the Pyrenees and intensity VII-IX (MSK). In Barcelona, the assumed intensity is V-VI. The highest part of Eastern tower collapsed, and it was rebuilt in the 20th Century.

2. In 1427 there is a long list of earthquakes in different places of Catalonia with intensities between III and VIII. Apparently, no damage is registered in Barcelona.
3. February 1428 there is an earthquake with the epicentre in the Pyrenees and intensity VIII. The estimated intensity on Barcelona is VI-VIII. The rose window of Santa.Maria del Mar collapses killing some people. There are also damages in Sta.Maria del Pi church.
4. May 1448 there is an earthquake with the epicentre near Barcelona and intensity V-VI, causing in Barcelona damage to houses and palaces, which were previously damaged by a flood. Except for some local damages (rose window and the tower), it is possible to conclude that Santa Maria del Mar has resisted earthquakes of some importance.

Figure 4.22 Current view of the third pier at left side, damaged due to 1936 fire.

The most important in 1373 (intensity V-Vi) and 1428 (VI-VIII). Even though some damages could not be reported in the documents found, it is rare that they have omitted important damages or partial collapses (given the associated high costs of repair). Therefore the building resisted earthquakes without important problems. As a conservative estimation, an intensity of VI could be associated with the maximum earthquake that the building has resisted all of its history. According to Roca (2007) and using the given correlation of an old Spanish Seismic Code, it is possible to relate the intensity with an acceleration:

$$\text{Log10 } a = 0{,}30103\, I - 0{,}2321 \quad (2.1)$$

Valid for T=500 years, being an acceleration (gals,10-2m/s2) and I the Intensity. Applying the formula the obtained acceleration for intensity VI is 0,375 m/s2 = 0,038g. According to the Spanish seismic code, the seismic action in Barcelona has a basic acceleration of 0,04 g (corresponding to T=500 years). This value is almost the same as the obtained one. This estimation has to be considered as an indicative value, but it is not possible to assure that the past earthquakes reached these values. However, the fact that the structure resisted earthquakes of this kind it will be taken into account when analysing the results of the numerical simulations (Murcia J., 2008).

4.2.3. Morphology

Vendrell et al. (2007) carried out a detailed study on the morphology of the structure, by means of a bibliographical research, inspection, Non Destructive Techniques (georadar, seismic tomography) and extraction of cores. In this way, it has been possible to take detailed characteristics of the different elements of the structure, including the vault infill. By using georadar and opening some holes in the foundations, it was possible to identify the foundation type and a considerable number of pre-existing constructions (figures 4.24).

Figure 4.23 Buttress (left) and piers (right) foundation.

These old constructions are integrated into the foundations. Their existence provided a pre-consolidation of the soil and makes the foundation condition heterogeneous. Walls and buttresses are three-leaf elements made of two external ashlar masonry layers and a rubble infill. This morphology can be seen from the holes made by bombing and shots from the1714 and 1936 wars. As the ashlar masonry is very thin, the load-carrying capacity is provided by the irregular masonry of the infill. By means of seismic tomography, it was possible to identify the massif condition of the piers (figure 4.25).

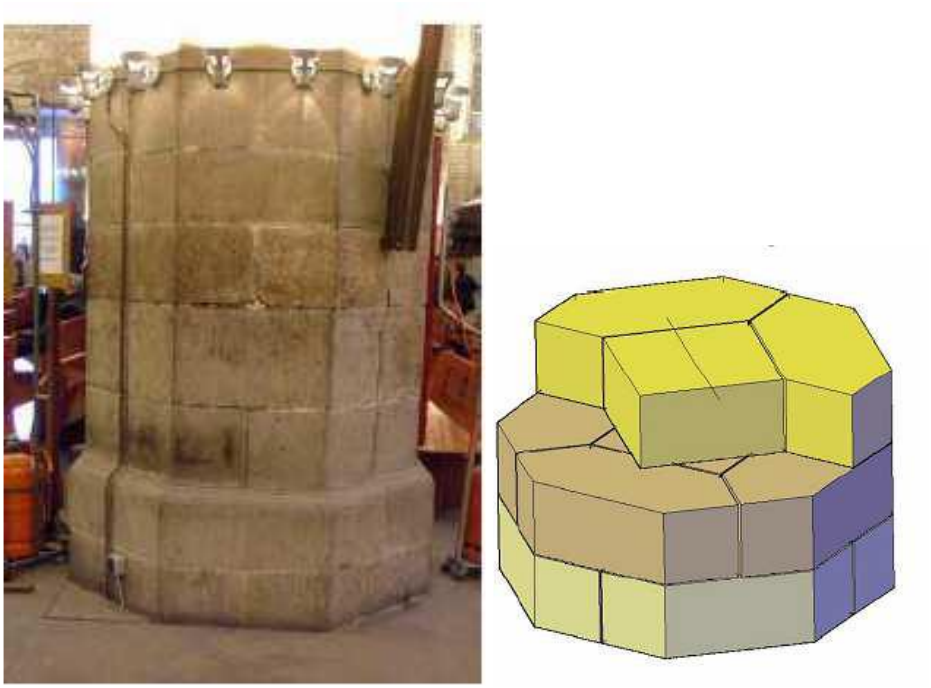

Figure 4.24 Pier base (left) and composition (right).

The section consists on one central squared ashlar of big dimensions surrounded by 4 hexagonal blocks giving an external octagonal shape (figure 2.25). The position of the internal block rotates 45º at each level in order to ensure stability, as it was found in Mallorca cathedral. Given the big dimensions of the stones, the thin layers of mortar and the massif condition of the pier, they are supposed to have a higher stiffness and strength than the rest of masonry elements of the structure. This hypothesis is in good agreement with their essential role in the global behaviour of the structure. The vaults morphology was characterized by means of information obtained from past interventions, combined with georadar and the opening of few holes (Mazziotti A., 2015). The vaults are made of blocks around 20cm thick. In the lateral vaults there is a supplementary layer of load-carrying material made by rubble masonry linked with lime mortar. In the central vault there is a light infill made by ceramic pieces, which is 0.7 to 1m thick (figure 4.26). In the top, there is a pavement 12cm to 15cm thick. The central and lateral vaults have different morphology due to structural reasons. The light infill in the central vault reduces the vertical load carried by the piers and the thrust that the buttresses need to counteract. However, the lateral vaults require this load-carrying infill as

their structural function is similar to a flying arch: transfer the thrust of the central vault to the buttress. That is the reason why they have almost the same height as the central vault.

Figure 4.25 Infill of the central vault (picture done in the 1990s).

This is a very significant characteristic of Santa Maria del Mar design, which is shared with Barcelona cathedral. In this case, as the vaults are squared and cover a bigger area the piers were improved to carry a bigger load. The arches supporting the vaults have been found to be diaphragmatic arches. They consist in vertical walls of load-carrying masonry up to the roof. It is thought their existence is justified by the need to support the timber beams of a previous temporary roof. However, previous calculations (Roca, 2007) showed that they also contribute in a significant way to the seismic capacity of the structure. The towers are very light elements, compared to the rest of the building. Their interior is empty, except a cylindrical 20cm thick wall that supports the steps of the stairs. The external wall is 40cm thick. Regarding the materials used, the masonry is mainly done with stones from Montjuic hill (siliceous gres) and lime mortar. The stone from Santa Maria del Mar Church has not been tested, but their mechanical properties are well characterized by previous studies and, in particular, they provided the value of the specific weight equal to 22kN/m3, the compressive strength (f_{cs}) equal to 30 MPa and the Elastic Modulus equal to 10GPa.

From this informations it has been possible to obtain the design values for masonry, as a material composed by stone and mortar.

4.2.4. Damage

A damage survey was carried out by Vendrell et al. (2007) by complementing an inspection with NDT techniques. A review of the main structural damages is here presented.
The perimeter walls show several slight and punctual damages: loss of mortar in joints, the opening of construction joints, holes due to the bombing. Behind them, there is a crack damage pattern associated with the openings of windows. Cracks starting from the base of the opening going down vertically or slightly inclined (figure 4.27). Some of them can be associated with differential settlements and other to the existence of tension stresses below the opening resulting from a deviation of the load as an arch. Besides, there are some cracks in the wall associated with the tower. The cracks start from the upper part of the first window from the corner towards the tower, and there is no continuity of the crack below the window (figure 4.27). These cracks could be caused by the leaning of the tower (possibly caused by an earthquake).

Figure 4.26 Vertical crack below windows (left) and inclined crack from windows towards tower.

The façade shows the same kind of vertical cracks associated with the windows and the towers, in both the East and West sides. Other cracks appear near the rose window, but they could be related to construction joints (figures 4.28). Finally, in the towers, the stone presents damage due to the corrosion and expansion of steel pieces.

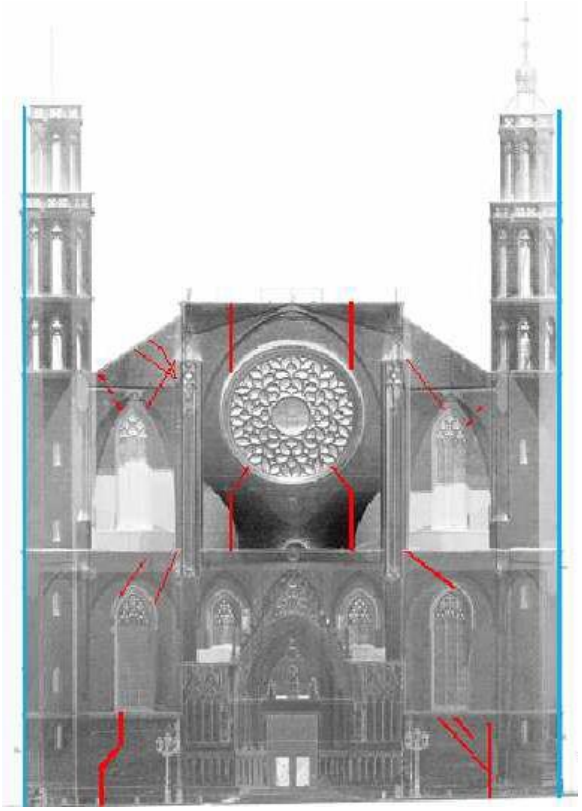

Figure 4.27 Vertical crack below windows (left) and inclined crack from windows towards tower.

Some cracks are also observed in the upper walls, both in the upper perimeter walls and walls of the central nave. The most characteristic pattern is the crack starting at the arches and going up inclined to the circle opening, that can be observed both from outside and inside (figure 4.29). It can be due to the existence of a relieving arch caused by the opening. As a result, the central part wouldn't be loaded.

Figure 4.28 Crack in central nave.

Some lateral vaults show loss of material and holes, also in the arches and nervures. This can be the result of the fires of 1379 and 1936. In fact, the central vaults were restored, but some lateral vaults still show this damage. Another damage that can be seen in the keys of some vaults and arches are longitudinal cracks and even relative displacements. This could be due to the 1379 fire when part of the structure was still under construction. Some work forms were burned and destroyed, while the mortar didn't still set. As a result, there was a loss of mortar and big deformations.

The piers are probably the most damage and vulnerable elements of the church. Their damage was mainly produced by the 1379 and 1936 fires. Some pillars show a significant loss of material (stone and mortar), for example, the third pier at the Western side (figure 4.30). There is also some splitting of material in the corner of some piers. This could be due to a high compressive stress concentration. However, the stresses are not expected to be so high. As the piers showing this problem are also in the affected area of the fire, it is thought that fire was the cause of this damage. The inclination of the piers and towers has been estimated. The piers showed a horizontal displacement between 2 and 8cm in the transversal direction and between 4 and 7cm in the longitudinal direction. The Eastern tower presented a longitudinal leaning of 6cm and the Western tower 15cm

longitudinally and 13cm transversally (to the exterior of the building in all cases).

Figure 4.29 Loss of material in pier.

The movements can be considered as small for an ancient structure like this one: for the piers equal or less than 1/200 and the towers below 1/300. The cracks in the wall near the tower could be associated with the leaning. However, it is worth to notice that the upper part of the Western tower rebuilt in 1496 doesn't show a leaning. This would mean that the movement stabilized before that date. Therefore, the movement could be associated with the 1427 earthquake. The existence of some cracks points out possible differential settlements. However, it is difficult to justify them, as the structure has been found to transfer the vertical load to the foundation in a uniform way. Possible reasons for differential settlements could be the heterogeneity of the soil conditions due to pre-existing constructions and the construction process. In fact, the perimeter walls were built before the piers. Even though the settlement could be similar in both elements, the difference of time between one and the other could cause the cracks in the structure. In other words, the settlement already existed in the wall when the rest of elements were built, so that the structure suffered this differential settlement due to the late settlement of the piers.

In addition to the damage mentioned above, Santa Maria del Mar Church shows other damages at the material level, namely: loss of material in stone

and mortar, cracking due to steel corrosion, dirt, biological colonisation, vegetal growth, moist spots and graffiti.

4.2.5. Finite element analysis

A non linear FEA of the typical bay of Santa Maria del Mar Church is presented. First, the material parameters used for masonry are described. Then, the results of analysing the structure subjected to gravity load and seismic load are presented. Second, the geotechnical characterization and calibration procedure adopted for the soil is described, followed by the description of its influence on the global masonry response during a pushover analysis.

4.2.5.1. Structural model

The masonry structure of Santa Maria del Mar is described through the Jointed Masonry Model. The Church portion analysed is located along a cross section that includes external walls, two pillars and three vaults, including their fillings (Fig.4.31). The section thickness is equal to 13.5 m, which corresponds to the distance between the centre of two consecutive spans.

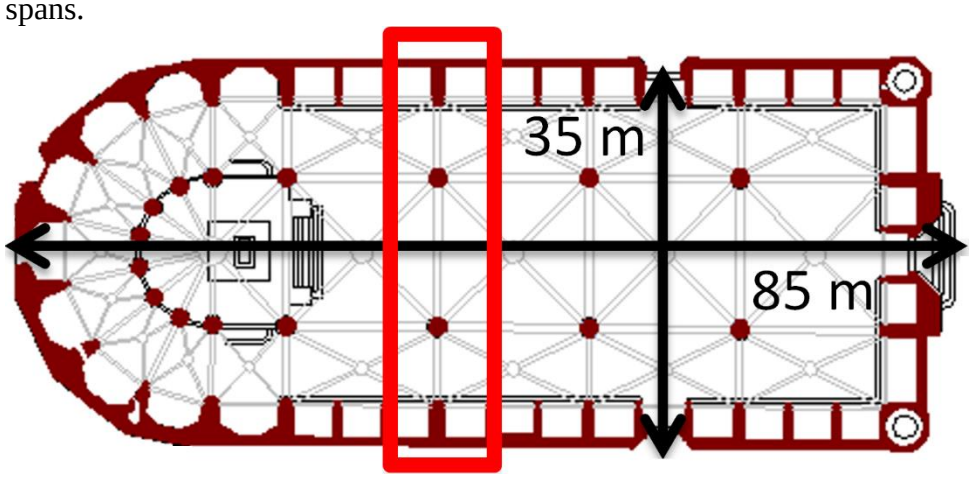

Figure 4.30 Portion of the structure considered in the numerical analysis.

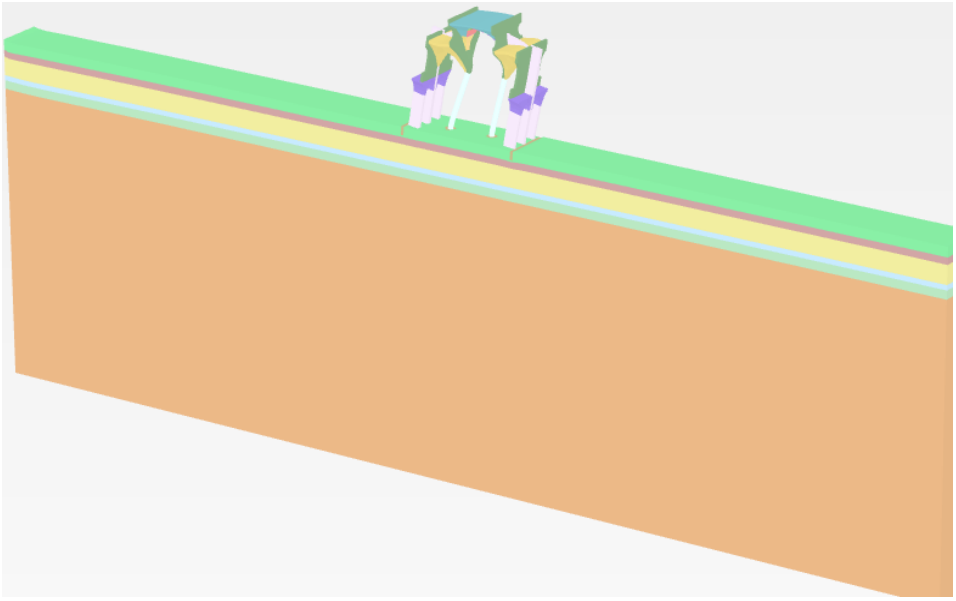

Figure 4.31 Whole model considered in the numerical analysis.

Different parameters are adopted with reference to distinct elements of which the considered section is composed. In particular, the same material properties are considered for both lateral vaults filling and inner core walls due to their similar composition.
Another set material is used for describing walls, footings and vaults taking into account, in the definition of the head and bed joints, the two different orientations of the walls. Two different sets of parameters are then used to describe pillars and the pottery fillings of the central vault. With reference to this letter, a partition of its intrados in eight portions is made to take into account the different orientation of the joints.
Starting from the mechanical parameters available for the masonry components, based on laboratory tests on cores taken from the buildings, the global compressive strength of each structure's element has been obtained as:

$$f_c = 0.45 \cdot f_{cs}^{0.7} \cdot f_{cm}^{0.3} \qquad 4.6$$

where f_{cs} and f_{cm} are respectively the compressive strength of stone and mortar. The value of cohesion is calculated as:

$$c = f_c \cdot \frac{(1 - sen\varphi)}{(2 - cos\varphi)} = 0.42\, f_c \quad (with\ \varphi = 10°) \qquad 4.7$$

The tensile strength is obtained as the 2% of the compressive strength, and the Young modulus is assumed equal to $500 \cdot f_c$.

Parameter	Pillar	Walls Footings Vaults Arches	Pottery filling in the central vault	Lateral vaults filling
γ (kN/m^3)	21.6	21.6	2.15	21.6
G (kPa)	3846000	3077000	1538000	1538000
ν (-)	0.3	0.3	0.3	0.3
C_{mc}(kPa)	12600	12600	1050	1050
φ_{mc} (°)	10	10	10	10
ψ_{mc} (°)	10	10	10	10
σ_{mc} (kPa)	120	80	50	50
SFβ (-)	1.25	0.69	0.58	1.25
$C_{planes1\text{-}2}$ (kPa)	840	840	840	840
$\varphi_{planes1\text{-}2}$ (°)	45	45	45	45
$\psi_{planes1\text{-}2}$ (°)	45	45	45	45
$\sigma_{planes1\text{-}2}$ (kPa)	40	40	40	40

Table 4.12 Parameters of the Jointed Masonry Model for the Church of Santa Maria del Mar.

4.2.5.2. Rigid base analyses

The following analyses are carried out assuming the structure lays on a rigid soil to provide a comparison with the results obtained using a more advanced constitutive model for masonry in which the structure response on a rigid base was analysed.

4.2.5.2.1. Gravity load

The analysis of a typical bay of Santa Maria del Mar subjected to gravity load is here described. All the construction stages of the Church were simulated: the configuration of the full perimeter including the buttress, chapels, lateral walls, choir and façade. This phase was succeeded by the formation of the arches, both longitudinal and transverse ones, and both at the lateral and central naves. Finally, the construction was completed by building the vaulted roof on the already existing arches starting in each bay with the lateral vault membranes and then the central one (Fig. 4.33-4.34).

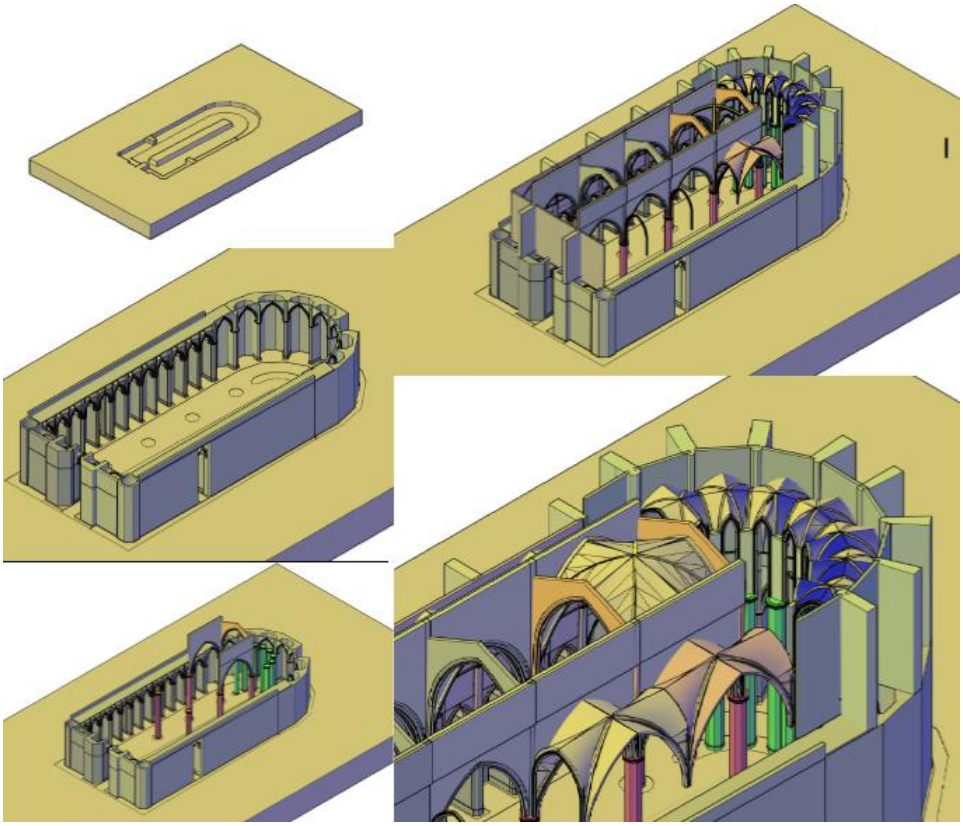

Figure 4.32 Construction of Santa Maria del Mar (Roca, 2008).

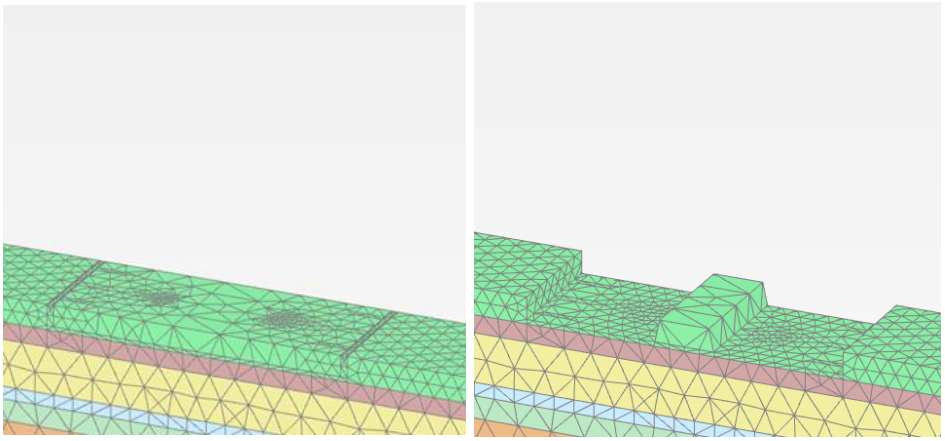

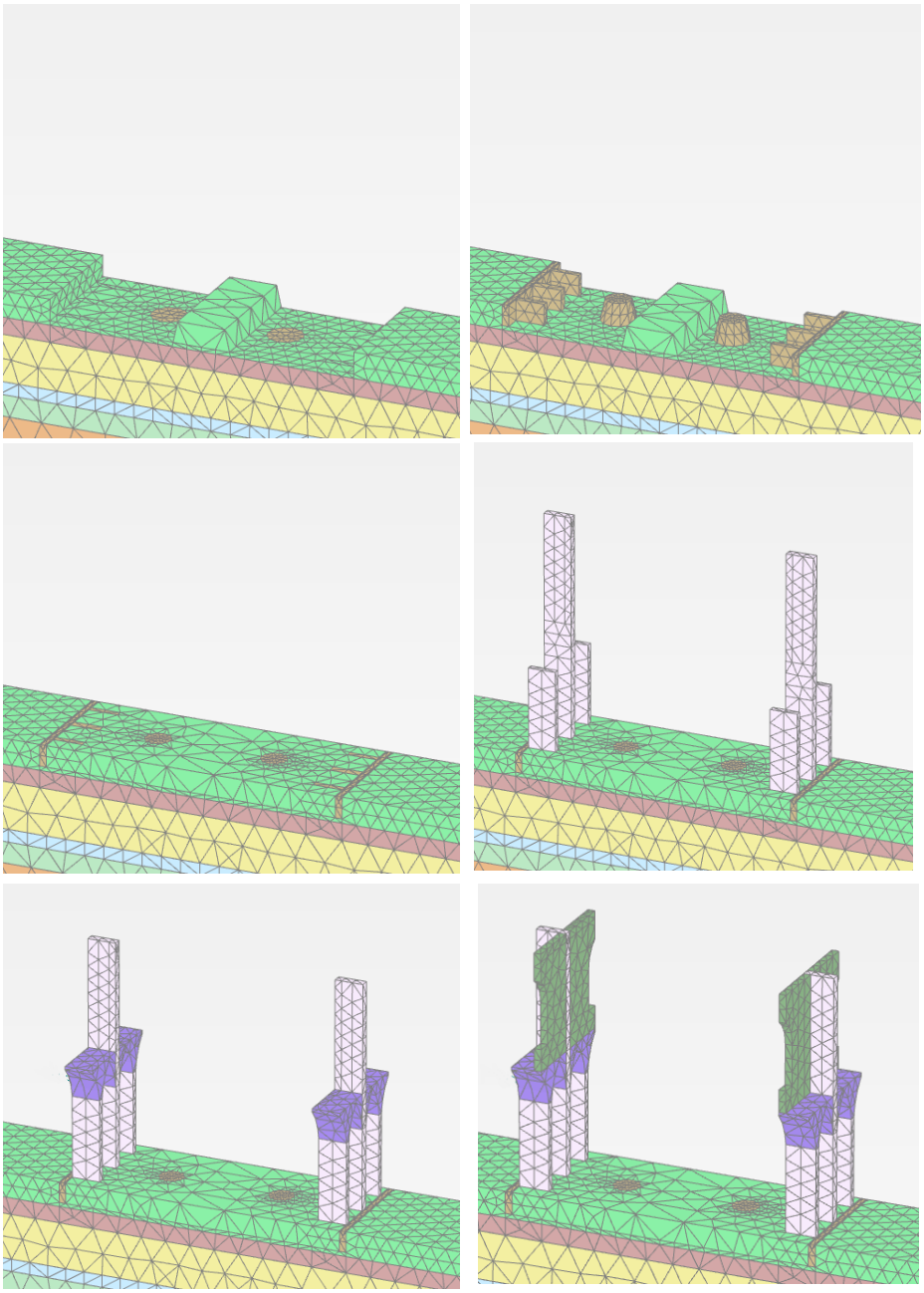

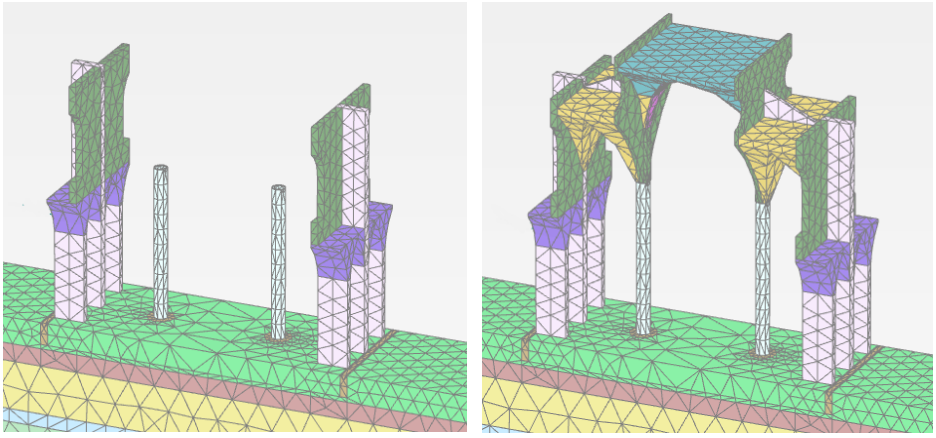

Figure 4.33 Phase sequence numerical analysis with Jointed Masonry Model, with real soil stratigraphy.

The comparison of the analysis results shows a very good agreement with the results obtained from both the corresponding numerical prediction provides by Roca (2007) equal to 2.9 MPa (Fig. 4.35) and the average compression stress measured at the base the two piers through the hole drilling test equal to 3.0 MPa. In fact, the numerical test carries out with Jointed Masonry Model provides a value of compression stress at the base of the two pillars equal to 2.98 MPa that agreed very well with the value expected (Fig. 4.36). This results confirmed a good parameter calibration was provided.

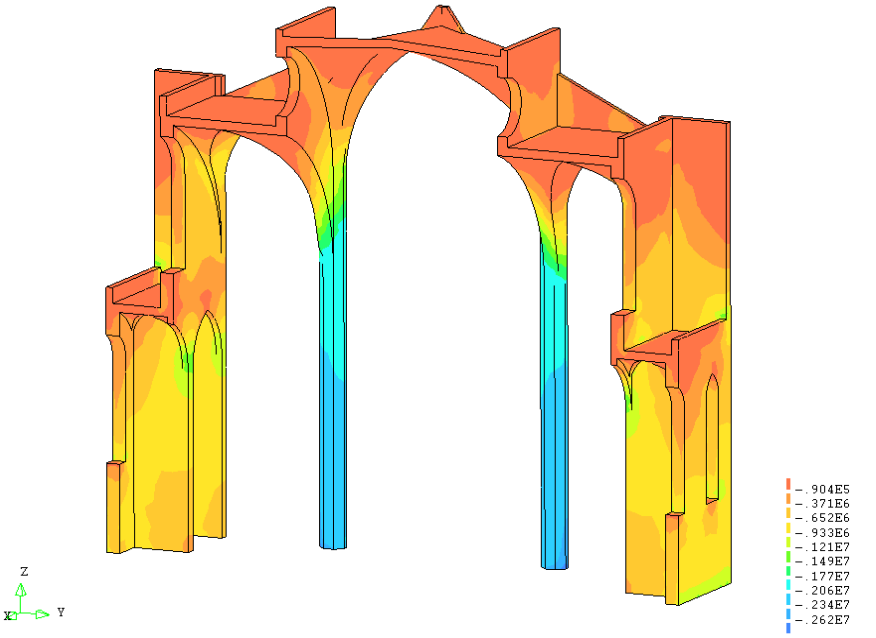

Figure 4.34 Compression stress distribution obtained by Roca 2007.

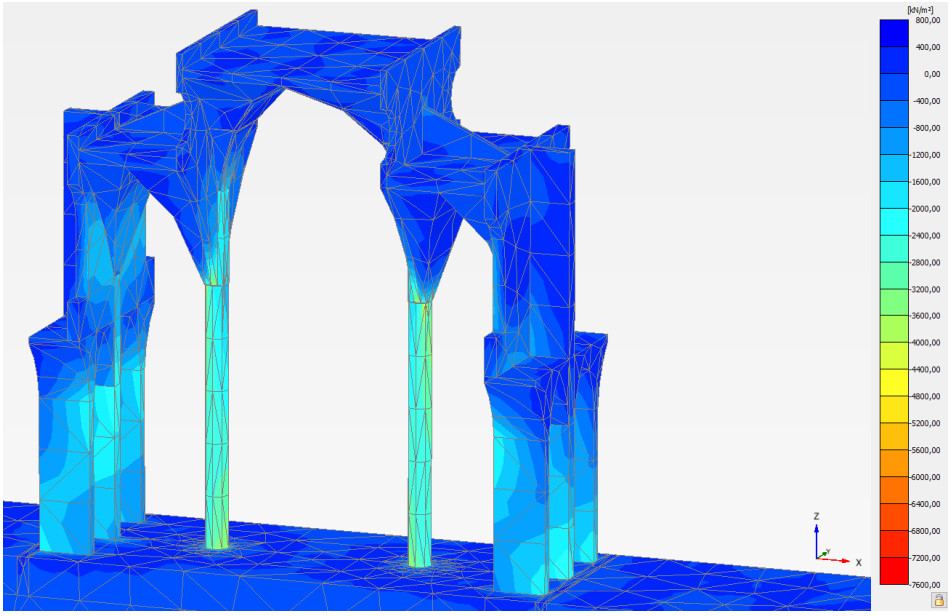

Figure 4.35 Compression stress distribution obtained with Jointed Masonry Model.

4.2.5.2.2. Seismic analysis: nonlinear static pushover

A pushover analysis has carried out to assess the behaviour of the structure under a seismic load. This is a simplified analysis approach since it is the equivalent nonlinear static analysis of one macro element of the structure. An accurate analysis would be a nonlinear dynamic analysis in the time-domain, introducing a time-acceleration spectrum. Nevertheless, this simplified analysis is admitted to evaluate the seismic performance of the structure. With the pushover analysis, it is possible to achieve the capacity curve of the structure. For a horizontal load proportional to the mass distribution, the obtained capacity curve is plotted in figure 4.10 together with that obtained by Roca et al. (2009). Jointed Masonry Model shows a more deformable behaviour compared to Roca et al. (2009), but the maximum value reached by the capacity curve, and corresponding to the structure multiplier, agreed very well with that expected, equal to 0.0997 since the obtained value is 0,1006 (Fig. 4.37).

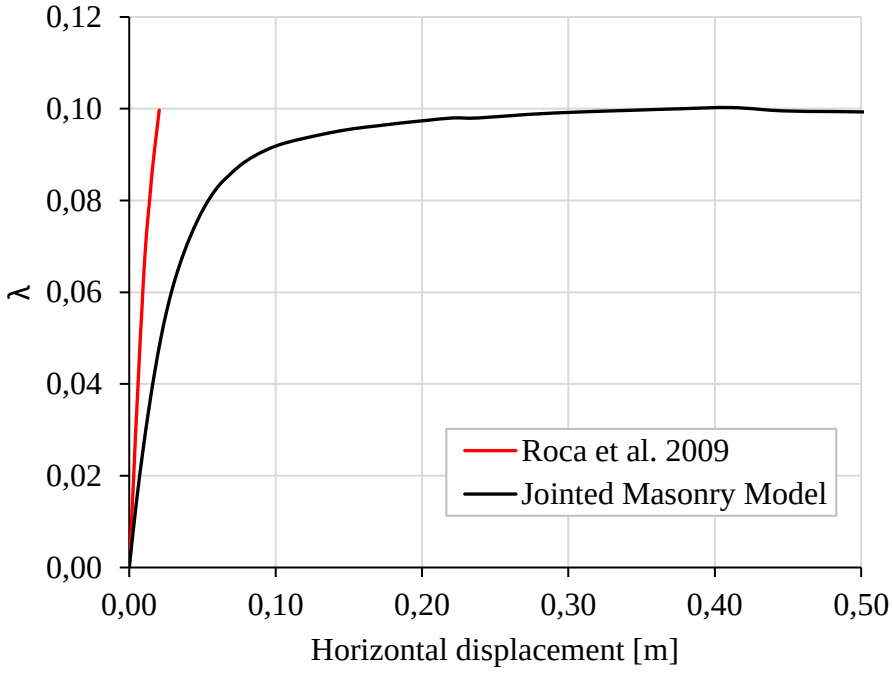

Figure 4.36 Capacity curve of a bay of the Church on a rigid base.

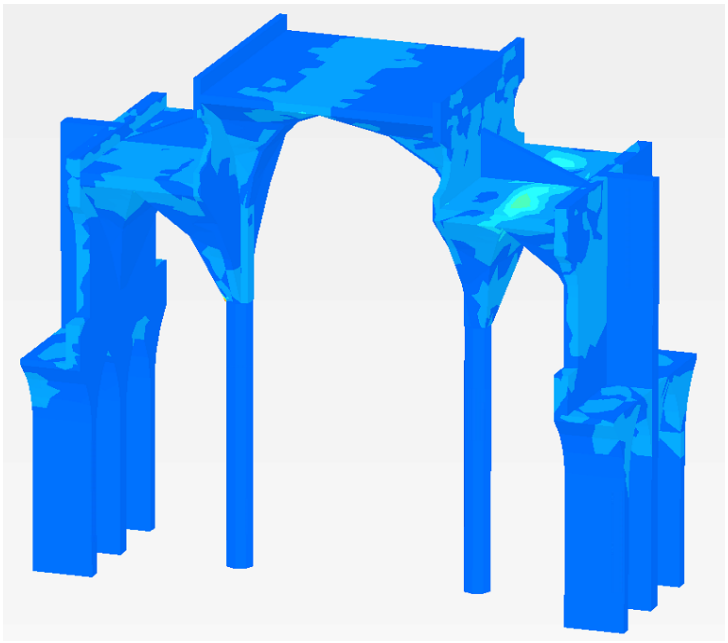

Figure 4.37 Tensile damage in Santa Maria del Mar at peak load for lateral forces distributed according to the mass (Jointed Masonry Model).

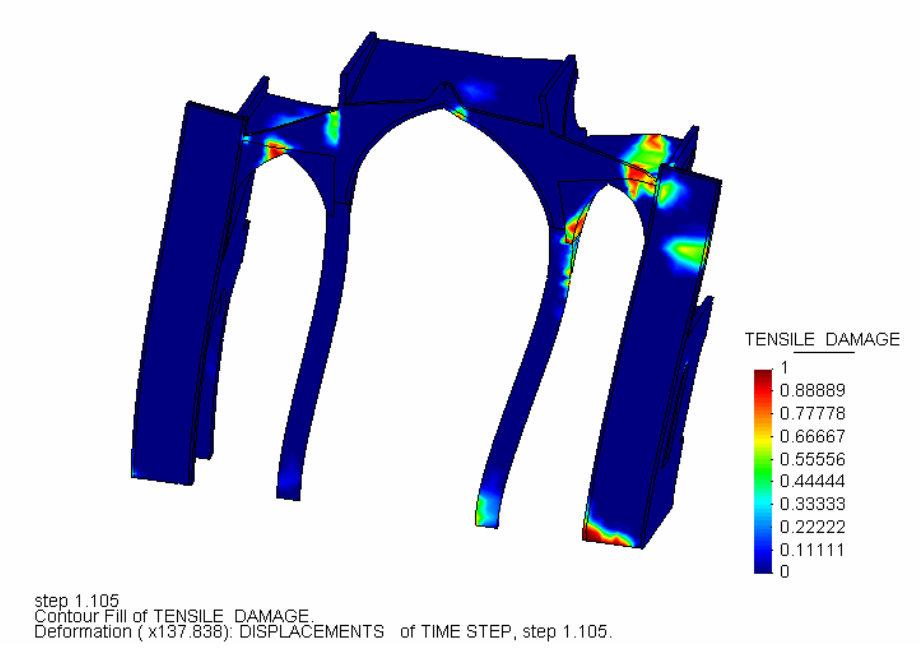

Figure 4.38 Distribution of the tensile damage parameter in Santa Maria del Mar at peak load for lateral forces distributed according to the mass (Roca et al. 2009).

Figure 4.37 shows the deformed configuration of the Church, achieved using the Jointed Masonry Model, at the end of the static non-linear pushover analysis. It resembles quite well what provided by the advanced numerical model shown in Fig. 4.38.

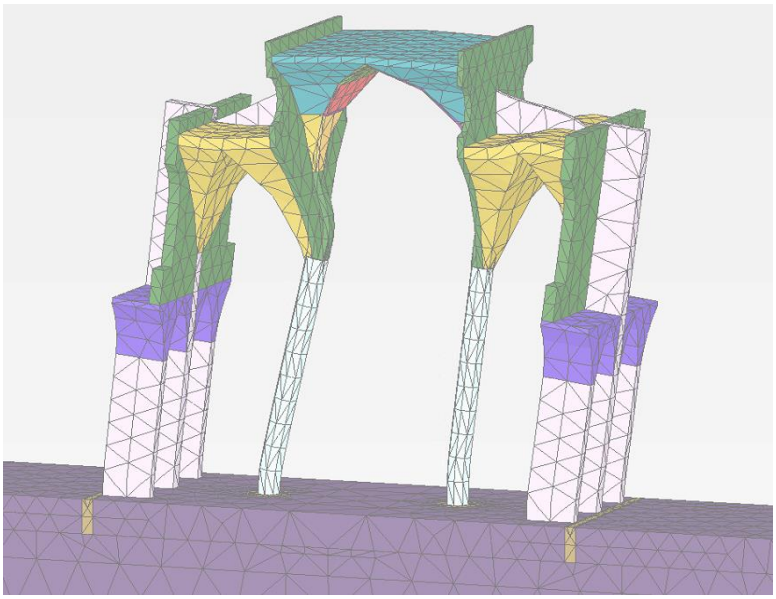

Figure 4.39 Deformed mesh in Santa Maria del Mar at peak load for lateral forces distributed according to the mass (Jointed Masonry Model).

Also for the tensile damage distribution, a good agreement is obtained. In both models, in fact, it is possible to observe a similar damage localization, concentrated at the intrados of the central vault and on the extrados of the lateral one. Plus, the damage observed on the external side of the right wall in the case of Jointed Masonry Model is quite coherent with that obtained by Roca et al. (2009).

4.2.5.3. Soil structure interaction analyses

4.2.5.3.1. Geotechnical characterization and soil model

The soil stratigraphy at the base of the Church was carried out starting from some in site investigations and laboratory tests. Three boreholes with continuous core retrieval were conducted to a depth of 10.00, 9.20 and 20.00 meters below the ground level. All of them were located inside the Church and indicated as "P" in the figure 4.40.

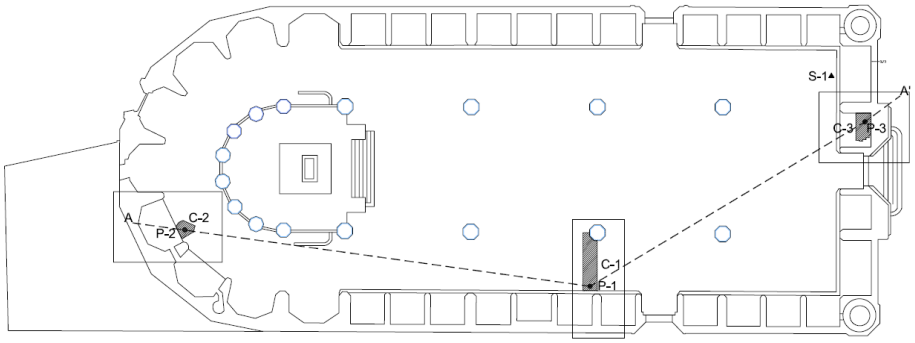

Figure 4.40 Tensile damage in Santa Maria del Mar at peak load for lateral forces distributed according to the mass (Jointed Masonry Model).

From the analysis of the stratigraphic sequence, it appears that the subsoil is constituted by a first layer of anthropological removal characterized by backfill and several typologies of structures like old house foundations, floors and mortuary vases. Under this stratum, a layer composed of sand of very low consistency and, for this reason, comparable to the first layer, was identified. From a depth of about 5 m below ground level, a layer of sand of medium consistency was encountered. A clay layer of about 2 m thickness is then found. A layer of sandy silt was suddenly recognized and, finally, a further sand layer, in this case of high consistency, was identified. All the layers are spread over the whole extension. The hydraulic conditions were evaluated through open standpipe piezometers installed within the boreholes P1, P2 and P3, indicating a position of the water 6 m below ground level, as it is shown in Fig. 4.41.

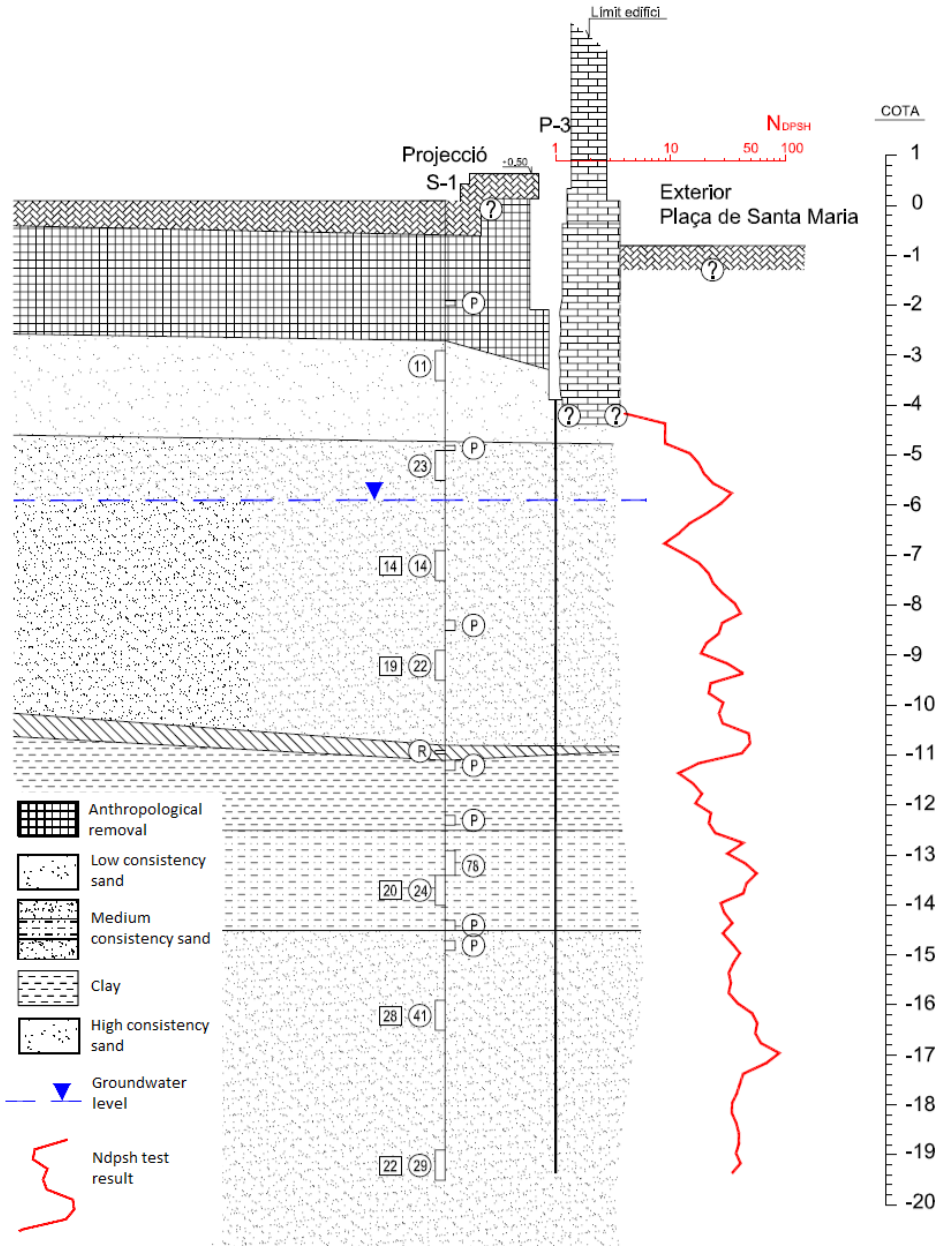

Figure 4.41 Detail of the lithostratigraphical section with reference to P3 borehole (Geotechnical Report of Santa Maria del Mar Church).

The first layer was described by a linear elastic-perfectly plastic Mohr-Coulomb model, characterized by the following parameters: γ =14.7 kN/m^3, E =30MPa, v = 0.20, c =14.7 kPa, φ =321° and ψ =0°.

Laboratory tests were conducted on two undisturbed samples collected along the borehole S1 between 12.30 and 13.50 m below ground level. The strength properties in terms of effective stresses were obtained by direct shear tests, indicating the values of cohesion and friction angle for the sandy silt equal to 72 kPa and 29.44° respectively. The undrained strength *cu*, equal to 127 kPa, was determined for the clay by an undrained unconsolidated triaxial tests that were carried out on a sample taken between 12.3 and 12.5 m below the ground level.
The mechanical response of the other foundation soils was described by the advanced constitutive *Hardening Soil model with small strain stiffness* (HSsmall, Benz, 2007), already described during the interaction analysis of the Nymphaeum of Genazzano. The physical and mechanical parameters used to model the soil in the interaction analysis of Santa Maria del Mar Church, are summarized in Table 13.

Parameter	1_Low consistency Sand	2_Intermediate sand	3_Clay	4_Sandy Silt	5_ High consistence Sand
γ (kN/m^3)	14.70	17.00	16.60	19.20	17.00
c' (kPa)	0	0	127	72	0
φ' (^{o})	27	29	16.80	29.40	29
ψ (°)	0	0	0	0	0
m (-)	0.50	0.65	1	1	0.70
$E'_{50}{}^{ref}$ (kPa)	14400	15600	18000	18000	20400
$E'_{oed}{}^{ref}$ (kPa)	14400	15600	13230	12010	18980
$E'_{ur}{}^{ref}$ (kPa)	28800	31200	36000	36000	40800
ν_{ur} (-)	0.20	0.20	0.20	0.20	0.20
$G_0{}^{ref}$ (kPa)	60000	65000	60000	60000	85000
$\gamma_{0.7}$ (-)	0.00011	0.00011	0.00028	0.00028	0.00011
p^{ref} (kPa)	100	100	100	100	100
$K_0{}^{nc}$ (-)	0.5460	0.5152	0.7110	0.5091	0.5152
R_f (-)	0.9	0.9	0.9	0.9	0.9
$\sigma_{tension}$ (kPa)	0	0	0	0	0
$c_{increment}$ (kPa/m)	0	0	0	0	0

Table 4.13 Parameters of the HSs model for the soil strata of Santa Maria del Mar Church.

The unit weight (γ) and the strength parameters (c' and φ') are derived from the geotechnical characterization. For all the soil layers a zero value dilatancy is assumed. The profile of the small strain shear modulus G_0 is estimated by the number of blows N_{SPT} determined by the SPT tests, and adopting the expression of Otha and Gotho (1978) for the shear wave

velocities (eq. 4.4) in which the values of f_A and f_B adopting for the different layers are shown in table 14.

Parameter	1_Low consistency Sand	2_Interme diate sand	3_Clay	4_Sandy Silt	5_ High consistence Sand
f_A	1	1	1	1	1
f_B	1	1.07	1.07	1.14	1.14

Table 4.14 Parameters for the Otha & Goto expression.

In order to have a continuous profile for G0, these values were interpolated by the expression of Viggiani and Atkinson (1995) through the parameters in table 15.

Parameter	1_Low consistency Sand	2_Interme diate sand	3_Clay	4_Sandy Silt	5_ High consistence Sand
A	3500	3500	1600	1600	3500
n	0.60	0.60	0.74	0.74	0.68
m	0.17	0.17	0.22	0.22	0.17

Table 4.15 Parameters for the Viggiani and Atkinson expression

This allowed to calibrate the parameters of the constitutive model Gref0 and m as shown in Figure 4.42.

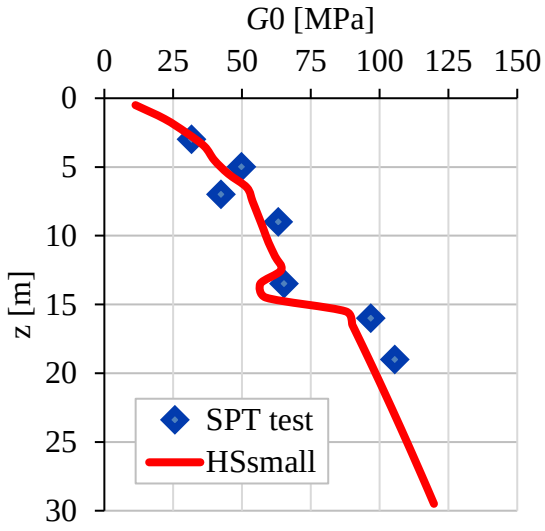

Figure 4.42 Profile of the small strain shear modulus G0 with depth for the soil underlying Santa Maria del Mar Church.

The parameter γ0.7 was selected with reference to the decay curves of G/G0-z proposed by Vucetic and Dobry (1991) for soil with plasticity index Ip equal to 0% and 20%, the latter used for Clay and Sandy Silt. The reference value of the small strainYoung's modulus, *Eref*0, was related to *Gref* 0 by the Poisson's ratio for unloading/reloading, *vur* , assumed to be equal to 0.2. The reference value of the unloading/reloading Young's modulus, E^{ref}_{ur} , assumed to be 0.2 E^{ref}_{0}, was calculated with reference to the stiffness decay curves. Finally, the parameters E^{ref}_{0} and E^{ref}_{oed} were set equal to 0.33 E^{ref}_{ur}, as proposed in the literature (Schanz, 1998).

4.2.5.3.2. Gravity load

The analysis of the typical bay of Santa Maria del Mar subjected to gravity load and already analysed with a rigid base, is here described in its interaction with the real soil underlying the Church. Also in this case, all the construction stages of the Church were taken into account, and the value of compression stresses at the base of the two piers resembles what was already obtained in the case of rigid soil. Nevertheless, a significant difference in the deformed configuration due to the presence of the real soil was obtained with reference to the rigid case (Fig. 4.43).

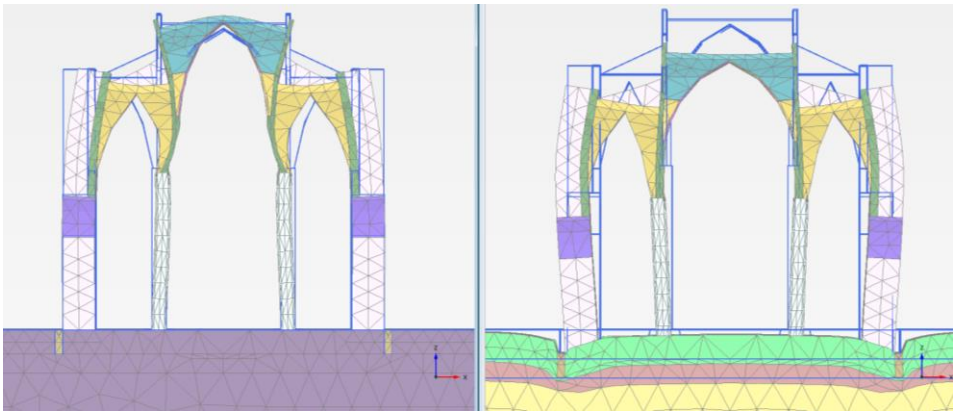

Figure 4.43 Deformed mesh at the end of gravity load scaled up 100 times: rigid soil (left), real soil (right).

This is connected to the differential vertical displacements between the two piers and the external walls. Therefore, in the case of real soil, the central nave is more damaged compared to the case with rigid soil. This is visible also with reference to the damage pattern shown in terms of plastic

deformations (Fig. 4.45) and plastic points (4.46). In the case of rigid soil the damage is localized in the lateral naves, while with the real soil the damage is also distributed in the central nave.

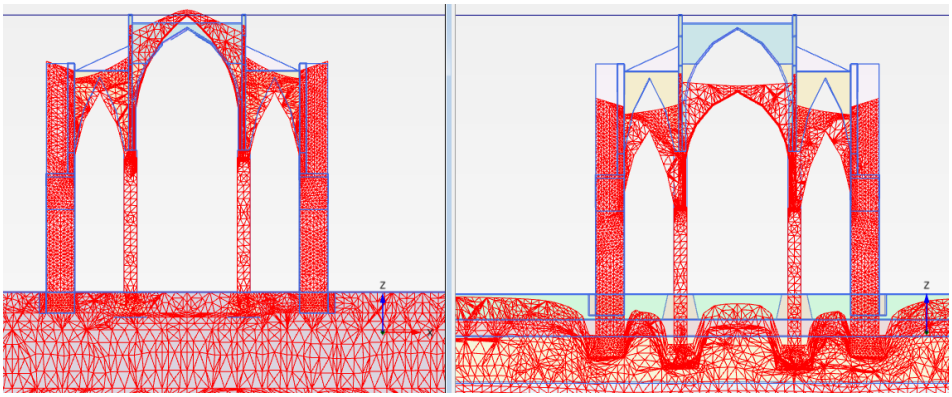

Figure 4.44 Vertical displacement at the end of gravity load scaled up 200 times (section): rigid soil (left), real soil (right).

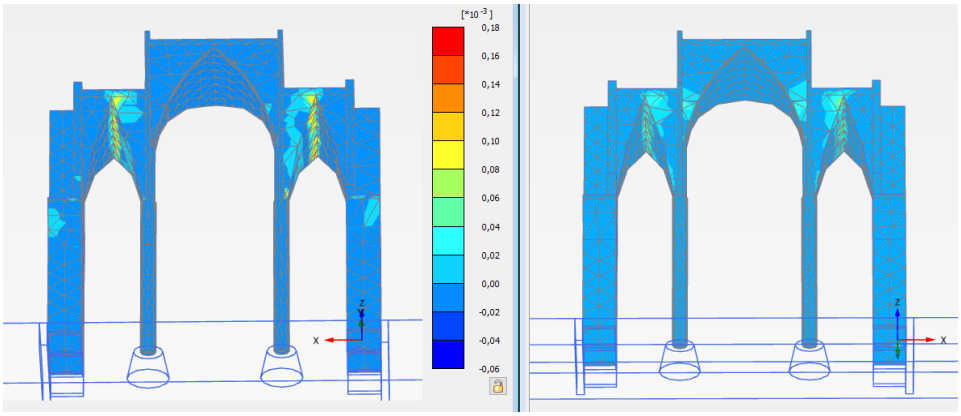

Figure 4.45 Plastic deformation distribution at the end of gravity load (bottom view): rigid soil (left), real soil (right).

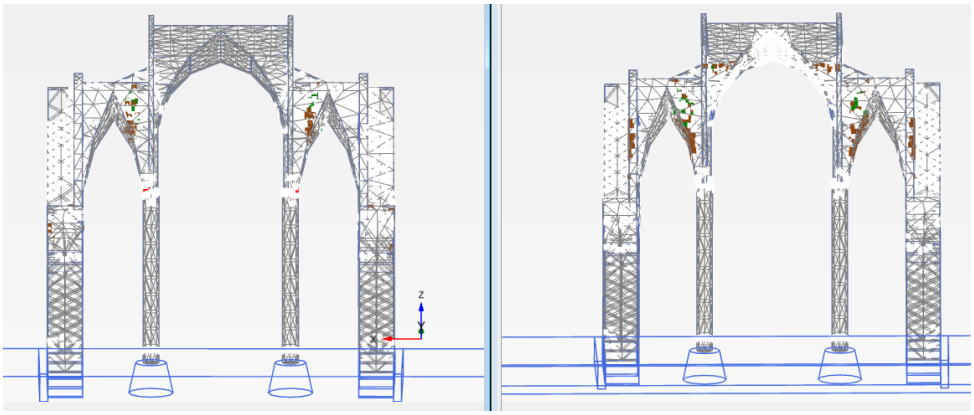

Figure 4.46 Plastic points distribution at the end of gravity load (bottom view): rigid soil (left), real soil (right).

Furthermore, it is worth noting that the damage occurred on the structure as a consequence of the soil settlements agrees very well with real observations. In fact, the plastic strain distribution resembles the actual sliding crack exists close to the keystone of the lateral vaults proves the capabilities of Jointed Masonry Model in describing this kind of structures.

4.2.5.3.3. Seismic analysis: non linear pushover

The seismic response of the Santa Maria del Mar Church was also analysed with reference to its interaction with real soil to understand how its behaviour changes due to the presence of soil.
The deformed configuration at the end of the analysis is very similar to the rigid base case, but the influence of the soil deformability on the Church seismic performance decreases the seismic capacity of the building as expected. The results obtained by the interaction non-linear analysis show a more deformable behaviour compared to that carried out with the rigid base and the maximum value reached by the capacity curve is equal to 0,093 (Fig. 4.47).

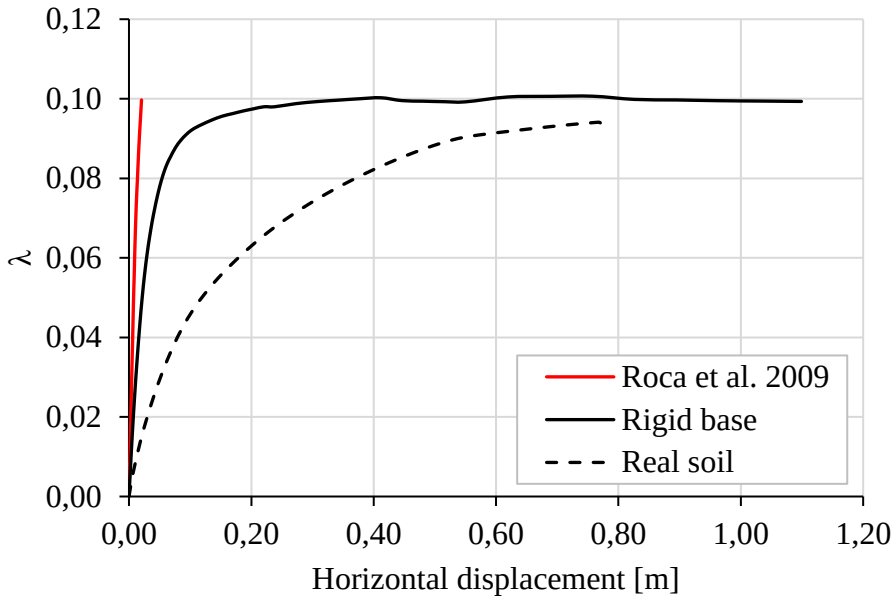

Figure 4.47 Capacity curve of a bay of the Church on the real soil.

4.2.5.3.4. Seismic analysis: non linear pushover with foundation supports element

A further analysis was carried out to try to take into account the possible influence of pre-existing structures, on which the Church was built, on its seismic performance. These elements were described with the same material used for the soil foundations, and they extend for the whole encumbrance of the external wall foundation of the Church (Fig. 4.48).
Figure 4.49 shows the capacity curves obtained from the seismic analyses performed with Jointed Masonry Model compared with the results obtained by Roca et al. (2009).

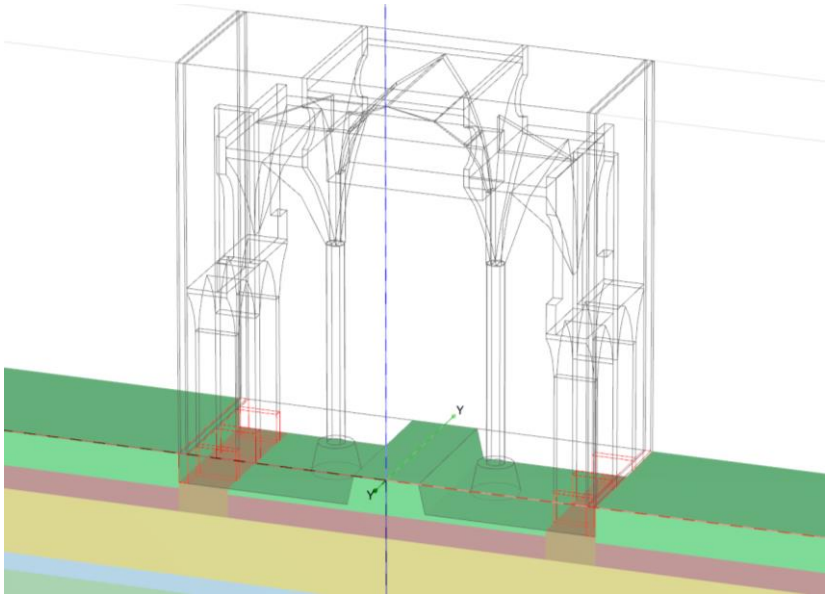

Figure 4.48 Supports element under foundations of Santa Maria del Mar Church.

The seismic capacity of the structure does not seem to be reduced considering real soil and supports foundations elements. It suggests that the supports elements are massive and still enough as to preserve the seismic performance in spite of the deformable soil.

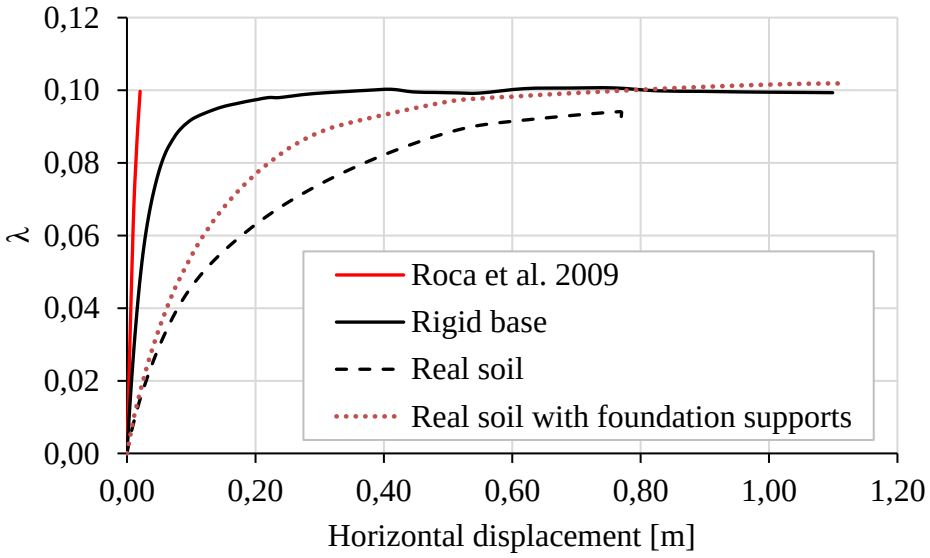

Figure 4.49 Capacity curve of a bay of Santa Maria del Mar.

4.3. Tunnelling-induced deformation and damage on masonry walls

The local ground deformations inevitably generated by the construction of shallow tunnels, such as for a new underground transportation system, could be dangerous for all the existing building present in the urban context in which the geotechnical work is acting.
This is particularly true for a particular kind of structure for which, due to their high cultural heritage, the even minor damage is undesirable.
This is the reason why any kind of tunnel design in an urban area cannot ignore its effects on a historic buildings. Therefore, the starting point is to quantify the settlements of underground infrastructures during their design projects, to try subsequently to have an estimation of the related damage induced on the surface buildings and provide the most appropriate mitigation techniques to be eventually adopted to minimise it (Mair & Taylor, 1997; Mair, 1998; Puzrin et al., 2012).
In the case of urban tunnelling projects, more detailed calculation procedures are required to identify buildings at risk and to make good evaluations of the likely extent of any tunnel-induced structural damage (Burghignoli, 2012; Rampello et al. 2012).
The performance of different example masonry buildings, described through the Jointed Masonry Model, in their interaction with the soil is here analysed, starting from the simple wall without opening to a complete 3D structure. The influence of eccentricity and inclination of the structure respect to the tunnel axis is also considered.

4.3.1. Modelling of excavation

The filling of a shield tunnel is usually built using prefabricated concrete ring segments, which are bolted together within the tunnel boring machine (TBM) to make the tunnel lining. The construction stages of the tunnel excavation have to consider that during the installation of the tunnel lining, the TBM has to remain stationary (Fig. 4.50).

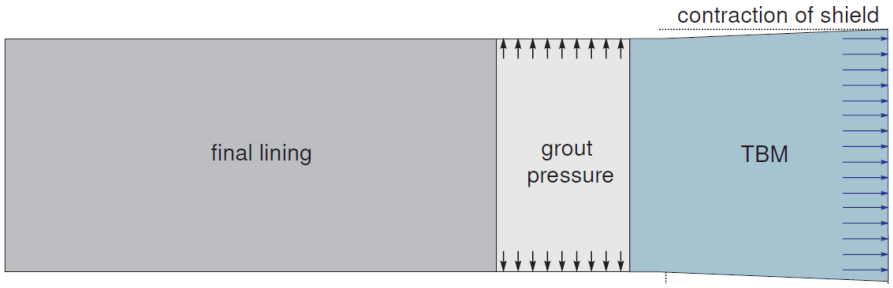

Figure 4.50 Sketch of a tunnel excavation process (Plaxis 3D Manual).

The excavation process can restart once a tunnel lining ring has been completely built, and it can continue only until enough soil has been excavated to erect the next lining ring. Due to this, the construction stages can be divided into as many steps as the number of portions in which the tunnel has to be divided to obtain segments 1.5 m width, which is the length of a tunnel ring.

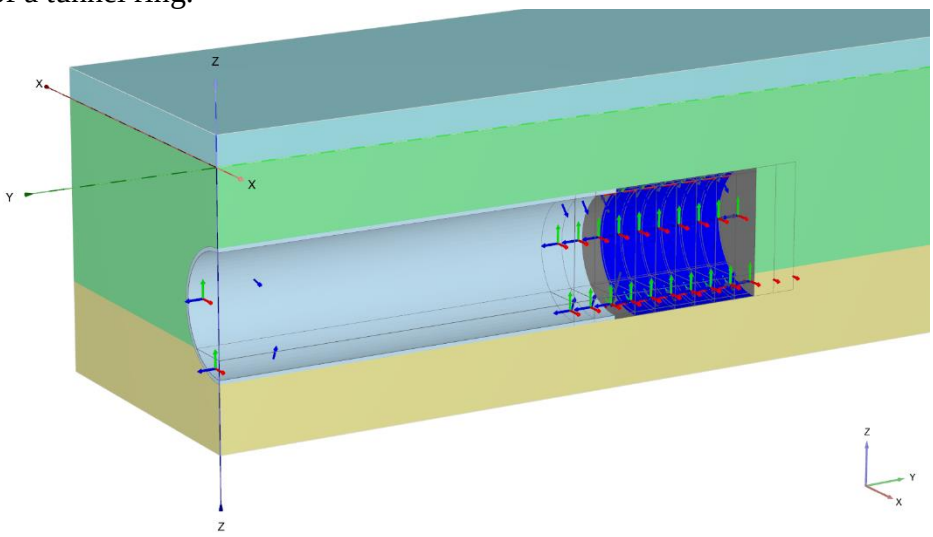

Figure 4.51 Construction stages of a shield tunnel model.

In each of these construction stages, the same steps are repeated over and over again. In fact, the input for the calculation phase is always the same exception made for its position, which will be shifted by 1.5 m each phase. In detail, the tunnel excavation consists of the following steps (Fig. 4.51):

- The support pressure at the tunnel front needed to prevent active failure at the face;
- The conical shape of the TBM shield;
- The removal of the soil and pore water within the TBM;

- The installation of the tunnel filling;
- The grouting of the hole between the soil and the newly installed lining.

In the following analyses, the soil portion considered has dimensions of 80x80x20 m^3 to avoid any influence from the boundaries. The tunnel, having a diameter equal to 8m, is assumed already excavated for the first 20m. After the activation of gravity in the masonry structure, the following 40m of the tunnel are simulated through the deactivation of soil slices 1,5m thick.
The distance between the tunnel axis and the ground level is equal to 9m.
The soil behaviour is described by the Mohr Coulomb Model, and the mechanical parameters are provided in Tab. 15. Drained conditions were assumed for the soil during the whole analysis.

Material properties	
γ (kN/m^3)	17
E (kPa)	75000
ν (-)	0.3
c (kPa)	1
φ (°)	31
ψ (°)	0

Table 4.16 Parameters of the Mohr Coulomb Model for the soil in tunneling analyses.

Figure 4.52 shows the free-field surface settlements for a value of volume loss equal to 0.4%, which is quite typical for a well-performing earth pressure balance machine since its use guarantees volume losses at the surface lower than 0.5%. The settlement profile obtained by numerical analyses for a volume loss of 0.4% is in good agreement with those predicted by the Gaussian distributions for trough width parameter K equal to 0.25.

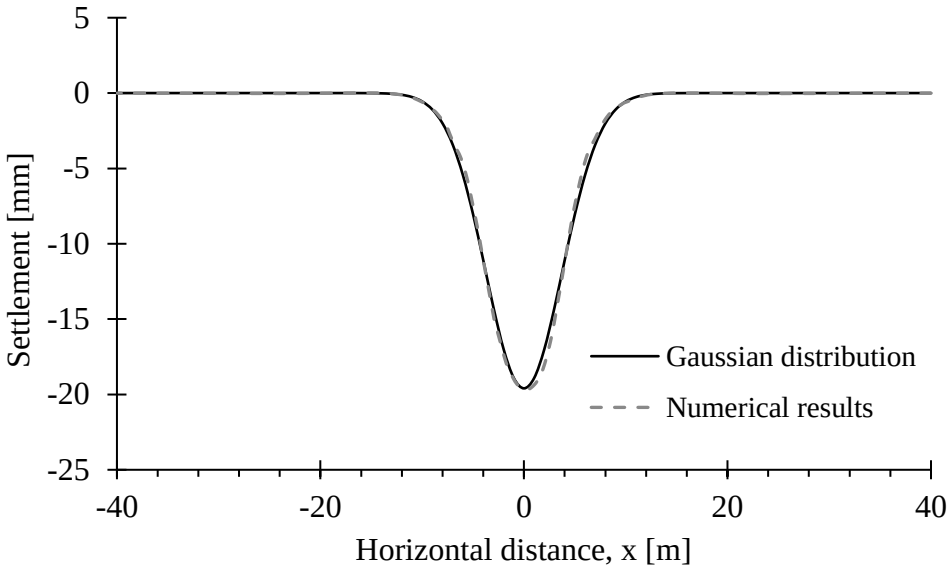

Figure 4.52 Modeling strategies for masonry structures: (a) masonry sample; (b) detailed micro-modeling; (c) simplified micro-modelling; (d) macro modelling.

The accordance between the numerical results and the empirical predictions indicates that the relatively simple constitutive assumptions and the simulation technique adopted for the tunnel excavation are adequate to the purpose of the present study.

4.3.2. Masonry wall without openings

The masonry wall, 4m high and 0,5m thick, rests on the ground and it is extended to the entire width of the soil model along the transversal section perpendicular to the tunnel axis. The excavation moves until it has no more effects on the masonry wall.
The mechanical parameters adopted for the masonry structure are the ones used for the traction test and summarized in Tab. 1. A more accurate mesh is used for both masonry and tunnel compared to the soil, as shown in Fig.4.53. At the final stage of excavation, the central part of the masonry suffers a vertical displacement equal to 3cm.
For this kind of geotechnical works, the damage is usually associated with the opening of tensile cracks and, due to this, it is useful look to the contour

of tensile plastic strain as an appropriate indicator of this phenomenon. In this way, different categories of damage can be correlated to different levels of tensile strain in according to Boscardin & Cording (1989).

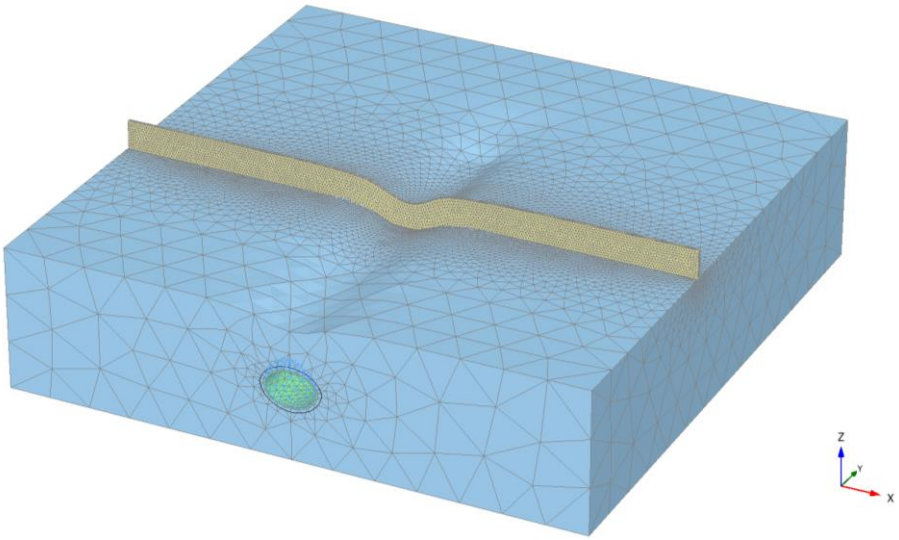

Figure 4.53 Deformed mesh for the tunneling analysis.

The extensional strain distribution, shown in Fig.16, reach a value equal to 0,53% at which correspond a severe damage in according with Boscardin and Cording (1989).

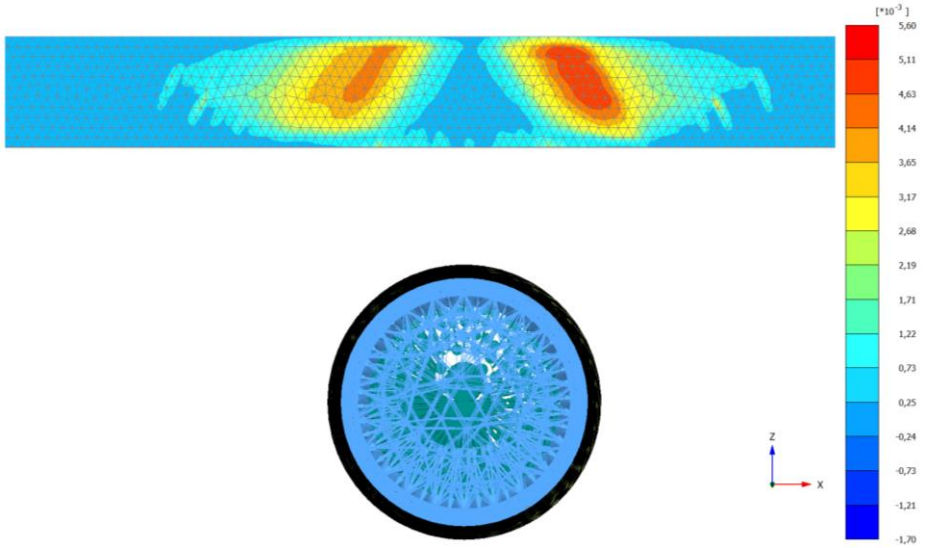

Figure 4.54 Distribution of extensional strain on the masonry wall central portion.

It is worth noting that the pattern of extensional strain on the masonry clearly resembles what is expected in literature when a short settlement located in the middle of the structure is considered (Mastrodicasa, 2012). In fact, the cracks are both inclined of 45° towards the centre of the wall, and they are located at the half height. Due to the large extension of the wall, the distribution of the vertical displacements at the base of the structure do not differ significantly from those obtained under free field conditions (Fig. 4.55).

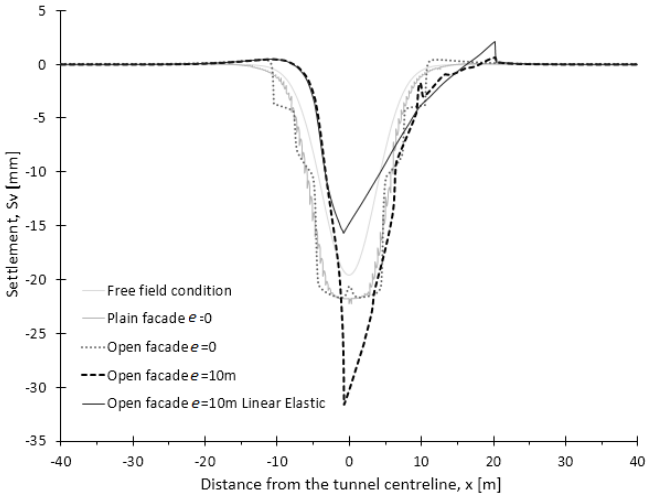

Figure 4.55 Vertical displacement at the foundation level.

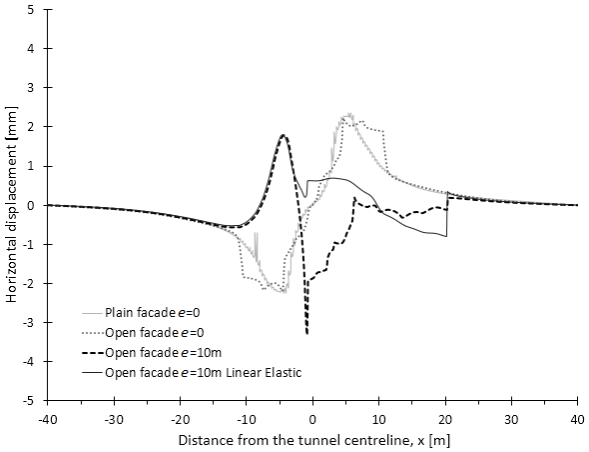

Figure 4.56 Horizontal displacement at the foundation level.

4.3.3. Masonry wall with opening

The dimensions of the building and the layout of the openings are based on previous work (Burd et al., 2000; Wisser et al., 2005; Pickhaver et al., 2010; Yiu et al. 2017) and shown in Figure 4.55. The structure height is equal to 8 m and its thick is 0.5 m.

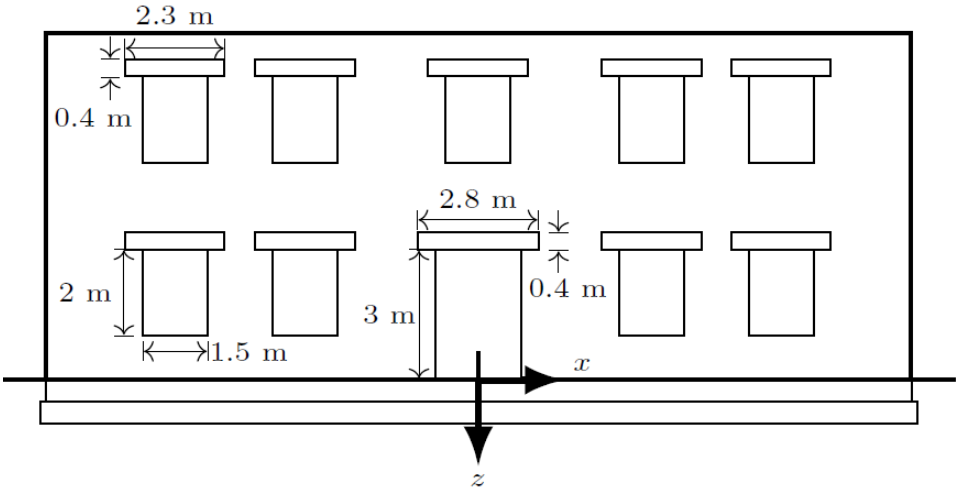

Figure 4.57 Dimensions of façade openings and lintels, also showing coordinate axes.

In this kind of geotechnical problems, it is useful provide an appropriate representation also of the foundations. For the following analyses the foundations is modelled as a strip footing of width 1 m, thickness 0.5m and embedded depth 1 m (Fig. 4.56). These dimensions are based on the foundations of the low-rise residential masonry building described in Withers (2001).

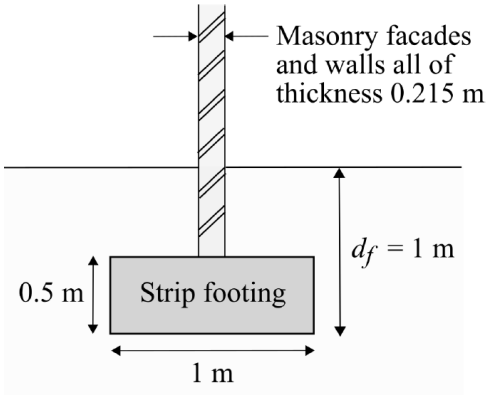

Figure 4.58 Detail of masonry and foundation (Yiu et al. 2017).

Lintels are included above all of the window and door openings in the facades to avoid tensile failure in the masonry due to local sagging effects and they are modelled as elastic elements (G = 3.75E6 kPa, ν = 0.2). For this masonry wall the eccentricity influence is also taking into account.

4.3.3.1. Without eccentricity

The results of a 3D isolated façade modelled in isolation are presented below. The façade meshes include the geometric arrangement of openings shown in Fig. 4.59. Due to the presence of the opening in the façade, the settlement profile induced by the excavation at the base of the foundation shows a stepped profile (Fig. 4.55). Apart from this peculiar shape, its average profile is in good agreement with that of the full wall. The corresponding horizontal displacements are lower in magnitude and in the opposite direction to those occurring in the soil adjacent to the base of the footing (4.56).

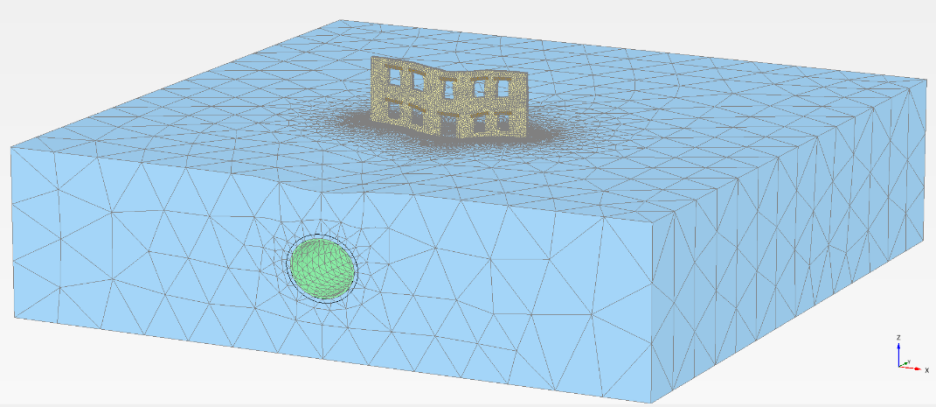

Figure 4.59 Deformed mesh for the tunnelling analysis of a masonry wall with opening.

The computed tensile strains induced in the façade for a tunnel excavation wihout eccentricity are shown in Fig. 4.60. The façade with openings exhibits a significant concentrations of strain occuring around the windows and coerent with the pattern observed in the plain wall, since a comparable distribution of tensile strain is observed.This indicates the importance of accounting for openings when determining the pattern and magnitude of the tensile strains developed in a façade.

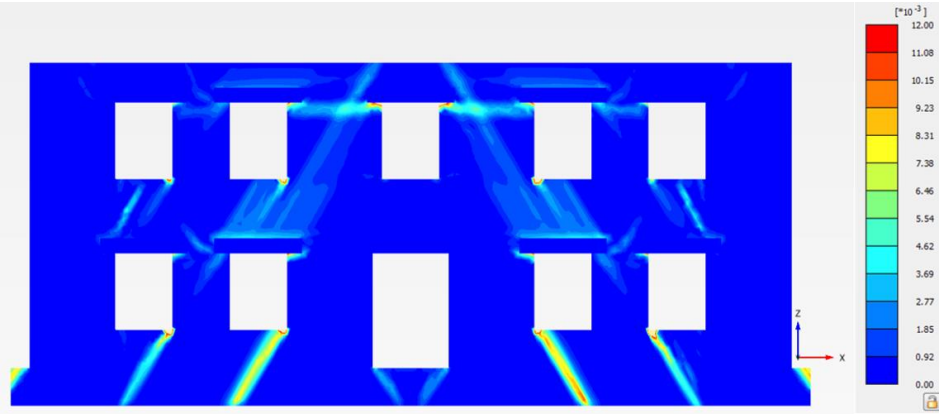

Figure 4.60 Extensional strain distribution at the end of the tunnelling analysis.

The extensional strains occurred in the wall with openings are larger then in the plain wall (Fig. 4.60). This is due to the different stiffness of the two structures since the plain façade is stiffer than the case where openings are present, which reduces the severity of the tunnel.

4.3.3.2. With eccentricity

The isolated facade with eccentricity is here described. In this case, the masonry wall with openings is shifted with respect to the tunnel axis such that the latter corresponds to the left corner of the wall.

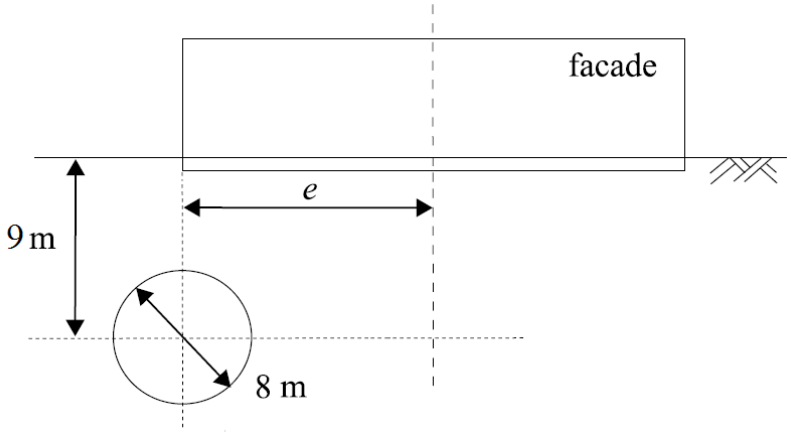

Figure 4.61 Tunnel dimensions and definition of eccentricity e.

The Fig. 4.62 shows the deformed configuration at the end of the tunnelling analysis. It is clear how the maximum deformation suffered by the structure regarding the portion more close to the tunnel.

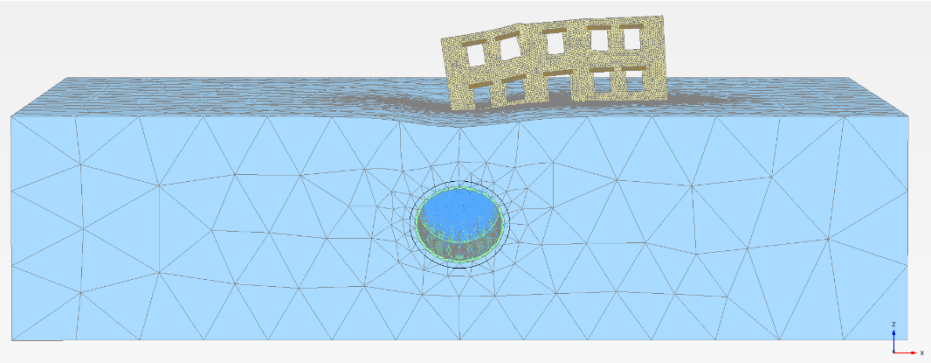

Figure 4.62 Deformed configuration at the end of the tunnelling analysis.

Figure 4.63 shows the extensional strain distribution at the end of the analysis. As a consequence of the tunnel excavation, the wall seems to be subdivided into three portions, the first one on the left being characterised by an almost rigid rotation towards the tunnel. In particular, a maximum strain value of 0.91% is reached on the upper right corner of this portion, in correspondence of the inflection point of the subsidence trough as evaluated at the foundation intrados (Fig. 4.55). While the right side, far from the tunnel axis, is exposed to a moderate deformation pattern. This is an expected outcome since the deformations distribution resembles the typical damage observed in terminal settlements problems.

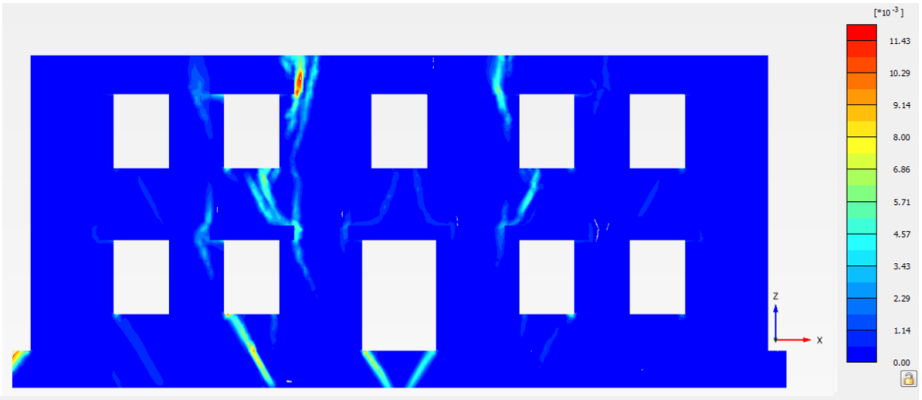

Figure 4.63 Deformed configuration at the end of the tunnelling analysis.

The same analysis was carried out describing the masonry façade as an elastic continuum. Figures 4.55 and 4.56 highlight that, in this case, the settlements profile can be strongly underestimated as compared to that

observed when the non-linear behaviour of the masonry is taken into account.

4.3.4. 3D complete building

A 3D complete building analysis in which both facades, internal and end walls are considered in the model, is presented. The internal facades of the 3D structure have the same geometrical characteristics of the masonry wall with openings, while the end walls are plain facades (4.64).
Due to the symmetry of the structure to its longitudinal axis, a deformation pattern very similar to the previous ones, obtained for the wall with openings, was expected if both cases with and without eccentricity were analyzed. This is the reason why it was preferred to carry out a specific analysis in which eccentricity and inclination of the structure respect to the tunnel axis are considered together.

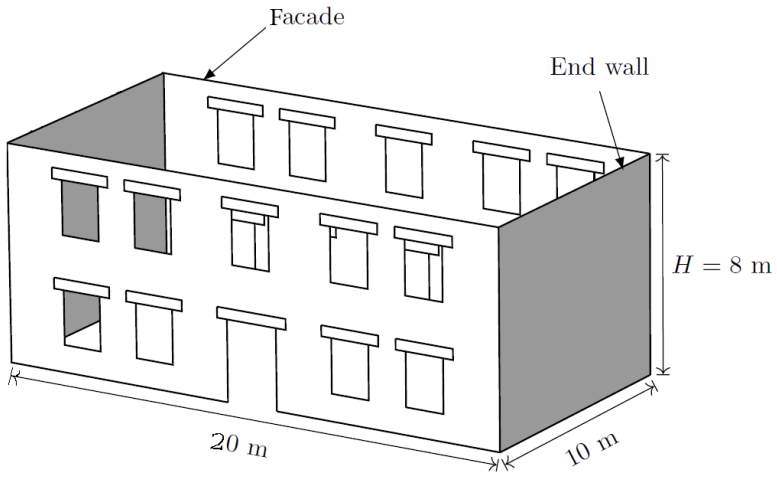

Figure 4.64 Layout and dimensions of building.

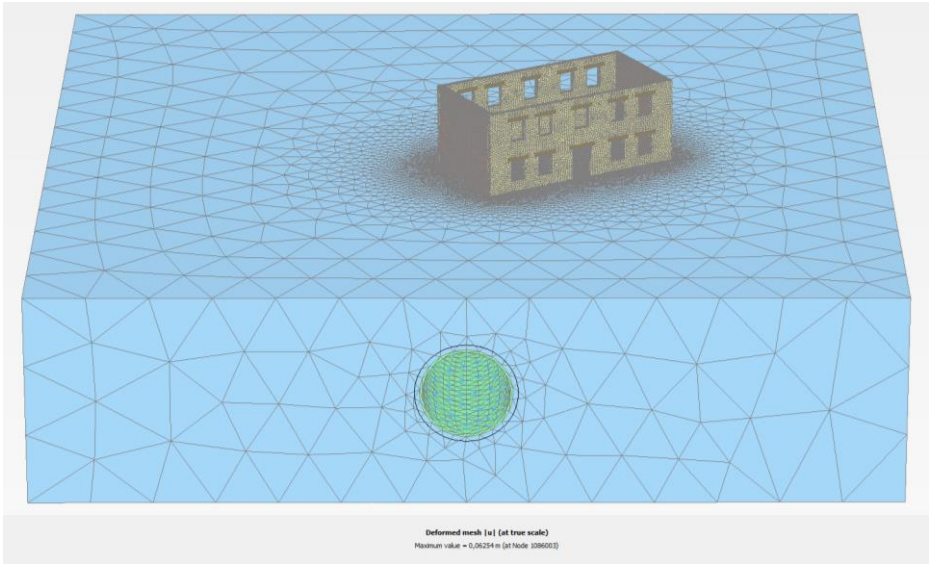

Figure 4.65 Whole model of a 3D building.

The eccentricity is such that the tunnel axis is in line with the point positioned at the middle of the left end wall. Starting from this point, an inclination of 30° with respect to the horizontal line perpendicular to the tunnel axis is considered (Fig. 4.65-4.66).

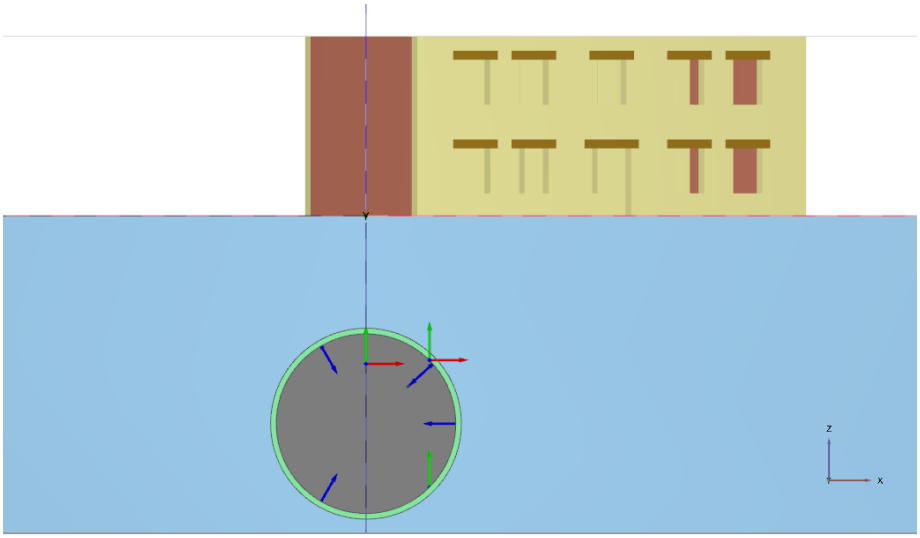

Figure 4.66 Detail of the 3D building model.

Fig. 4.67 shows the extensional distribution for the whole building. The differential settlements induced in the skew tunnel case are less than those in orthogonal tunnel case. Data on computed tensile strains in the front façade are shown in Fig. 4.68 and 4.69. The information related to the end walls are not presented since their damage categories remains at Cat. 0.

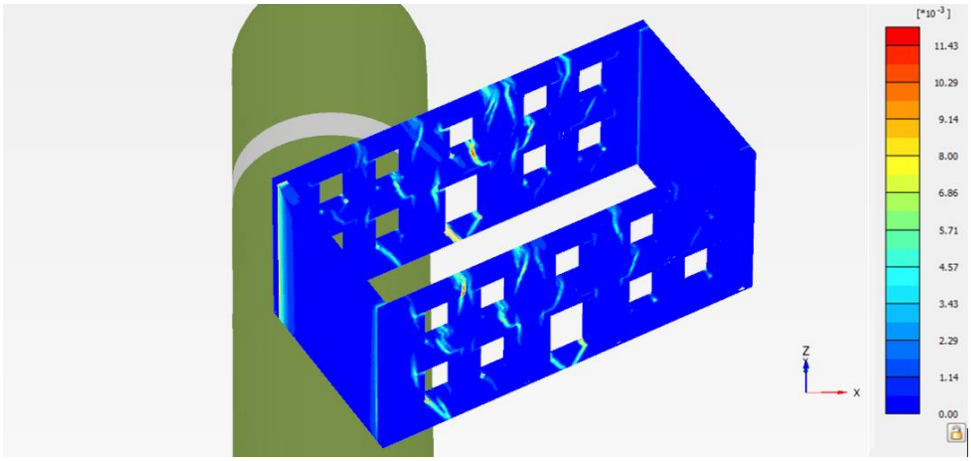

Figure 4.67 Detail of the 3D building model.

It is clear as the Jointed Masonry model is able to catch the how the damage is distribuited according to the tunnel axis. In fact, how it can be observed in the following figures, the tensile deformation concerne the left side of the front façade and then is shifted to the right side of the rear façade.

Figure 4.68 Front façade damage.

Figure 4.69 Rear façade damage.

On the base of this comparison, the orthogonal tunnel case seems to produce a more moderate damage estimation. It is worth noting that transient effects associated with the incremental tunnel construction and taken into account in the analysis, are particularly significant for the skew tunnel configuration since also twisting deformation effects, here catch from a qualitative point of view, are induced in the structure as the tunnel heading passes beneath it.

5. CONCLUSIONS

The conservation of cultural and architectural heritage, is an issue of great interest, due to their intrinsic historical and artistic value. In the contest of urban geotechnical works, like underground transportation system, this issue assumed a particular importance. Therefore, the design of these kind of works has to take into account the effect induced on the cultural heritage as a consequence of their interaction with the area in which they are located. A specific kind of analyses that integrates both geotechnical and structural aspects is needed in order to make an accurate estimation of the damage produced on masonry buildings.

The aim of this work is to provide an instrument with which a quantitavely assessment of high heritage value buildings at a risk of tunnell-induced settlements damage, can be obtained.

At this scope a new masonry model called Jointed Masonry Model has been developed starting from an already existing Jointed Rock Model originally developed to describe the rock mass behavior and implemented in a Geotechnical Finite Element Code.

This latter model, anisotropic elastic perfectly plastic, could be adapted to the description of masonry wall since it allows to define the orientation of a maximum three planes along which a possible failure mechanism can occur and on which of them a local Mohr-Coulomb yield criterion is applied. In order to adapt the Jointed Rock Model to structural applications, and to provide a more realistic representation of the masonry behaviour, a modified version of the Jointed Rock Model named Jointed Masonry model has been developed. In this constitutive model the mechanical and geometrical characteristics of masonry components are take into account through the SFBeta parameter, which is the main innovation of the new model. Thanks to it, the enhanced shear and tensile strength on the head joints due to the contribution of the bed joints which are subjected to a vertical stress state increases with depth and depending on the dimensional ratio of the blocks, is taking into account.

In this way, although the model is formulated in a continuum context, the geometrical character of the single block composing the masonry is retained. It is worth noting that by using mainly three parameters as cohesion, friction angle and SFbeta, which are available in the majority of cases (c and φ) and easily obtained (SFbeta), it is possible take into account the non-linear and anisotropic behaviour characterising masonry structures.

In addition, the other great advantage of the Jointed Masonry Model consists in the fact that it is implemented in a 3D Geotechnical Finite Element Code. This provide the opportunity to produce interaction analyses in which the behaviour of both soil and masonry structure is described taking also into account the three dimensionalities of the problem. In fact, especially during geotechnical works, like new underground transportation system in urban areas, it is essential being able to reproduce all the tunnel construction stages to better understand and make a more accurate quantitate estimation of the damage induced in historical buildings as a consequence of this kind of works.

The model is validated against experimental and analytical results, this letter performed with more advanced constitutive model developed for masonry structure. The good agreement between the results has assess the capability of the Jointed Masonry model in describing historical buildings. Two important masonry structures are thus analysed for the first time in their interaction with soil, taking into account the conditions evolution characterising the singular monument's history during their construction and their lifetime, allowed to understand and reproduce with sufficient degree of accuracy what happened to structures over time. In particular, for the Nymphaeum of Genazzano, a Renaissance structure attributed to Bramante, the numerical results have reproduced the same damage observed during in situ survey, proving the reliability of the proposed model in describing this kind of structure. The second case study, represented by the Church of Santa Maria del Mar in Barcelona, has confirmed what the previous studied had already shown since, once again, the results are perfectly corresponding to those obtained using a more advanced constitutive model to describe masonry structure. In this case, the possibility to take into account the real soil stratigraphy has allowed to analyse for the first time the influence of soil on the global masonry response during a non-linear static pushover analysis, valuated in terms of collapse load.

Further analyses are also conducted in order to assess the performance of different example masonry buildings during a tunnel excavation taking into account both eccentricity and inclination of the structures with respect to the tunnel axis. The general trends indicated by the finite element analyses are consistent with the expected behaviour.

This work has demonstrated that this approach based on a 3D finite element modelling and carried out adopting advanced constitutive hypotheses for both the structure and soil, being the first described by the new Jointed

Masonry Model within a geotechnical code, allows to capture the key factors affecting the overall response of masonry buildings in soil structure interaction problems, including the construction sequence and interaction with the surrounding environment.
Further analyses are needed to acquire a complete model calibration in order to take also into account the out of plane behaviour and to extend the study to a complete 3D structure with reference to high heritage-value buildings.
This could allow that this kind of approach can be usefully extended in future to the identification of possible retrofitting measures of this type of structures.

REFERENCES

AMOROSI A., BOLDINI D., DE FELICE G., LASCIARREA W.G., MALENA, M. 2015. *Analisi geotecnica e strutturale del Ninfeo di Genazzano*, Rivista Italiana di Geotecnica, 1, 29-44.

AMOROSI A., BOLDINI D., DE FELICE G., LASCIARREA W. G., MALENA M. 2016. *An integrated approach for geotechnical and structural analysis of the Nymphaeum of Genazzano*. Structural Analysis of Historical Constructions, pp. 503-510.

AMOROSI A., BOLDINI D., DE FELICE G., LASCIARREA W. G., MALENA M. 2018. *Jointed Masonry Model: a new versatile constitutive law for 3D analysis of masonry structures*. In preparation.

AMOROSI A., BOLDINI D., DE FELICE G., MALENA M. 2012. *Tunnelling-induced deformation in a masonry structure: a numerical approach*. Proc. 7th International Symposium on Geotechnical Aspects of Underground Construction in Soft Ground, Rome, pp. 353–359.

AMOROSI A., BOLDINI D., DE FELICE G., MALENA M., SEBASTIANELLI M., 2014a. *Tunnelling-induced deformation and damage on historical masonry structures*. Géotechnique, 64, No. 2, pp. 118-130.

BARUCCO P. 2000. *I restauri del Ninfeo di Genazzano. Verifica di tre interventi conservativi del XX secolo*. Atti del Convegno Internazionale di Scienza e Beni Culturali, Bressanone, pp. 511–523.

BENZT. 2007. *Small-strain stiffness of soils and its numerical consequence*s. Ph.D. thesis, Universität Stuttgart.

BERTO L., SAETTA A., SCOTTA R., VITALIANI R., 2002. *An orthotropic damage model for masonry structures*. Int J Numer Methods Eng 55:127–157.

BILOTTA, E., PAOLILLO, A., RUSSO, G. & AVERSA, S. (2017). *Displacements induced by tunnelling under a historical building*. Tunnelling and Underground Space Technology 61, 221–232.

BORRI, CORRADI, GALANO, VIGNOLI, 2004. *Analisi sperimentali e numeriche per la valutazione della resistenza a taglio delle murature*.

BOSCARDIN M., CORDING E. J., 1989. *Building response to excavation-induced settlement.* Journal of Geotechnical Engineering, ASCE, Vol. 115, 1-21, January.

BURD, H. J., HOULSBY, G. T., AUGARDE, C. E. & LIU, G., 2000. *Modelling tunnelling-induced settlement of masonry buildings*. Proc. Instn Civ. Engrs – Geotech. Engng 143, No. 1, 17–29.

BURGHIGNOLI A., 2012. *L'attraversamento sotterraneo del centro storico di Roma*. Rivista Italiana di Geotecnica, n. 3, pp. 13–50 (in Italian).

BURLAND J.B., 1995. *Assessment of risk of damage to buildings due to tunneling excavations*. Invited Special Lecture to IS-Tokyo 1995: 1st Int. Conf. On Earthquake Geotechnical Engineering.

BURLAND J.B., VIGGIANI C. 1994. *Osservazioni sul comportamento della Torre di Pisa*. Rivista Italiana di Geotecnica, n. 3, pp. 179–200.

BOURLAND J.B., WROTH C.P., 1974. *Settlement of buildings and associated damage*. State of the Art Review, Conf on Settlement of Structure, Cambridge. Pentech Press, London, pp. 611-654.

A. BRIGNOLA, S. FRUMENTO, S. LAGOMARSINO, S. PODESTÀ, *Identification of Shear Parameters of Masonry Panels Through the In-Situ Diagonal Compression Test*. International Journal of Architectural Heritage, 3:1, 52-73"

CALABRESI G. 2013. *The role of Geotechnical Engineers in saving monuments and historic sites*. Proc. 18th International Conference on Soil Mechanics and Geotechnical Engineering, Paris, pp. 71–83.

C. CALDERINI, S. CATTARI, S. LAGOMARSINO, *The use of the diagonal compression test to identify the shear mechanical parameters of masonry*. Costruction and Building Materials.

C. CALDERINI, S. CATTARI, S. LAGOMARSINO, *Identification of shear mechanical parameters of masonry piers from diagonal compression test*. 11th Canadian Masonry Symposium, Toronto, Ontario.

CLEMENTE R., 2006. *Structural analysis of historical buildings by localized cracking models* (in Spanish). PhD dissertation, Universitat Politècnica de Catalunya, Barcelona, Spain.

M. CORRADI, C. TEDESCHI, L. BINDA, A. BORRI, 2003. *Experimental evaluation of shear and compression strength of masonry wall before and after reinforcement: Deep repointing*. Costruction and Building Materials.

CROCI G., 1995. *The Colosseum: safety evaluation and preliminary criteria of intervention*. Structural Analysis of Historical Constructions, Barcelona.

DE BUHAN P., DE FELICE G., 1997. *A homogenization approach to the ultimate strength of brick masonry*, J. Mech. Phys. Solids 45, No. 7, pp. 1085-1104.

DE FELICE G., AMOROSI A., MALENA M., 2010. *Elasto-plastic analysis of block structures throught a homogeneization method*. Int. J. Numer. Analyt. Methods Geomech. 34, No. 3, pp.221-247.

FARGNOLI, V., GRAGNANO, C. G., BOLDINI, D. & AMOROSI, A. (2015). *3D numerical modelling of soil–structure interaction during EPB tunnelling*. Geotechnique 65, No. 1, 23–37.

FRANZIUS J.N., 2004. *The behaviour of buildings due to tunnel induced subsidence*. PhD Thesis, Imperial College, University of London.

FROMMEL C.L. 1969. *Bramantes "Ninfeo" in Genazzano*. Römische Jahrbuch für Kunstgeschichte, 12, pp. 137–160.

GAMBAROTTA L., LAGOMARSINO S., 1997. *Damage models for the seismic response of brick masonry shear walls Part I & Part II*. Earthq Eng Struct Dyn 26.

Geotechnical Report of Santa Maria del Mar Church.

GHIASSI B., SOLTANI M., TASNIMI A.A., 2012. *A simplified model for analysis of unreinforced masonry shear walls under combined axial, shear and flexural loading*. Engineering Structures 42, pp. 396-409.

GONZALEZ A., CASALS A., ROCA P., GONZALEZ J.L., 1993. *Studies of Gaudi's Cripta de la Colonia Güell.* IABSE Symposium, Structural Preservation of the Architectural Heritage, Rome, pp 457–464.

HARDIN B., DRNEVICHV. 1972. *Shear modulus and damping in soils: design equations and curves*. J. Soil Mech. Found. Div., 98, n. 7, pp. 667–692.

HARRIS, D. I. & FRANZIUS, J. N., 2005. *Settlement assessment for running tunnels – a generic approach*. Proc. International Symposium of Geotech. Aspects of Underground Construction in Soft Ground, Amsterdam, 2005.

LANCELLOTTA R., 2013. *La Torre Ghirlandina: una storia di interazione struttura-terreno*. Rivista Italiana di Geotecnica, 2, pp. 7-37.

LOTFI H.R., SHING P.B., 1994. *Interface model applied to fracture of masonry structures*. J Struct Eng ASCE 120(1):63–80.

LOURENCO P.B., 1996. *Computational strategies for masonry structures*. PhD thesis. Delft University of Technology, Delft, The Netherlands.

LOURENÇO P.B., ROTS J.G., 1997. *A multi-surface interface model for the analysis of masonry structures*. J Eng Mech ASCE 123(7):660–668.

MACCHI G., RUGGERI M., EUSEBIO M., MONCECCHI M., 1993. *Structural assessment of the leaning tower of Pisa*. In: Structural preservation of the architectural heritage, IABSE, Zürich, Switzerland, pp 401–408.

MAIR, R. J., (1998*). Tunnelling and geotechnics: new horizons.* 46th Rankine Lecture. Géotechnique 58, No. 9, 695–736,

MAIR R., TAYLOR R. N., BRACEGIRDLE A., (1993). *Subsurface settlement profiles above tunnels in clays*. Geotechnique, Vol. 43, No. 2, pp. 315 – 320.

MAIR, R. J., TAYLOR, R. N. & BURLAND, J. B. (1996*). Prediction of ground movements and assessment of risk of building damage due to bored tunnelling*. In Proc. 4th Int. Symp. Geotechnical Aspects of Underground Construction in Soft Ground, AA Balkema, pp. 713–718.

MAIR, R. J., TAYLOR, R. N. (1997*). Bored tunneling in the urban environment: State-of-the-art report and theme lecture*. Proceedings of the 14th International Conference on soil mechanics and foundation engineering, Hamburg, Vol. 4, pp. 2353-2385. Rotterdam, the Netherlands: Balkema.

MALLARDO V., MALVEZZI R., MILANI E., MILANI G., 2008. *Seismic vulnerability of historical masonry buildings: a case study in Ferrara*. Eng Struct 30:2223–2241.

MASTRODICASA S., 2012. *Dissesti statici delle strutture edilizie.*

MAZZIOTTI A., 2015. *Structural Analysis of Historical Masonry Buildings*. Ph.D. Thesis. University of Naples Federico II.

MOH Z. C., HWANG R.N., JU D. H., 1996. *Ground movements around tunnels in soft ground*. In Mair et al. (eds) Geothecnical Aspects of Underground Construction in Soft Ground, London: Balkema.

MOLA F., VITALIANI R., 1995. *Analysis, diagnosis and preservation of ancient monuments: the St. Mark's Basilica in Venice*. In: Structural analysis of historical constructions I. CIMNE, Barcelona, Spain, pp 166–188.

MURCIA-DELSO J., DAS A.K., ROCA M., CERVERA M., 2009. *Seismic safety analysis of historical masonry structures using a damage constitutive model*. In: Thematic conference on computational methods in structural dynamics and earthquake engineering.

MURCIA J., 2008. *Seismic analysis of Santa Maria del Mar Church in Barcelona*. Master's Thesis in Structural Analysis of Monuments and Historical Construction.

O'REILLY, P. AND NEW, M. *Settlement above tunnels in the United Kingdom - their magnitude and prediction*. Proceedings of Tunneling Symposium 1982:173-181.

OTHAY., GOTO N. 1978. *Empirical shear wave velocity equations in terms of characteristic soil indexes.* Earthquake Engineering and Structural Dynamics, 6, pp. 167–178.

PAPA E.A., 1996. *Unilateral damage model for masonry based on a homogenization procedure*. Mech Cohes-Frict Mater 1:349–366.

PELA' L., APRILE A, BENEDETTI A., 2009. *Seismic assessment of masonry arch bridges*. Eng Struct 31:1777–1788.

PELÀ L., CERVERA M., ROCA P., 2013. *An orthotropic damage model for the analysis of masonry structures*. Construction and Building Materials 41, 957-967.

PICKHAVER, J. B., BURD, H. J. & HOULSBY, G. T., 2010. *An equivalent beam method to model masonry buildings in 3D finite element analysis*. Computers and Structures 88, No. 19/20, 1049–1063.

PLAXIS 3D, 2016. *Material Manual*.

POTTS D.M., ADDENBROOKE T.I., 1997. *A structure's influence on tunnelling-induced ground movement*. Proc. Instn, Civ. Engrs. Geotech. Engineering, 125, 109-125.

PUZRIN A.M., BURLAND J.B., STANDING J.R., 2012. *Simple approach to predicting ground displacements caused by tunneling in undrained anisotropic elastic soil*. Géotechnique, vol. 62, n°4, pp.341-352

RAIJMAKERS TMJ, VERMELTFOORT ATH, 1992. *Deformation controlled tests in masonry shear walls*. Research report TNO-Bouw. Report B-92-1156 [in Dutch].

RAMPELLO, S., CALLISTO, L., VIGGIANI, G. & SOCCODATO, F., 2012. *Evaluating the effects of tunnelling on historical buildings: the example of a new subway in Rome*. Geomech. Tunnelling 5, No. 3, 275–299.

ROCA,P., 2007. *Basílica de Santa Maria del Mar: estudi de l'estructura*. Technical University of Catalonia.

ROCA P., 1998. *Studies of Gaudi's Cripta de la Colonia Güell*. In: Structural analysis of historical constructions II. CIMNE, Barcelona, pp 377–393.

ROCA P., CERVERA M., GARIUP G., PELA' L., 2009. *Structural analysis of masonry historical constructions*. Classical and Advanced Approaches. Arch. Comput. Methods Eng. 17, pp. 299-325.

ROCA P., MASSANAS M., CERVERA M., ARUN G., 2004. *Structural analysis of Küçük Ayasofya Mosque in Ístanbul*. In: Structural analysis of historical constructions IV. Balkema, Amsterdam, pp 679–686.

SANTOS J.A., CORREIRA A.G. 2001. *Reference threshold shear strain of soil. Its application to obtain a unique strain dependent shear modulus curve for soil*. Proc. 15th Int. Conf. on Soil Mechanics and Geotechnical Engineering, 1, Istanbul, pp. 267–270.

SCHANZ T. 1998. *Zur modellierung des mechanischen verhaltens von reinbungsmaterialien*. Tesi per *l'Abilitazione, Inst fur Geotechnik, Universitat Stuttgart.*

SEBASTIANELLI M., AMOROSI A., BOLDINI D., DE FELICE G., DI MUCCI G., MALENA M. 2012. *Settlement prediction of an historic masonry due to tunnel excavation taking into account soil-structure interaction*. In. 8th International Conference on Structural Analysis of Historical Constructions, Wroclaw, pp. 567–574.

SKEMPTON A.V. 1986. *Standard Penetration Test Procedures*. Géotechnique, 36, n. 3, pp. 425–557.

SUTCLIFFE DJ, YU HS, PAGE AW., 2001. *Lower bound limit analysis of unreinforced masonry shear walls*. Comput. Struct. 79(14):1295–1312.

TZAMTZIS A.D., 1994. *Dynamic finite element analysis of complex discontinuous and jointed structural systems using interface elements*. PhD Thesis, Department of Civil Engineering, QMWC, University of London.

VENDRELL, M., GIRÀLDEZ, P., CABALLÉ, F., GONZÁLEZ, R., ROCA, P., 2007. *Estudi històricoconstructiu, materials de construcció i estabilitat estructural de Santa Maria del Mar*. Departament de Cultura i Mitjans de Comunicació, Generalitat de Catalunya.

VIGGIANI G., ATKINSON J.H. 1995. *Stiffness of fine-grained soils at very small strains*. Géotechnque, 45, n. 2, pp. 249–265.

VUCETIC M., DOBRY R. 1991. *Effects of the soil plasticity on cyclic response*. J. Geotech. Engng Div. ASCE 117, No. 1, pp. 89–107.

WISSER, C., AUGARDE, C. E. & BURD, H. J., 2005. *Numerical modelling of compensation grouting above shallow tunnels*. Int. J. for Numer. and Anal. Meth. in Geomech. 29, No. 5, 443–471.

WITHERS, A. D., 2001. *Murdoch, Neptune and Clegg Houses in Moodkee Street, Rotherhithe*. Building Response to Tunnelling 2, 811–828.

YIU, W. N., BURD, H. J. & MARTIN, C. M., 2017. *Soil-building interaction in finite element analysis of tunnelling-induced building damage*. In Proc. IV International Conference on Computational Methods in Tunneling and Subsurface Engineering, pp. 381–388.